Measuring techniques to determine hydrophobicity of polymer insulators

by
Emile Kleyn

Thesis presented in partial fulfilment of the requirements for the degree of Master in Engineering (Electrical and Electronic) in the Faculty of Engineering at Stellenbosch University

Study leader: Dr. Johannes M. Strauss

December 2020

Declaration

By submitting this report electronically, I declare that the entirety of the work contained therein is my own, original work, that I am the sole author thereof (save to the extent explicitly otherwise stated), that reproduction and publication thereof by Stellenbosch University will not infringe any third party rights and that I have not previously in its entirety or in part submitted it for obtaining any qualification.

Date: February 2020 .....

Abstract

High voltage insulators play an important role in power grid networks. Maintaining high voltage insulators is essential in creating a reliable grid. Various factors such as pollution can influence the hydrophobicity characteristics of an insulator, affecting its ability to insulate. Therefore, it is imperative that techniques should exist to determine the insulator's hydrophobicity properties. Several techniques already exist, all with some shortcomings.

Two techniques were developed in the quest to create a field ready hydrophobicity measurement method. Machine learning was used to do image analysis of the insulators. Several convolutional neural networks were investigated and tested. A good correlation was found from the convolutions neural network results and the insulator's surface hydrophobicity.

A 3D laser surface constructor was developed to accurately scan an insulator's surface, creating a 3D computer model of the water formations present on its surface. Analysis was done on the 3D model, displaying the correlations between the insulator's surface hydrophobicity and features extracted from the 3D model. Promising results were achieved with this method. Both these methods can be used in the field to obtain the surface hydrophobicity of an insulator.

Uittreksel

Hoogspanningsisolators speel 'n belangrike rol in ons nationale krag netwerk. Die instandhouding van hoogspanningsisolators is noodsaaklik om 'n betroubare krag toevoer netwerk te skep. Verskeie faktore, soos besoedeling, kan die hidrofobisiteitseienskappe van 'n isolator beÃ¯nvloed. Die gevolg is nadelige effek op die isolators se isoleringsvermoÃ«. Daarom is dit noodsaaklik dat daar tegnieke moet bestaan om die hidrofobisiteitseienskappe van die isolator te bepaal. Daar bestaan reeds verskeie tegnieke, almal met enkele tekortkominge.

Twee tegnieke was ontwikkel om 'n veldgereedheidsmetode om hidrofobisiteit graduering te bepaal. Masjienleer is gebruik om beeldanalise van die isolators te doen. Verskeie indrukwekkende neurale netwerke is ondersoek en getoets. 'n Goeie korrelasie was gevind tussen die resultate van die neurale netwerk en die oppervlakhidrofobisiteit van die isolator.

'n 3D-laseroppervlakte-konstruktor was ontwikkel om die oppervlakte van 'n isolator akkuraat te skandeer. Die water formasies op die oppervlakte was dan ontrek vanuit die 3D-rekenaarmodel. Analise was gedoen op die 3D-model. Korrelasies tussen die isolator se oppervlaktehidrofobisiteit en karakterastieke was toe gevind uit die 3D-model. Belowende resultate was behaal met hierdie metode. Albei hierdie metodes kan in die veld toegepas word om die oppervlakhidrofobisiteit van 'n isolator te verkry.

Contents

List of Figures

List of Tables

Chapter 1

Introduction

1.1 Hydrophobicity of polymer insulators

1.1.1 Environmental effects on HVI

The stability of a power network is a continuous problem, as the dielectric materials which HV insulators are being manufactured with are constantly affected by environmental factors, inevitably causing failure over time [4].

Natural pollutants can contribute to the degradation of a high voltage insulators. When pollutants accumulate on an insulator's surface, it causes the surface to become a conductive electrolyte when it is exposed to wet conditions such as rain or fog. As a result, leakage currents increase as the electrical insulation properties on the insulator's surface decrease. Hence, the polluted insulator's surface acts as a preferential flow path for current to flow [5, 6].

UV radiation from the sun can also present significant degradation on the insulators surface [7]. Sun ray radiation can be classified into three different UV wavelengths [8]:

- UVA (320 - 400 nm)
- UVB (290 - 320 nm)
- UVC (100 - 290 nm)

UVC has the lowest wavelength range and the atmosphere acts as a natural filter preventing it from penetrating the earth's surface, hence having no effect on the insulators structure. Therefore, UVA and UVB are the primary wavelengths penetrating the insulator's structure, making it crucial to have insulators that can withstand these UV wavelengths.

Insulators also experience UV radiation while they are in service by means of radiation discharge in flashover currents [9, 10]. When flashover occurs, UV radiation can have a severe impact on insulator degradation. UVC is also present during electrical discharge, where effective atmospheric filtering is not present. The duration, frequency and intensity during a flashover incident determines the severity of degradation. Although the deterioration due to UV exposure is not destructive on its own, the long-term effects can cause mechanical and electrical issues that can lead to structural failure [9, 10]. Atmospheric deposits on the insulator's surface can also provide protection from UV radiation [11].

As renewable energy generation becomes more common, the development of in-field insulator performance classification techniques becomes more important. Most renewable energy

sources, such as wind and marine, are present in hilly or coastal areas, where the probability of salt and water contamination is high, causing a higher probability for flashover currents [12].

1.1.2 Pollution

Environmental pollution can either be active or inert [12, 13]:

- Active pollution consists out of salt fog, fly ash, metallic particles, salt deposits, chemicals, fertilizers, etc.
- Inert pollution is composed of non-soluble substances, such as deposits from cement factories, sand and dust.

Climate conditions such as high moisture levels, radiative exposure and counter-diffusion of hydroxide ions also have an effect on insulator degradation [4]. Other major sources of pollution include snow, rain forest algae/moss, industrial and lighting. Insulators in coastal environments are more susceptible to greater risks of pollution [4, 14]. Factors such as high wind speed and wind direction along coastal environments where distance from the sea, salt accumulation, diffusion and penetration rates are all closely related to the degradation rate of an insulator. The carrier of coastal pollutants can be described as follows: Soluble salts (NaCl and Na_2SO_4) present in water droplets are carried by nano/micro bubbles and are deposited on insulator surfaces. Pollutants cause the water to accumulate on the surface, forming a film of water which can cover the surface either partially of completely. The salts that dissolve in the film of water cause the insulator to become conductive, providing a path for leakage currents to flow [4, 15, 16].

Since pollutants can create a high risk of failure on high voltage power lines, which are essential to a countries power distribution, it is important to understand where potential points of failure may occur on the power grid. With all of these pollutants that accumulate on the insulator's surface, measuring the effect it has on the performance of the insulator can be complicated and time consuming.

The main concern for insulator performance is water accumulation on the surface of an insulator. As described above, pollutants enhance water accumulation. Instead of measuring the pollutant deposits on an insulator's surface, measuring the ability of an insulator to repel water is more beneficial. This gives rise to measuring an insulator's hydrophobicity characteristics.

1.2 Hydrophobicity measurement techniques

1.2.1 Hydrophobicity vs. hydrophilicity

In the scientific community, two definitions exist to describe the behaviour of water on a surface: these are hydrophobicity and hydrophilicity. Hydro refers to water, phobicity refers to a lack of affinity and philicity refers to affinity. A surface can be described as hydrophilic when the static water contact angle θ is $<90°$ and as hydrophobic when the contact angle θ is $>90°$(See figure 1.1) [1].

Different types of hydrophobicity measuring techniques will be described below.

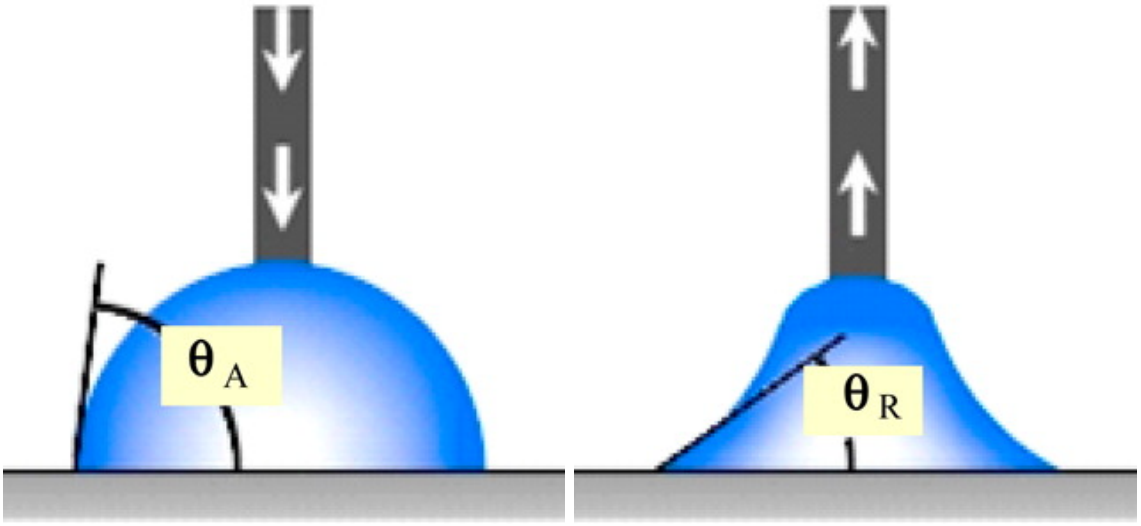

(a) (b)

Figure 1.1: (a) Hydrophobic contact angle and (b) hydrophilic contact angle [1].

1.2.2 STRI hydrophobicity classification

This method is a relatively easy method to implement in field conditions. The insulator's ability to repel water is measured by categorizing water accumulation patterns on the surface between seven classes hydrophobicity classes (HC 1 - 7). Classes with higher numbers represent and increasing degree of hydrophilicity behaviour of the insulator surface.

Method description:

- The insulator's surface should be at an angle of 10 - 35° to the horizontal plane.
- 50 - 100 cm^2 of the insulator surface is sprayed with a fine mist of water.
- Examine the water droplet formations on the wetted surface and compare it to a guide of reference images with HC1 - HC7 seen in figure 1.2.

1.2.3 Sessile drop technique

By measuring the contact angle of water droplets on silicon rubber materials, it is possible to determine the surface hydrophobicity. A method called the sessile drop technique can be used to measure the contact angle of a water droplet to the insulator's surface. Using a syringe, a water droplet is placed onto the surface. A goniometer is used to measure the static angle of the water droplet to the surface, as seen in figure 1.3.

The sessile drop method is applicable in laboratory environment only since it requires good illumination and optimal view of single drops on flat horizontal samples. This drawback in the methods for estimating hydrophobicity of insulators in the field conditions led to popularity of STRI hydrophobicity classification method [17].

1.2.4 ESDD, NSDD, and TSDD measurements

Another method is to measure salt deposits on an insulator. The weight of the insulator is measured with a sensitive microgram scale and then an area ($2cm^2$) of the salt deposit is removed from the surface of the insulator, after which the weight is measured again.

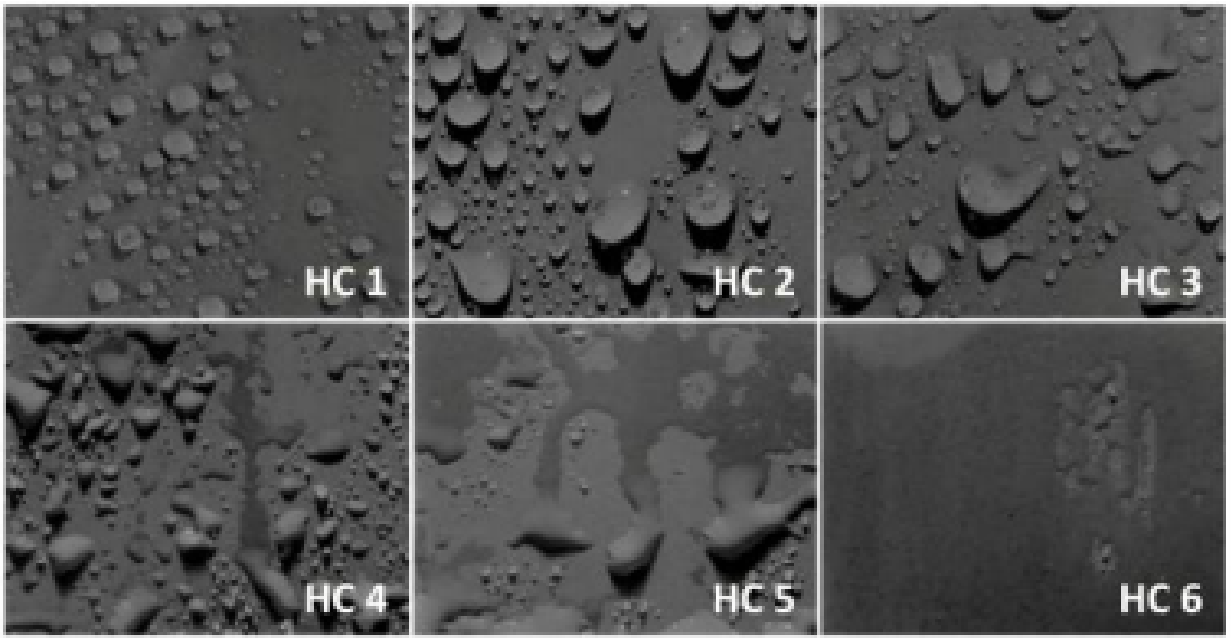

Figure 1.2: Hydrophobicity classification guide for classes HC1 - HC7 [2]

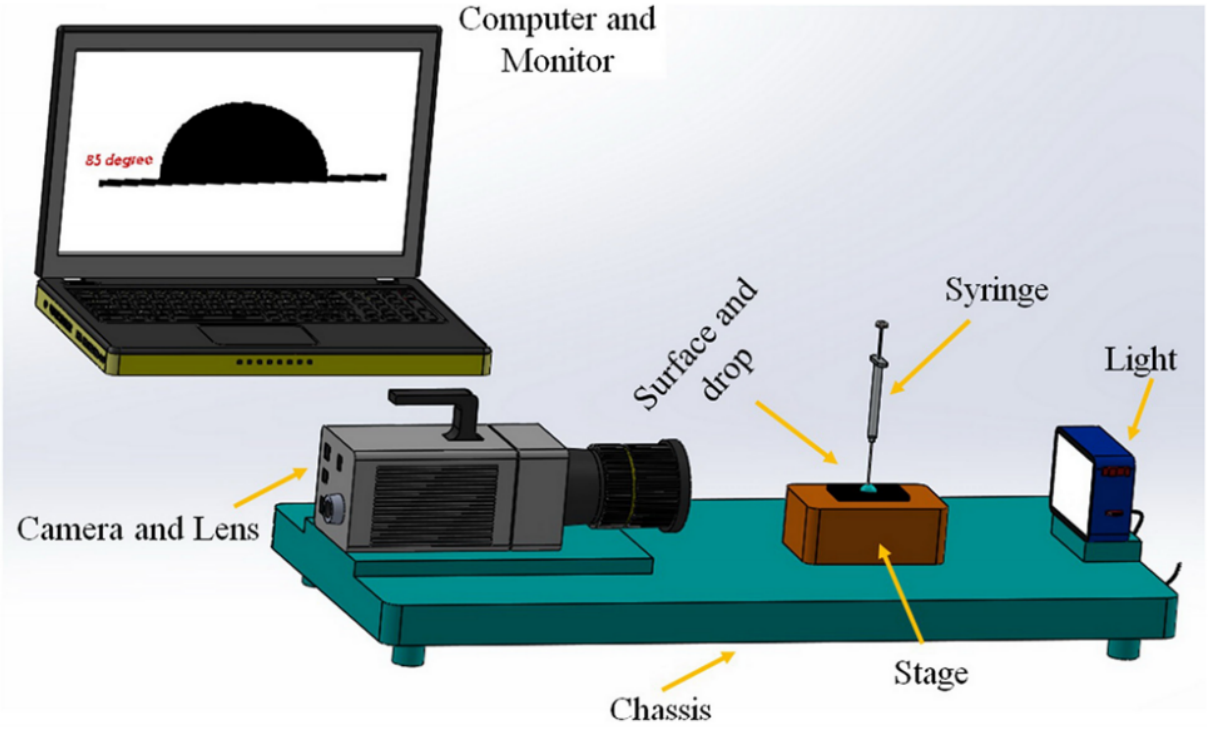

Figure 1.3: Sessile drop device setup [3]

A ratio of salt weight to area is then determined. This ratio is called Total Salt Deposit Density (TSDD) with dimensions as mg/cm^2 [17]. Analysis for non-soluble salt content is then determined of the salts that were removed. This gives rise to Non-Soluble Salt Deposit Density (NSDD) and Equivalent Salt Deposit Density (ESDD) which is proportional to soluble salt [17].

1.2.5 Scanning electron microscopy

A scanning electron microscope gives a magnified image of a micro section of the insulator's surface. It can be used to analyse micro cracks as well as surface roughness, which both play an important role in loss of hydrophobicity [17].

1.2.6 Advantages and disadvantages of methods

Table 1.1 provides a summary of the advantages and disadvantages of the different hydrophobicity measurement methods that were discussed.

Table 1.1: Summary of hydrophobicity measurement methods

Method	Advantage	Disadvantage	Measurement accuracy	Is it practical for field usage
Sessile drop	On a single point, the measurement is accurate.	Multiple samples are needed.	High for multiple measurements.	No
ESDD, NSDD, TSDD	Accurate measurement of salt deposits	Time consuming	Medium	No
Electron microscope	Accurate and precise measurement.	Can only be done in a lab and requires trained people.	High	No
STRI (manually)	1) This method is field ready. 2) Provide an overall measurement of the surface	Training is required and is perceptive based.	Medium	Yes
STRI (Image analysis)	Not based on human perception. Little training is required.	Light exposure has to be uniform over entire insulator.	Medium	Yes

1.2.7 Hydrophobicity measurement instructions

In order to achieve accurate and reputable results, hydrophobicity measurements taken of a surface using the STRI or Sessile drop technique should be done immediately after the insulator is removed from its supporting structure. Due to the ability of the insulator's silicone surface to recover, measurements would be inaccurate if there is a significant delay between the time of measurement and the time when the insulator is removed from its environmental stressors [18].

1.3 Problem statement

High voltage insulators are essential in providing electricity to a country, and so they play a crucial role in power grid infrastructure. For a grid to provide a stable performance, it is important to keep all its critical components in top condition.

It is important to do regular checkups on insulator performance quality to prevent unforeseen events from occurring. Thus, having a quantifiable method to conduct insulator quality analysis while the insulator is still intact to the grid's infrastructure is desired.

As described in section 1.2, current measurement techniques have several disadvantages, making it inappropriate for conducting in-field measurements. Although the STRI method can be used for in-field measurements, it is subjective to human perception. Therefore, it is important to develop a method that can conduct repeatable in-field measurement results and that can be used universally without extensive training. A few desired characteristics for such a method are:

1. Results should be repeatable and constant.
2. Results should not be subject to individual interpretation.
3. Minimal to no training on method/device.
4. Interpretation of insulator's condition should be straightforward.
5. Multiple insulator condition classification techniques that can possibly support the results of one another and not only classify hydrophobicity states, but also provide an indication of where preferential flow paths for leakage currents may exist.
6. It should be usable outside in the field.
7. Lightweight.
8. The device should be affordable.
9. It would be beneficial if analysis can be done using a cellular device with a camera.
10. It should not be affected by external lighting.
11. Detailed measurements should be easily transferable into a cloud database for possible future analyses.

1.4 Method of approach

1.4.1 Machine learning technique

Machine learning has the ability to recognize patterns between different sets of images which may not be obvious to the human eye. The advantage of using machine learning for image classification is that, after training has been done, image analyses can be done on photos without the need for a supercomputer. The more image data harvested, the more accurate the algorithm becomes after training.

Machine learning algorithms can be trained to be unaffected by change of external lighting conditions, as long as a large enough dataset is provided. Water droplet formations tend to

differ for different classes of hydrophobicity, yet for each class, a pattern can be recognized. This makes it an ideal approach for developing a hydrophobicity measurement device.

Several machine learning algorithms will be investigated to determine which provides the best results.

1.4.2 3D Laser profiling technique

When looking at measuring the hydrophobicity of an insulator, it is essential to investigate the structure of the water droplets. As was discussed in section 1.2.3, the sessile drop technique provides an indication of the water droplet contact angle to the insulator's surface, which in turn correlates the hydrophobicity of the insulator at the specific point of measurement.

It is desired to use the sessile drop technique over the entire surface of the insulator, but this would be tedious and unfeasible to implement in the field. A 3D laser profiling technique will be investigated to try to replicate a modified idea of the sessile drop technique over the entire surface of the insulator. 3D laser profiling techniques are widely used to do fine measurements for quality control on production lines. Some of the best 3D laser profilers can measure with an accuracy deviation of less than tens of micrometers [19].

1.5 Requirements and limitations

Machine learning technique

Machine learning algorithms require a dataset that it can be trained on. The size of the dataset plays an important role in the accuracy of the algorithm, but more importantly, the quality of the dataset is essential to achieve consistent results. Since water droplet formations can differ vastly, a large dataset is essential. However, creating a large dataset is very time consuming. A drawback to this technique is that limited human resources are available to create such a dataset. As this technique will be used in the field, the dataset should be harvested such that it represents conditions that reflect insulators that are in the field. Different illumination sources should also be present in the dataset.

The goal of this technique is to take a picture of an insulator's surface, feed it into a machine learning algorithm and provide a hydrophobicity classification. A set of instructions should be defined that describes the method of preparing the insulator's surface as well as how the pictures should be taken.

3D Laser profiling technique

In order to use a 3D laser technique, an algorithm should be able to identify a light source projected onto the surface that is being evaluated. External lighting can be a drawback to this technique if it is greater that the light source. A simple solution to this would be to increase the light source intensity; however, a high intensity light source could be dangerous to the naked eye and can also cause potential damage to the surface of an insulator.

Chapter 2

Image based hydrophobicity analysis by means of machine learning

2.1 Introduction to machine learning

Differentiating between a hydrophobic and hydropilic insulator can seem like an arbitrary task for the human eye, but creating an image processing algorithm to be implemented with a computer is a whole other level of difficulty. Even more so is that various classes of hydrophobicity should be differentiated from each other. One person may classify an insulator on the STRI guide as a class 1, while someone else may classify it as a class 2. This discontinuity of borders between different classes of hydrophobicity can pose an even more difficult task to create an image processing algorithm that can be implemented by a computer to do analysis.

Let's take the example of creating an image processing algorithm to search for a dark spot on an apple, which may indicate that the apple is starting to rot. One might create different windows (also known as kernals) of round dark spots surrounded by a green or red background. Sliding these windows over the entire image of an apple and searching for high match thresholds, one might successfully identify rotten apples. However, using such a technique for identifying water droplets will require that hundreds to thousands such windows must be created to successfully identify different water droplets that represent different degrees of hydrophobicity on the insulator's surface. Machine learning algorithms have the ability to recognize patterns in datasets that might not be visible to human perception.

Machine learning involves changing system parameters of already performing systems or new systems, such that enhancement can be achieved to better perform planning, recognition, diagnosis, or robot control [20]. This, often described as artificial intelligence (AI), has the ability teach itself by observing the effect on the output when a certain parameter is changed. After such an observation has been made, an even better alteration to the system's parameters can be made to improve the output [20].

Applying machine learning in the quest to do analysis on the hydrophobicity state of insulators can prove beneficial in recognizing different patterns for different hydrophobicity states. One such pattern might be to detect different water droplet shapes on the insulator's surface. Highly hydrophobic surfaces have uniform round droplet formations and hydrophilic surfaces have a film of water dispersed over the insulator's surface.

In this chapter, the building blocks of neural networks will be discussed, followed by convolutional neural networks with application to image recognition.

2.2 Artificial neural networks

According to Dr. Wang [21], artificial neural networks can be described as the nervous system of the human body. The nervous system consists out of three layers. These are:

1. **Input layer:** This resembles signal sources from outside the body that are fed into the hidden layer's neurons / nodes. Neurons are hidden in the body and are used for processing the signals received from outside.
2. **Hidden layer:** The hidden layer consists of multiple neurons connected to signals from outside the body. These neurons are activated by activation functions.
3. **Output layer:** The output layer is an activation function that represents the overall response of the processed signals that were fed into the hidden layer.

As with the human body, multiple hidden layers can exist, consisting of multiple neurons [21]. A basic three-layer neural network is displayed in figure **??**. The input signals to the neural network are x_1 to x_3. The output / answer of the neural network is $\hat{y}_1$. Let's take an example of a neural network predicting whether you will require to wear a jacket for a given day. The input signals are:

x_1 : The current temperature.

x_2 : The current humidity.

x_3 : Are there any clouds, yes or no.

The output, $\hat{y}_1$, of this neural network will be a yes or no answer.

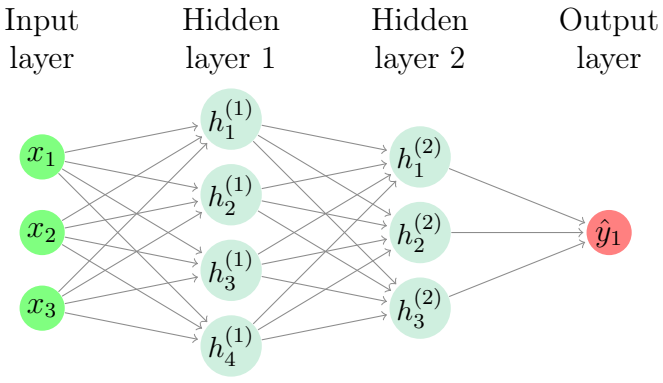

Figure 2.1: Three layer neural network

Each neuron in the neural network has a similar structure, as seen in figure 2.2. Each input signal carries a certain weight into the hidden layer's neuron. The summation of all the weighted inputs are then fed through an activation function [22]. The output of the activation function is also the output signal of the neuron [23]. The output of the neuron can then be fed into a neuron in a subsequent layer as an input signal to that neuron. A neural network is trained by using a data set with known input and output values / signals. By training / adjusting the weights w_1 to w_3 for each neuron of the network, the more accurate the network becomes at predicting the desired output from only the input signals of the network.

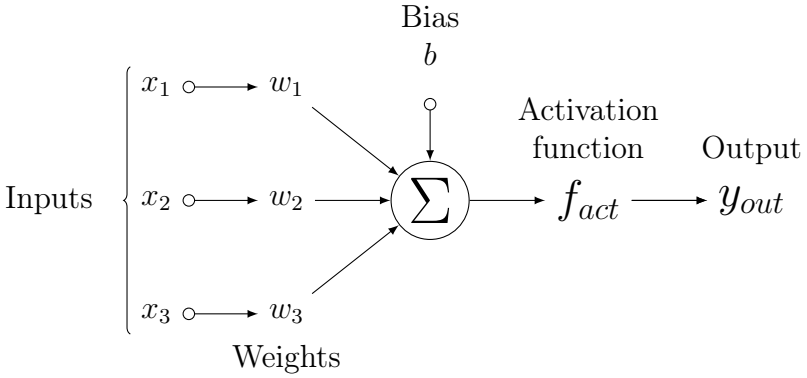

Figure 2.2: Single neuron in neural network

Overfitting and biasing

One caveat of a neural network is that it can be prone to overfitting. Overfitting is when a neural network becomes so good at learning how to predict the output values from the given inputs of a data set, that it is unable to provide similar degrees of accuracy for unseen data [24]. To combat this behaviour, a bias input signal is also fed into the neurons to prevent overfitting from occurring. A bias value is a constant value and is not affected by the input signals of a neural network.

Dataset size

Variance measures the degree to which the predictions of the classifiers developed by a learning algorithm differ from training sample to training sample [25]. It is known that the more data a learning algorithm has, the better learning can be achieved [25]. However, this is only true up to where the difference between the variance of a dataset, which is larger than another, is negligible.

Neural network size

As the complexity of the dataset grows, so does the complexity of the classifiers. The more complex the datasets are, the more hidden layers and neurons in those layers can be introduced to keep up with the complexity of the neural network. However, as discussed earlier, when there are too many hidden layers, a network can become so good at learning the data set it had trained with, that it is unable to accurately predict unseen data, also known as overfitting. The result is that the neural network learned the dataset instead of the pattern in the dataset.

Activation functions

An activation function, also known as a threshold function or transfer function, is a function that performs a transformation of the sum of all the weighted input signals [22]. Some of the most common activation functions are used to solve non-linear problems [22]. Examples of such function are:

$$Sigmoid : h_\theta(x) = \frac{1}{1 + e^{-\theta^T x}} \tag{2.1}$$

$$ReLU : h_\theta(x) = \begin{cases} 0 & x < 0 \\ x & x \geq 0 \end{cases} \tag{2.2}$$

$$Tahn : h_\theta(x) = tahn(x) = \frac{(e^x - e^{-x})}{(e^x + e^{-x})} \tag{2.3}$$

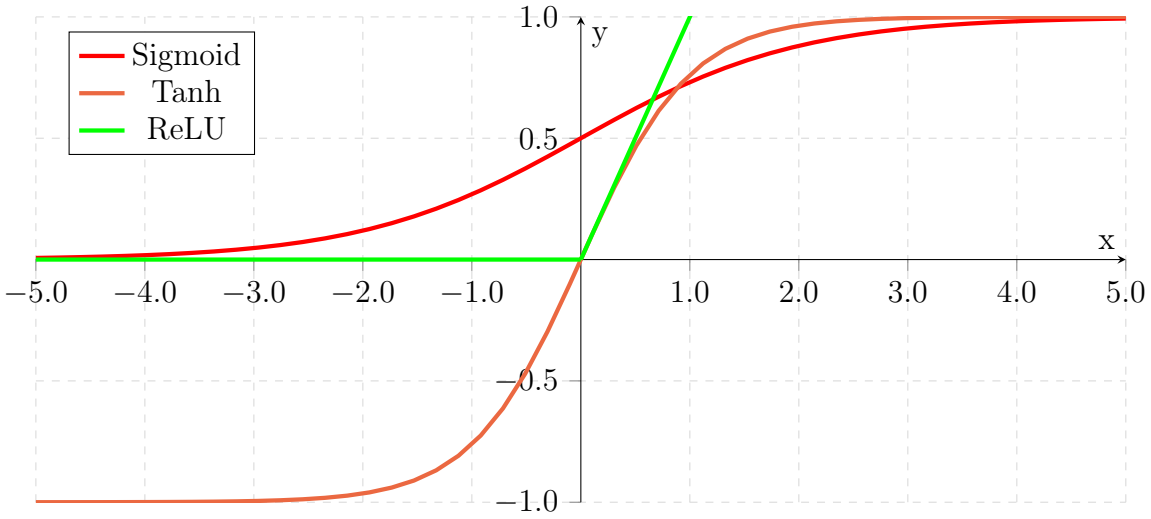

Figure 2.3: Activation functions

Types of learning

Two main types of machine learning exist. These are supervised and unsupervised machine learning:

- In supervised machine learning a data set is presented with values / answers to that data set [20]. A hypothesis is then constructed to closely match the values / answers to the data set. If a hypothesis is found, it can then be used to make an accurate guess of the values of the data set or unseen related data [20].
- In unsupervised machine learning, a data set is provided without the values / answers to that data set. Functions are then trained to classify the data into meaningful categories [20].

Supervised machine learning was used in this project. The dataset is made up of images of different insulators for which the hydrophobicity states are known. The known hydrophobicity states are the answers to the data set for which a hypothesis is required.

2.2.1 Training neural network

A neural network consists out of many other parts which makes it function. Such as back propagation, weights initialization, cost functions and the list go on. A good understanding was obtained in order to build the neural network in the sections that follows.

2.3 Machine learning Image processing technique

A convolutional neural network development approach was done and will be discussed in the following section. Convolutional neural networks are ideal for image processing as it can easily learn abstract features and effectively identify objects [26].

Convolutional neural networks use a sliding window. This window consists out of a filter with many weights. These weights are trained in order to recognize patterns in images.

2.4 Existing machine learning techniques for hydrophobicity analysis

A study was done in order to obtain an estimation of the hydrophobicity of a composite insulator based on an improved probabilistic neural network [27]. A Radial Basis Function feedforward network was used to do hydrophobicity analysis. At first, an image of a wet surface was pre-treated to de-noise the image [27]. Image segmentation followed with the use of a Sobel operator to isolate the water droplets from the background (i.e. the insulator's surface). Three features were obtained that include the shape factor and the area of the largest water droplet [27]. These features were then used as inputs to the neural network. The accuracy of this network provided good results [27]. The downside is that pre-treatment can require some additional fine tuning in order for the Sobel operator to effectively eliminate the water droplets from the background.

Another study was done by training a support vector machine. The flow of image to data was as follows [28]:

1. Preprocessing of Insulator Images
    - Convert images to grayscale.
    - Denoise images.
    - Histogram equalization: Water droplets in areas with too bright or dark foreground could be more easily recognized with histogram equalization.
2. Feature extraction and segmentation of water droplets:
    - The eccentricity e of the aspect ratio of water droplets

$$e = \frac{b}{a} - 1 \tag{2.4}$$

      With a and b respectively representing width and length of the rectangle over which feature extraction is being done.
    - fc: The shape factor of the largest water droplets

$$f_c = \frac{4\pi s}{l^2} \tag{2.5}$$

      With s,l representing the area and circumference of the largest water droplets. With $f_c = 1$ representing good water repellency and $f_c < 1$ representing poor water repellency.
    - The minimum distance d between two water drops

$$d = \sqrt{(x_1 + x_2)^2 + (y_1 + y_2)^2} \tag{2.6}$$

      d is the distance between one central point of a water droplet and another.
    - The area ratio of the maximum water drops in the entire image K

$$K = \frac{S_{max}}{S} \tag{2.7}$$

      S_{max} represents the area of the water droplets and S the total area over which feature extraction is being done.

The features obtained were fed into a support vector machine model, back propagation model and into a generalized regression neural network. It was found that the support vector machine provided the most promising results.

The general approach of hydrophobicity analysis was to use various techniques to isolate water droplets from the insulator. Certain features were extracted from the water droplet formations and used to train a neural network to recognize patterns within those features. Hydrophobicity classifications could then be made using the trained network.

Unlike the methods described above, a different approach to hydrophobicity analysis was used to train a neural network. Instead of obtaining features/patterns by isolating a water droplet from the background, the water droplet itself with the background will be fed into a neural network to obtain patterns within images. No other research could be found that used a similar approach with hydrophobicity analysis on high voltage insulators.

2.5 Neural network development approach

2.5.1 Overview

When developing a neural network to do image analysis, it is important to identify possible obstacles that a neural network can encounter and then design it accordingly. Successful development of neural networks can be achieved by developing several neural network models and applying iterative improvements to those models. There can be more than one network topology that might work for a given neural network requirement. Having several models and observing the outcome of those models is beneficial in making better decisions in designing the neural network for a specific classification requirement [29].

2.5.2 Design goals

One of the requirements for analysing the hydrophobicity of an insulator of an image is that the neural network algorithm should not be affected by variations in external lighting present within the image. The neural network should detect changes in hydrophobicity over the insulator's surface, as certain areas on the insulator can have different hydrophobicity states. The neural network performance should not be affected by the shape of the insulator's surface. It should be applicable to a variety of insulator shapes. The neural network should differentiate between nine different classes of hydrophobicity states instead of just six states, as described in the STRI guide.

2.5.3 Design approach

Analyzing individual water droplets on an insulator's surface, a classification can be made on the insulator's hydrophobicity at a given area. As seen in figure **??** one can observe the change in hydrophobicity by looking at the form of the water droplet. It was from this observation that it was decided that an image of an insulator would be divided up into a grid of smaller images. The subset of small images would then be fed into a neural network to do analysis with. This approach has the advantage to provide grid sized hydrophobicity states of the insulator, rather than an overall hydrophobicity classification. Further analysis could also be done on the grid hydrophobicity states to determine the path of least resistance that leakage currents would follow over the insulator's surface.

Design specifications

- Grid image size: Different image sizes inside the grid were used to test the effect that it had on the neural network performance.
- Neural network input image resolution: The resolution of all the images fed into the neural network were resized to a 50 x 50 pixel image size. Using a 50 x 50 image resolution is ideal because it will speed up the training time while still maintaining enough detail to differentiate between hydrophobicity states.

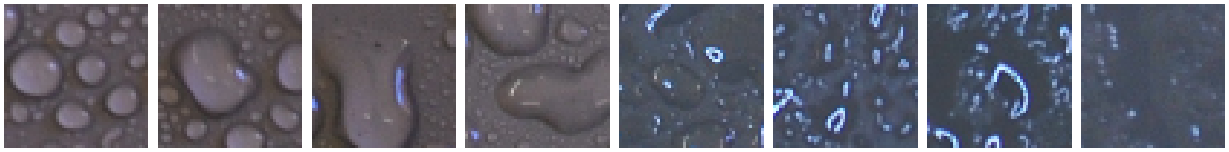

(a) (b) (c) (d) (e) (f) (g) (h)

Figure 2.4: Water droplets on insulator ranging from hyrophobic (a) to hyrophilic (h).

2.5.4 Convolution neural networks (CNN)

As discussed in section 2.3, convolutional neural networks are great for doing machine learning on images. CNN will be implemented only on the sub-images of the grid as described in 2.5.3. A series CNN models were tested, as of which only the more successful models will be described.

Some terms that will be used in discussion of the neural network designs are as follows:

Same padding: After an image is convoluted, the output is smaller than the original image. Zeros are then added around the output, also known as zero padding, to achieve the same dimensions as the input image. This can be seen in figure 2.5

0	0	0	0	0	0	0	0	0	0
0	0	0	0	0	0	0	0	0	0
0	0	118	51	253	101	180	185	0	0
0	0	210	176	142	3	206	107	0	0
0	0	28	14	248	136	253	120	0	0
0	0	140	102	129	103	58	164	0	0
0	0	175	225	207	46	9	138	0	0
0	0	224	113	137	45	93	60	0	0
0	0	0	0	0	0	0	0	0	0
0	0	0	0	0	0	0	0	0	0

Figure 2.5: Zero padding 8×8 matrix to a dimension of 10×10.

Conv: It is a convolutional layer.

Max Pool: Max pooling takes the maximum number for every n-strides to create a new matrix with less elements, as seen in figure 2.6. This new matrix is the output of the max

pooling operation and is generally then fed into another convolutional layer, or flattened and fed into a fully connected layer.

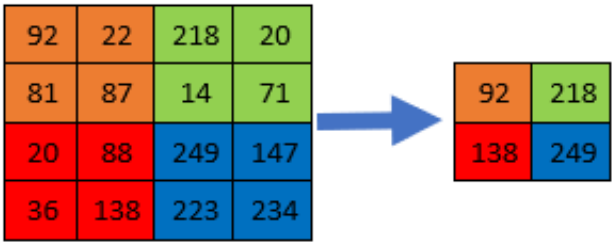

Figure 2.6: Max pooling with stride of 2.

Output dimension calculation

The output width and height of each layer is calculated as follows:

1. W: Input width
2. H: Input height
3. F_w: Filter width
4. F_h: Filter height
5. P: Padding
6. S_w: Width stride
7. S_h: Height stride

$$\begin{aligned} output\ width &= \frac{W - F_w + 2P}{S_w} + 1 \\ output\ height &= \frac{H - F_h + 2P}{S_h} + 1 \end{aligned} \tag{2.8}$$

2.5.5 Convolutional neural network topology: Network 1

This convolutional neural network was one of the first amateur network designs. It was included to display the errors made during the design process. Although this network was flawed, it did manage to perform some classifications that will be discussed in section 2.8. The following is a description of the CNN design with a visualization of the network in figure 2.7.

1. Input: Color images of size $44 \times 44 \times 3$.
2. Conv-1: The first convolutional layer is made up of a kernel with 4 channels, each having a dimension of 40×40. The convolutional layer is applied with a stride of 1 and same padding.
3. MaxPool-1: A maxpool layer is applied on the output of Conv-1. The maxpool layer has a pooling size of 2×2, a stride of 2 and same padding.

4. Conv-2: The second convolutional layer is made up of a kernel with 4 channels, with each having a dimension of 30×30. The convolutional layer is applied with a stride of 1 and same padding.

5. MaxPool-2: A maxpool layer is applied on the output of Conv-2. The maxpool layer has a pooling size of 2×2, a stride of 2 and same padding.

6. Conv-3: The first convolutional layer is made up of a kernel with 4 channels, with each having a dimension of 20×20. The convolutional layer is applied with a stride of 1 and same padding.

7. MaxPool-3: A maxpool layer is applied on the output of Conv-3. The maxpool layer has a pooling size of 2×2, a stride of 2 and same padding.

8. Conv-4: The second convolutional layer is made up of a kernel with 4 channels, with each having a dimension of 10×10. The convolutional layer is applied with a stride of 1 and same padding.

9. MaxPool-4: A maxpool layer is applied on the output of Conv-4. The maxpool layer has a pooling size of 2×2, a stride of 2 and same padding.

10. Conv-5: The second convolutional layer is made up of a kernel with 4 channels, with each having a dimension of 5×5. The convolutional layer is applied with a stride of 1 and same padding.

11. MaxPool-5: A maxpool layer is applied on the output of Conv-5. The maxpool layer has a pooling size of 2×2, a stride of 2 and same padding.

12. Flatten-1: The output of MaxPool-5 is flattened to a single column with 16 elements.

13. FC-1: The final step is a fully connected layer that has 16 input elements with a softmax activation to classify between 9 outputs.

The design was flawed because filters used in the convolution process were too large. Excessive zero padding was applied to keep the dimensions right for the next layer. With excessive zero padding, the network does not have enough parameters on which it can train on to recognize valuable information about the patterns in the original image.

Analysing point (1) in figure 2.7, an image of size 44×44 is convoluted by filters of size 40×40. The output dimension with no zero padding is calculated with equation 2.8. The result is an output dimension of 5×5 which can be considered as valuable data regarding the input. Zero padding does not contribute any valuable info about the input, other than adding zeros so that the dimensions of the output is correct for the next layer's input.

After zero padding the output, the dimensions of the output are ready for the next layer of max-pooling at point (2). This flawed implementation is present at every layer of the network.

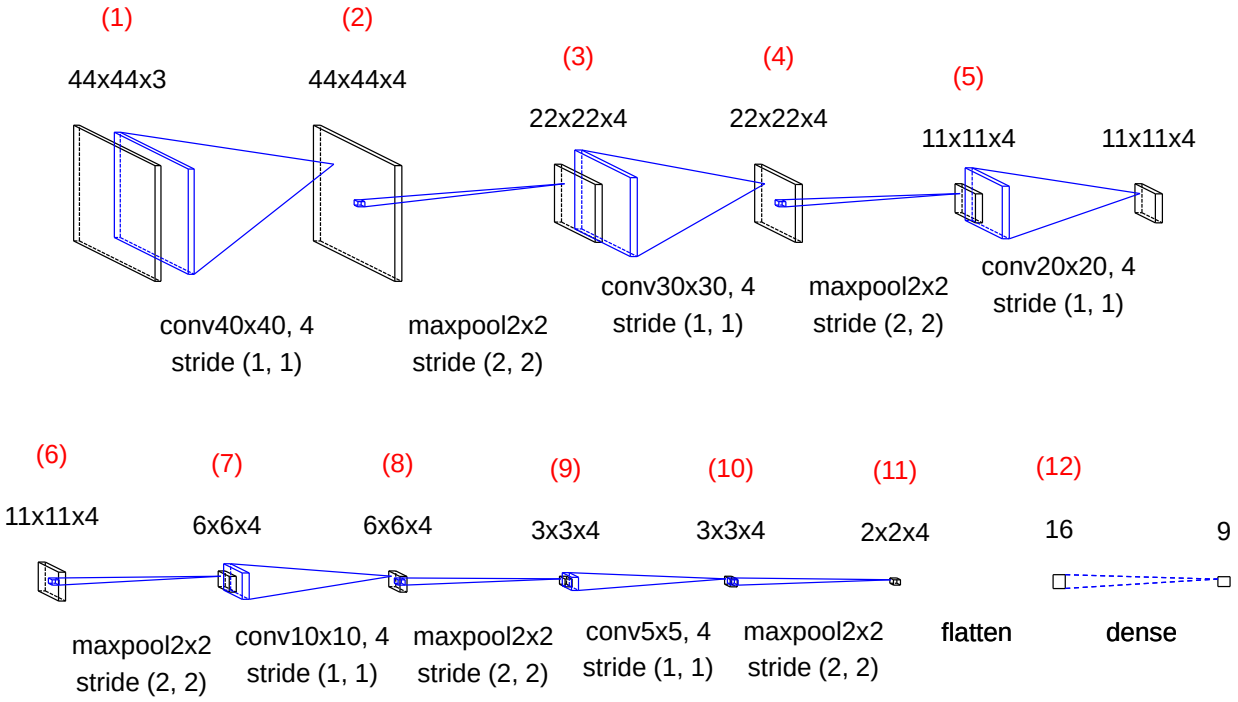

Figure 2.7: Convolutional neural network architecture of network 1.

2.5.6 Convolutional neural network topology: Network 2

This convolutional neural network followed a simpler design than network 1. It only had two convolutional layers with max pooling and two fully connected layers. The goal was to determine if a simple network design would also perform adequately. This network design does not contain flaws as described in network 1. The network design is described below and visualized in figure 2.8.

1. Input: Color images of size $44 \times 44 \times 3$.
2. Conv-1: The first convolutional layer is made up of a kernel with 15 channels, with each having a dimension of 10×10. The convolutional layer is applied with a stride of 1 and no padding.
3. MaxPool-1: A maxpool layer is applied on the output of Conv-1. The maxpool layer has a pooling size of 2×2, a stride of 2 and no padding.
4. Conv-2: The second convolutional layer is made up of a kernel with 20 channels, with each having a dimension of 6×6. The convolutional layer is applied with a stride of 1 and no padding.
5. MaxPool-2: A maxpool layer is applied on the output of Conv-2. The maxpool layer has a pooling size of 2×2, a stride of 2 and no padding.
6. Flatten-1: The output of MaxPool-2 is flatten to a single column with 720 elements.
7. FC-1: The first fully connected layer has 720 input elements with a tanh activation with 180 outputs.
8. FC-2: The final fully connected layer that has 180 input elements with a softmax activation to classify between 9 outputs.

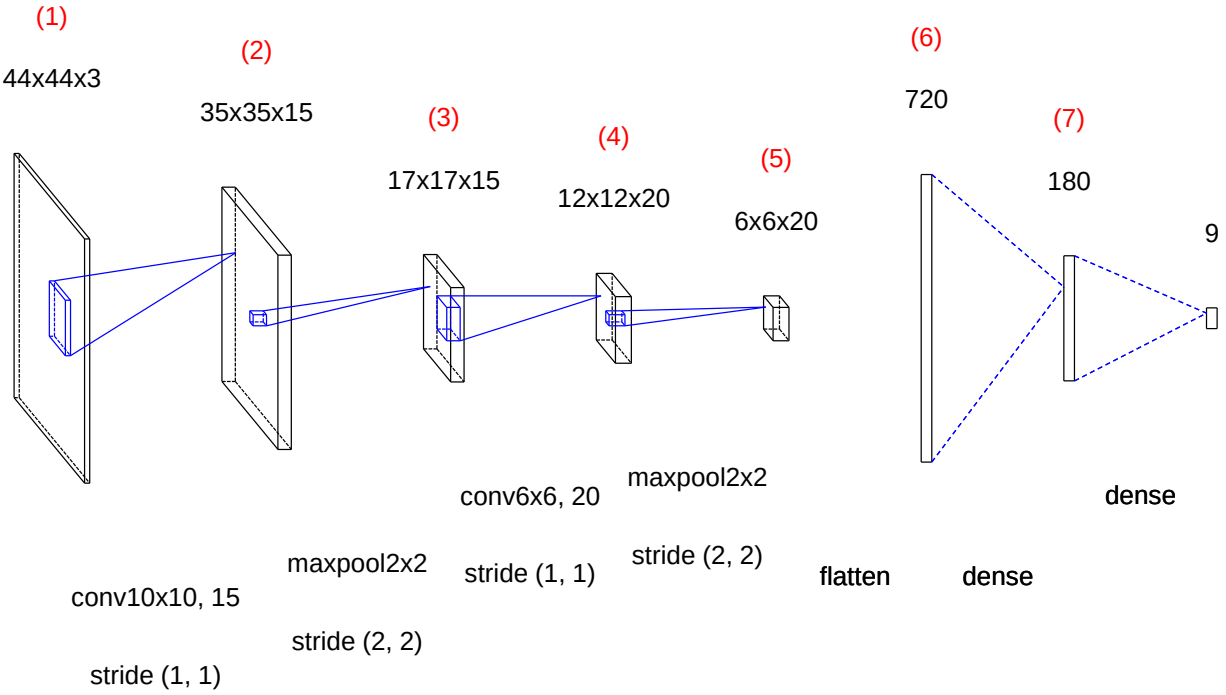

Figure 2.8: Convolutional neural network architecture of network 2.

2.5.7 Convolutional neural network topology: Network 3

The goal of this neural network was to evaluate the effect of kernels with many channels. Additional fully connected layers were also added. Below is a description of the CNN visualized in figure 2.9. It is expected that this network will deliver desirable results, given that it has many weights to train to recognize more complex patterns. Also note that there was no zero padding applied to any of the layers.

1. Input: Color images of size $44 \times 44 \times 3$.
2. Conv-1: The first convolutional layer is made up of a kernel with 18 channels, with each having a dimension of 7×7. The convolutional layer is applied with a stride of 1 and no padding.
3. MaxPool-1: A maxpool layer is applied on the output of Conv-1. The maxpool layer has a pooling size of 2×2, a stride of 2 and no padding.
4. Conv-2: The second convolutional layer is made up of a kernel with 40 channels, with each having a dimension of 6×6. The convolutional layer is applied with a stride of 1 and no padding.
5. MaxPool-2: A maxpool layer is applied on the output of Conv-2. The maxpool layer has a pooling size of 2×2, a stride of 2 and no padding.
6. Conv-3: The second convolutional layer is made up of a kernel with 50 channels, with each having a dimension of 2×2. The convolutional layer is applied with a stride of 1 and no padding.
7. MaxPool-3: A maxpool layer is applied on the output of Conv-3. The maxpool layer has a pooling size of 2×2, a stride of 2 and no padding.
8. Flatten-1: The output of MaxPool-3 is flattened to a single column with 450 elements.

9. FC-1: The first fully connected layer has 450 input elements with a tanh activation with 225 outputs.

10. FC-2: A fully connected layer has 225 input elements with a tanh activation with 112 outputs.

11. FC-3: The final fully connected layer that has 112 input elements with a softmax activation to classify between 9 outputs.

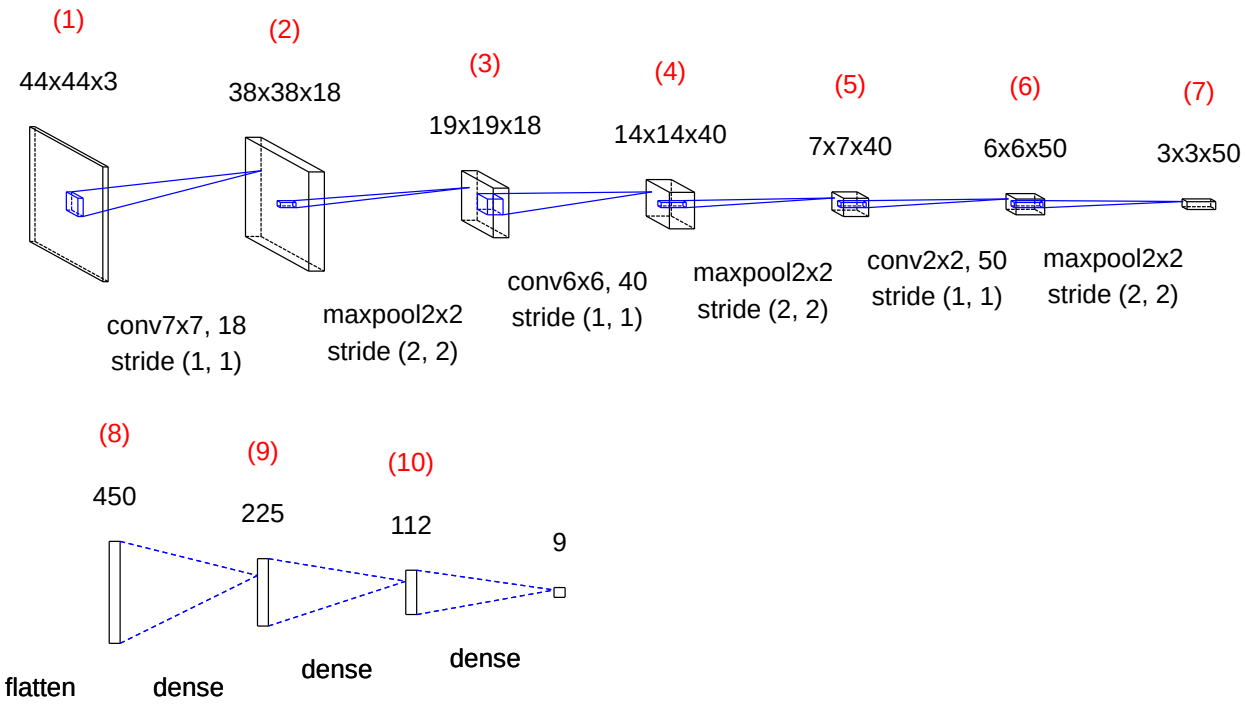

Figure 2.9: Convolutional neural network architecture of network 3.

2.5.8 Convolutional neural network topology: Network 4

This convolutional neural network followed a more complicated model. It was inspired by AlexNet convolutional neural network with some modifications applied. A description of the network follows with the architecture layout in figure 2.10. Note that certain layers had zero padding while others had no padding. It is expected that this network will perform well given all the parameters that it can be trained on. Overfitting might be present.

1. Input: Color images of size $44 \times 44 \times 3$.

2. Conv-1: The first convolutional layer is made up of a kernel with 24 channels, with each having a dimension of 21×21. The convolutional layer is applied with a stride of 1 and no padding.

3. MaxPool-1: A maxpool layer is applied on the output of Conv-1. The maxpool layer has a pooling size of 2×2, a stride of 2 and no padding.

4. Conv-2: The second convolutional layer is made up of a kernel with 66 channels, with each having a dimension of 4×4. The convolutional layer is applied with a stride of 1 and no padding.

5. Conv-3: The third convolutional layer is made up of a kernel with 66 channels, with each having a dimension of 3×3. The convolutional layer is applied with a stride of 1 and same padding.

6. Conv-4: The fourth convolutional layer is made up of a kernel with 44 channels, with each having a dimension of 3×3. The convolutional layer is applied with a stride of 1 and same padding.

7. MaxPool-2: A maxpool layer is applied on the output of Conv-4. The maxpool layer has a pooling size of 2×2, a stride of 2 and no padding.

8. Flatten-1: The output of MaxPool-3 is flattened to a single column with 176 elements.

9. FC-1: The first fully connected layer has 176 input elements with a tanh activation with 225 outputs.

10. FC-2: A fully connected layer has 225 input elements with a tanh activation with 112 outputs.

11. FC-3: The final fully connected layer that has 11 input elements with a softmax activation to classify between 9 outputs.

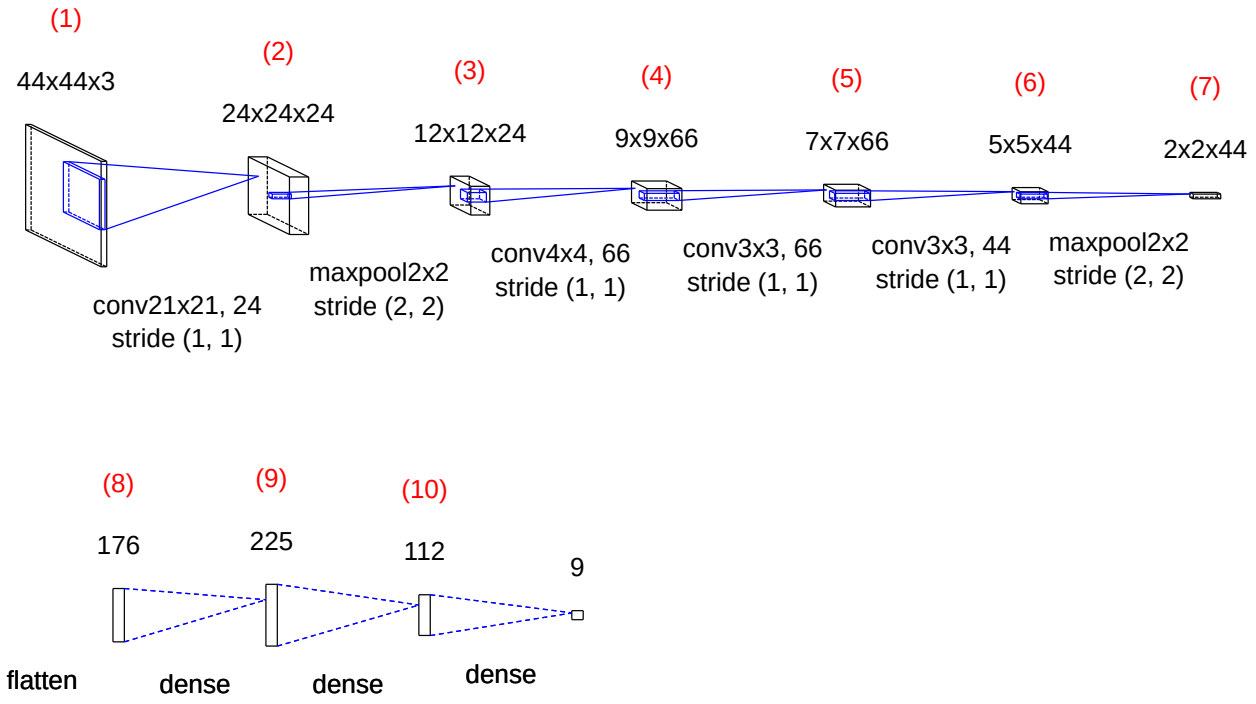

Figure 2.10: Convolutional neural network architecture of network 4.

2.5.9 Convolutional neural network topology: Network 5

This network was designed by trial and error. The output dimension of each layer was decreased gradually up to point (7) in figure 2.11. The fully connected layers were also decreased gradually to 9 possible output classes. This network is expected to perform well, as this was a systematic improvement over the other networks that were tested. Note that zero padding was not applied to any layers of the network. A description of the network follows with the architecture layout in figure 2.11.

1. Input: Color images of size $44 \times 44 \times 3$.
2. Conv-1: The first convolutional layer is made up of a kernel with 18 channels, with each having a dimension of 8×8. The convolutional layer is applied with a stride of 1 and no padding.
3. MaxPool-1: A maxpool layer is applied on the output of Conv-1. The maxpool layer has a pooling size of 2×2, a stride of 2 and no padding.
4. Conv-2: The second convolutional layer is made up of a kernel with 40 channels, each having a dimension of 6×6. The convolutional layer is applied with a stride of 1 and no padding.
5. MaxPool-2: A maxpool layer is applied on the output of Conv-2. The maxpool layer has a pooling size of 2×2, a stride of 2 and no padding.
6. Conv-3: The second convolutional layer is made up of a kernel with 50 channels, each having a dimension of 3×3. The convolutional layer is applied with a stride of 1 and no padding.
7. MaxPool-3: A maxpool layer is applied on the output of Conv-3. The maxpool layer has a pooling size of 2×2, a stride of 2 and no padding.
8. Flatten-1: The output of MaxPool-3 is flattened to a single column with 200 elements.
9. FC-1: The first fully connected layer has 200 input elements with a tanh activation with 120 outputs.
10. FC-2: A fully connected layer has 120 input elements with a tanh activation with 84 outputs.
11. FC-3: The final fully connected layer that has 84 input elements with a softmax activation to classify between 9 outputs.

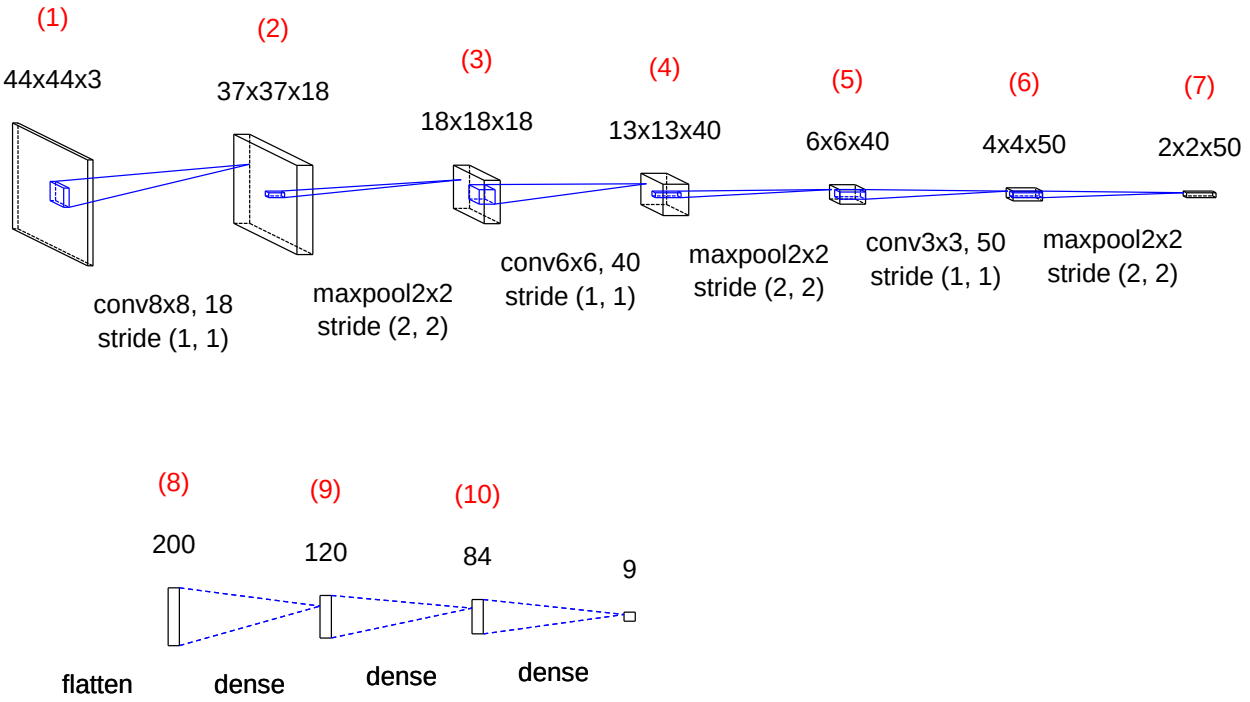

Figure 2.11: Convolutional neural network architecture of network 5.

2.5.10 Convolutional neural network topology: Network 6

Small modifications were made to network 5 to create a new network 6 in an attempt to improve even more on network 5. This network contains the same number of layers as network 5, with a slight change in the dimensions of the layers. Similar results are expected for this network compared to network 5. A description of the network follows with the architecture layout in figure 2.12.

1. Input: Color images of size $44 \times 44 \times 3$.
2. Conv-1: The first convolutional layer is made up of a kernel with 18 channels, with each having a dimension of 7×7. The convolutional layer is applied with a stride of 1 and no padding.
3. MaxPool-1: A maxpool layer is applied on the output of Conv-1. The maxpool layer has a pooling size of 2×2, a stride of 2 and no padding.
4. Conv-2: The second convolutional layer is made up of a kernel with 40 channels, each having a dimension of 6×6. The convolutional layer is applied with a stride of 1 and no padding.
5. MaxPool-2: A maxpool layer is applied on the output of Conv-2. The maxpool layer has a pooling size of 2×2, a stride of 2 and no padding.
6. Conv-3: The second convolutional layer is made up of a kernel with 50 channels, with each having a dimension of 2×2. The convolutional layer is applied with a stride of 1 and no padding.
7. MaxPool-3: A maxpool layer is applied on the output of Conv-3. The maxpool layer has a pooling size of 2×2, a stride of 2 and no padding.
8. Flatten-1: The output of MaxPool-3 is flattened to a single column with 450 elements.
9. FC-1: The first fully connected layer has 450 input elements with a tanh activation with 120 outputs.
10. FC-2: A fully connected layer has 120 input elements with a tanh activation with 84 outputs.
11. FC-3: The final fully connected layer that has 84 input elements with a softmax activation to classify between 9 outputs.

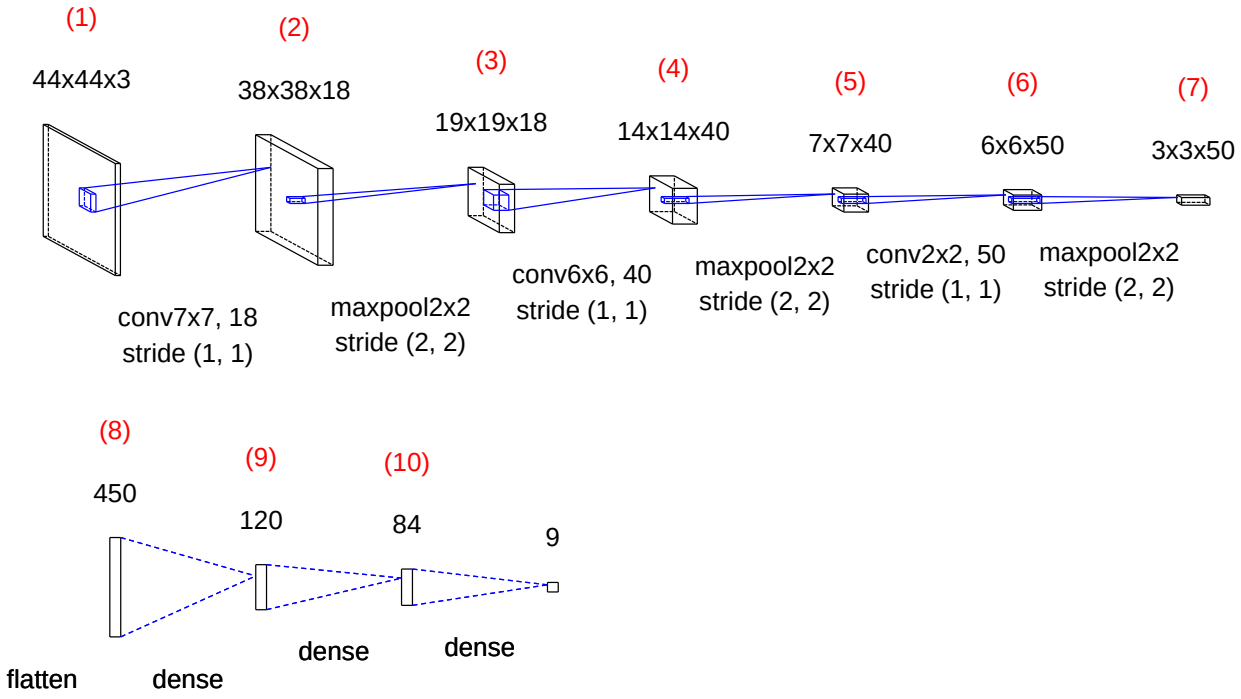

Figure 2.12: Convolutional neural network architecture of network 6.

2.6 Training dataset

2.6.1 Image harvesting process

The process of acquiring images was done under lab conditions. Deionised water was used to clean all the insulators and left to dry before tests were conducted. The focus of the image harvesting process was not to get insulators to behave such that it falls within a certain class, as described in the STRI guide. Rather, the focus was placed on getting a large number of images of water droplets or puddles with different contact angles on the insulator's surface. The water surface tension was altered by mixing different mixtures of water and isopropyl.

The experimental setup

The image harvesting setup was as follows:

- *Insulators used in setup:* Eight square polymer insulators sheets (200 mm x 150 mm) were used in this test. All the insulators had good hydrophobicity characteristics.
- *Illumination:* As described in chapter 1, the ideal hydrophobicity technique should be unaffected by external lighting conditions. Images of the insulators where taken under outdoor and indoor conditions, with various light exposures. The goal was to generate a dataset that encompasses many variations in lighting conditions that the classifier might encounter when it is applied on samples that were taken in the field.
- *Insulator placement:* Two insulators were used at a time. The insulators were placed next to each other, one at 30° and the other at 45°.
- *Camera setup:* A Nikon D60 digital camera was used with a Nikon 18200 mm 1:3.5-56 Lens. A Thule tripod was used to mount the camera on. The camera was set up 80 cm from ground level at an inclination of 45° to the horizontal plane.

- *Image capture sequence:* An image was taken every 5 seconds for about 180 seconds. By doing so, a large dataset was acquired. As the water droplets grew over time with the misting system, images taken at subsequent time increments could be seen as new data to the data set.

- *Misting system:* A water misting system was developed by using fine water misting nozzles. The goal behind this system was to set up an environment that, when a mist is applied on the insulator's surface, it will gradually form water droplet formations evenly across the entire surface of the insulator. Having a single nozzle, such as on a spray bottle, can result in uneven distribution of water droplet accumulations on the insulator's surface. Two water misting nozzles, 20 cm apart, were placed 50 cm above the insulator's surface, perpendicular to the ground. A reservoir filled with water and isopropyl alcohol was then injected into the water nozzle supply line by means of compressed air. The nozzle diameter size was 0.406 mm with a spray angle of 90°. The reservoir was pressurized at around 1000 psi. The median water droplet size was specified to be around 11 µm.

  The result was evenly distributed water droplets across the insulator's surface. At first, small water droplets would form on the insulator's surface, developing into larger and larger water droplets. Depending on the surface tension, the water droplets continued to grow until the force of gravity overcame the adhesion of the water droplets to the surface and sliding occurred. When a water droplet slid off the insulator's surface, it would eliminate all other water droplet formations in its path. This aided in creating a new set of water droplet formations on the sliding path, generating an even larger variety of data for the dataset. The misting system can be seen in figure 2.13

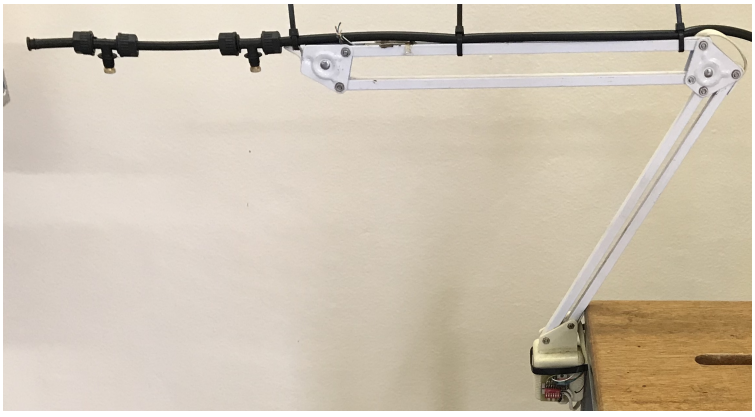

Figure 2.13: Misting system.

2.6.2 Image classification classes

In section 2.5.3 it was set out that an image would be divided into a grid of sub images for classification. These sub images were then analyzed for different classes of hydrophobicity. It was important to first get an understanding on how the image classification classes were defined. The sub-image harvesting, and labeling was then done based on the classified classes.

What follows is a description of the different classes that were constructed to separate water droplet formations from one another. The sub-image sizes are 120 x 120 pixels of the original image captured with the camera, down scaled to a lower resolution of 50 x 50 pixels. Starting

at class 1, with water droplets hinting to a hydrophobic surface, to class 9, resembling water droplet formations typically found on hydrophilic surfaces.

- **Class 0**
  This sub image would typically be a patch on the insulator's surface where water droplets just slide off with no trace left behind, as seen in figure 2.14c. These sub image patches could also be found where the misting system had a water penetration dead zone on the insulator's surface. Images in this class resembled two features:

  1. Very small water droplets.
  2. Empty patches with no trace of any water droplets.

(a) (b) (c) (d) (e) (f) (g) (h) (i)

Figure 2.14: Class 0 sub-images.

- **Class 1**
  This class encompasses water droplets that behave as if they have a large contact angle to the insulator's surface, as described in chapter 1. These water droplet formations would typically be found on highly hydrophobic patches on the insulator's surface. The water droplets in this class have the following features:

  1. They are almost perfectly round.
  2. The inner part of the water droplet looks bright and clear, almost as if light is traveling through it without distortion. This is due to the large contact angle.
  3. They are medium sized.

(a) (b) (c) (d) (e) (f) (g) (h) (i)

Figure 2.15: Class 1 sub-images.

- **Class 2**
  Water droplets in this class are on the verge off sliding of the insulator, while still maintaining their hydrophobic posture. These water droplets are typically found on hydrophobic patches on the insulator's surface. These patches on the insulator surface were exposed to water misting for a longer duration than the patches in class 1, thus the bigger sizes of the hydrophobic water droplets. This class has the following features:

  1. The water droplets are large but still inhibit a firm look, as in class 1.
  2. The water droplets have a round form.
  3. The inner part of the water droplets has a clear reflective look.

(a) (b) (c) (d) (e) (f) (g) (h) (i)

Figure 2.16: Class 2 sub-images.

- **Class 3**
  This is the first class where a loss in hydrophobicity is displayed. The water droplets are on the verge of sliding. It can be seen that the water droplets have a little tail end. This is because, since the insulator is on an angle, gravitational force is pulling down on the water droplet and the majority of the mass is located in the lower part of the water droplet. This creates a flat tail end on the water droplet, where adhesion to the surface is still present. This class has the following characteristics:

  1. Water droplets do not display uniform roundness.
  2. A little tail is present on the water droplet.
  3. The water droplets have a general downward pointing direction.

(a) (b) (c) (d) (e) (f) (g) (h) (i)

Figure 2.17: Class 3 sub-images.

- **Class 4**
  A significant loss in hydrophobicity can be observed in this class. While still maintaining the appearance of a water droplet, deformation on the water droplet's structure is converging to a puddle-like structure. This can be classified by observing the following characteristics:

  1. Significant deformation on water droplet structure.
  2. Water droplet size is large, while empty patches can also be present around the water droplet
  3. The water droplet has low surface tension. It appears to be flatter than Class 3.
  4. No general pointing direction of water droplet. The adhesion of the water droplet to the surface is stronger than the force gravity has on it.

(a) (b) (c) (d) (e) (f) (g) (h) (i)

Figure 2.18: Class 4 sub-images.

- **Class 5**
  This class resembles patches on the insulator's surface that are becoming highly hydrophilic. The water droplet formations are very flat as a result of very low surface tension on the insulator's surface. Large puddle formations start to form, since the general hydrophobic shape of the water droplet is completely degraded. The sub-images in this class can be categorized by the following characteristics:

  1. Flat water droplet puddles present over a large part of the sub-image.
  2. Hints of a general water droplet structure can still be observed.

(a) (b) (c) (d) (e) (f) (g) (h) (i)

Figure 2.19: Class 5 sub-images.

- **Class 6**
  Total loss of hydrophobicity is present in this class. No trace of a round water droplet structure can be found. Features in this class can be described as follows:

  1. The surface is partly covered by water puddles.
  2. Water puddles seem very flat with no surface tension.

(a) (b) (c) (d) (e) (f) (g) (h) (i)

Figure 2.20: Class 6 sub-images.

- **Class 7**
  This class exhibits many of the same characteristics as class 6. The only difference is that the water puddles cover a larger area of the insulator's surface. Characterizing this dataset is done as follows:

  1. A large area of the sub-image is covered by water puddles.
  2. The water puddles seems flat to the surface, almost becoming a film of water.

(a) (b) (c) (d) (e) (f) (g) (h) (i)

Figure 2.21: Class 7 sub-images.

- **Class 8**
  Total hydrophilic behaviour is observed in this class. This will occur on large patches over an insulator's surface where the insulator's ability to repel water is totally degraded. The classification method for this class is as follows:

  1. A film of water is present over the entire sub-image.
  2. The water puddle is completely flat to the insulator 's surface.

(a) (b) (c) (d) (e) (f) (g) (h) (i)

Figure 2.22: Class 8 sub-images.

Figure 2.23: Sub-image classification guide.

2.6.3 Image labeling process

Having all the different classes defined, a labeling software had to be developed to label each individual sub-image according to its class classification index. The source code of an existing open sourced labeling software called Labelme was used as a basis in this project. Modifications were made in order to speed up the labeling process.

2.6.3.1 Sub-images

The goal of the labeling software was to divide an image up into a grid of sub-images and add labels to those sub-images. The specifications of the sub-images were as follows:

1. Several sub-image sizes had to be created. This was done to find the perfect sub-image size that would result in the highest accuracy for a given machine learning model. The smaller the sub-image size, the less information it exhibits on the water droplet formations for a given patch on the insulator. The larger the sub-image size, the more classification classes may be present. These effects can be seen in figure 2.24. The sub-image sizes were set out as follows:

   - 70 x 70 pixels (6.7 x 6.7 mm)
   - 100 x 100 pixels (9.5 x 9.5 mm)
   - 120 x 120 pixels (11.5 x 11.5 mm)
   - 200 x 200 pixels (19.1 x 19.1 mm)
   - 300 x 300 pixels (28.7 x 28.7 mm)

   Early tests indicated that a sub-image size of 120 x 120 pixels (11.5 x 11.5 mm) provided the best results for training a neural network with high accuracy. The sub-images of 120 x 120 pixels were down scaled to 50 x 50 pixels to improve the neural network training speed, since there is less pixels to analyze. All further analysis was done with sub-image size of 120 x 120 pixels (11.5 x 11.5 mm).

2. The sub-image should be easily classifiable into the predefined classes.

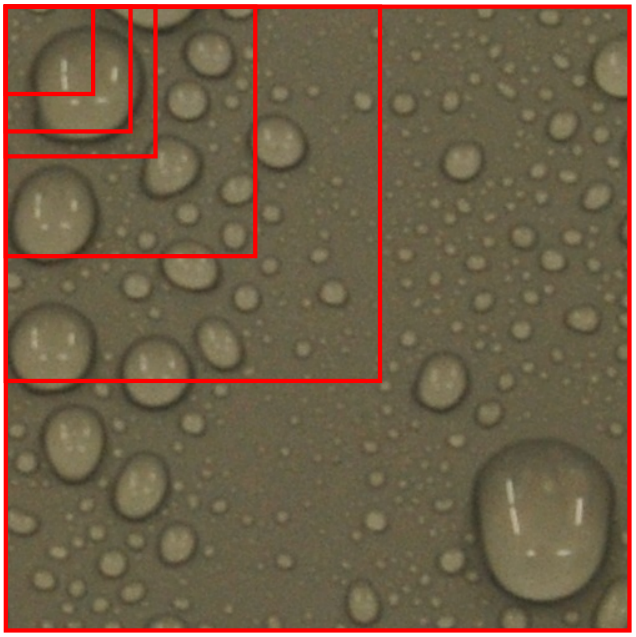

(a) Original sub-image 500 x 500.

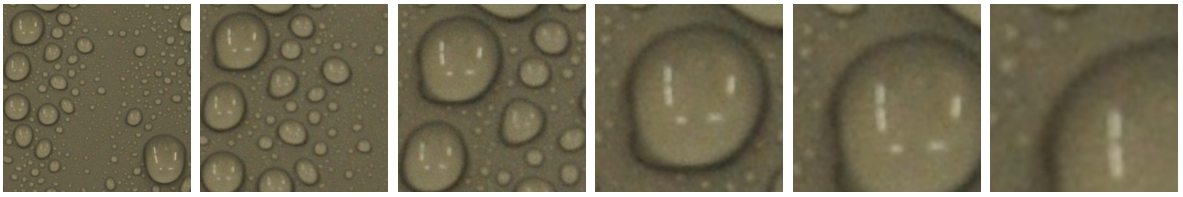

(b) 500 x 500. (c) 300 x 300. (d) 200 x 200. (e) 120 x 120. (f) 100 x 100. (g) 70 x 70.

Figure 2.24: Sub-image size reduced to smaller sizes.

2.6.3.2 Grids

Now that the different sub-image sizes were defined, grids could be created on the original image of the insulator's surface. Two methods were used to create grids on the original image:

1. **Class classification grid:**
   Different hydrophobicity patches were identified on the images in the image data set. A block was then drawn over those identified patches resembling a singular classification class. This block would then be divided up into as many as possible sub-images that could fit into the block. This was done for the entire range of sub-image sizes defined in section 2.6.3.1. Thus, each sub-image in this block would have the same classification class.

2. **Full image grid:**
   A block was drawn over the entire image that required classification. This block was then divided into equally sized sub-images. These sub-images were classified individually. The entire original image was divided up into a grid of sub-images with equal sizes. Each sub-image in the grid was then labeled. Sub-images that had a high degree of overlapping classification classes were discarded, as they would negatively influence the machine learning algorithm.

2.6.4 Assisted image labeling

Training a machine learning model that has accurate and consistent results requires a large number of images in the dataset. Unfortunately, labeling images is very time consuming, especially if one considers that a relatively small data set consists of thousands of images. This gave rise to assisted image labeling by means of an inexperienced machine learning model. An initial dataset was generated using the *class classification grid* described in section 2.6.3.2. This dataset was then used to do initial training with a machine learning model.

After the machine learning model was trained, a new dataset of sub-images was generated using the *full image grid* method described in section 2.6.3.2. Instead of manually classifying a class for each one of the sub-images in the grid, the trained machine learning model was used to predict the sub-image class. Although many of these classified sub-images were predicted incorrectly, it saved a considerable amount of time. The classified sub-images were moderated and the images that were in the wrong class were allocated to the correct classification class.

2.6.5 Data augmentation

Overfitting is a frequent occupancy in machine learning models. As described in section 2.2.1, the training set accuracy and the test set accuracy should be close to each other. A strong indication of overfitting is when training set accuracy is high while the test set accuracy is considerably lower. In order to combat overfitting, one of the methods is to acquire a larger dataset. The more images the model can learn on, the more likely it is that the model will find a distinct pattern for each of the classification classes.

Data augmentation can be applied without acquiring additional labeled images. Small changes in images can present themselves as a completely new images to the machine learning model. Two methods of data augmentation were used to enlarge the dataset considerably.

- **Mirroring:** By creating a mirror of the original sub-image along the vertical axis, the dataset was doubled in size. Unfortunately, creating another mirror image along the horizontal axis is not possible. The reason being, as water droplets become more hydrophilic, their shapes change in the vertical axis as a result of gravity forces enforced on them, as seen in figure 2.4c.

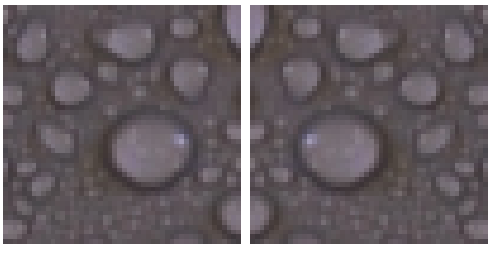

(a) Original image. (b) Flipped image.

Figure 2.25: Original image flipped along vertical axis.

- **Image shifting:** Instead of using the full 50×50 sub-image, new sub-images of 44×44 were created in each corner of and in the center of the original sub-image illustrated in figure 2.26. Using this method, the dataset was magnified by a factor of five.

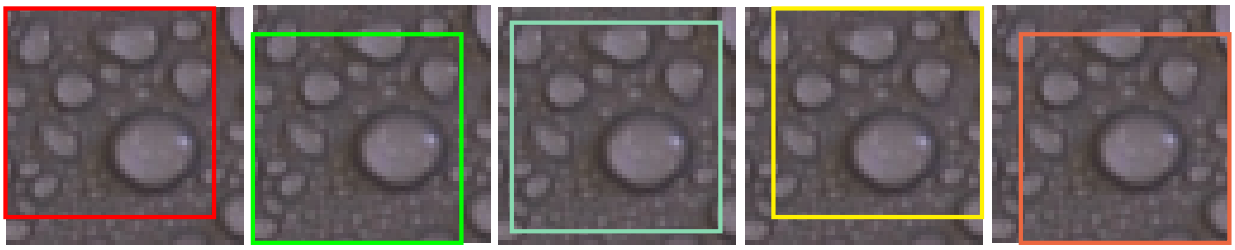

(a) Top left. (b) Bottom left. (c) Center. (d) Top right. (e) Bottom right.

Figure 2.26: New sub-images created by image shifting.

2.6.6 Images harvested

The total labeled images acquired was 5359 images. After mirroring the images in the dataset, it consisted of a total of 10718 images. Applying image shifting consequently magnified the dataset to 53590 label images.

The total labeled images in each class after data augmentation was as follows:

- **Class 0:** 1570 images
- **Class 1:** 5110 images
- **Class 2:** 7010 images
- **Class 3:** 9160 images
- **Class 4:** 2870 images
- **Class 5:** 2240 images
- **Class 6:** 7630 images
- **Class 7:** 8350 images
- **Class 8:** 9650 images

2.7 Neural network training

2.7.1 Programs and libraries used for neural network training

Two different machine learning libraries were used in the quest for building a neural network: Keras and Tensorflow. After experimentation, it was decided that Tensorflow would be used.

2.7.2 Model initialization

Before the neural network can be trained, the weights for all the filters and fully connected layers should be initialized. Usually, random values are used to initialize these weights, but for all the tests that will follow, a random number generator with a seed value was used to initialize these weights. This means that the same random weights would be generated repeatedly for all the tests that will follow.

2.7.3 Data set initialization

Training a machine learning model requires at least two datasets: training dataset and a test dataset. The training dataset is used to train the model with .The training dataset is also used to test the model's accuracy after each epoch in order to make changes to the model to improve accuracy. The test dataset is used to test the model's performance after training was done. The test dataset does not have any influence on training the model. The model has not seen the images in the test dataset. The test dataset results are therefore an accurate indication of the model's performance

The image dataset that was harvested was first randomized then split up into a ratio of 5:1 for train data to test data.

- Training data set: 42872 labeled images
- Test data set: 10718 labeled images

2.7.4 Learning rate

The learning rate is defined by the magnitude of change on the weights of the model. Finding the perfect learning rate can prove to be difficult. A fast learning rate is initially desired for accelerated learning. After convergence, a smaller learning rate will be used in attempt to improve the model even further.

2.7.5 Epochs

Epochs is the number of iterations that the full training data set used to update the weights of the neural network [30]. Usually, the more epochs, the better the accuracy becomes, up to the convergence point. The convergence point is where it does not matter how many epochs follows, as the accuracy will stay the same. Oscillation occurs around the convergence point. The convergence point can be extended by decreasing the learning rate.

2.7.6 Mini batch

The training dataset is divided up into smaller mini batches. These mini batches are then each used to train the neural network. The advantage of this method is that all the training data does not have to be in the system's memory. Therefore, less memory is required [31]. Mini batches are also computationally more efficient. Large mini batches generally take longer to converge, but provide a more accurate error gradient estimation [32].

2.7.7 Cost

The cost, also known as the loss function, is used to describe the total error between the correct output versus the predicted output of the neural network for a given data set [33]. The cost is used to determine if the network is improving from epoch to epoch. If the cost is getting lower for each n - number of epochs, then the network is still improving on its training results. If the cost is oscillating around a point for a certain n - number of epochs, then the network is unable to improve on its training results. Decreasing the learning rate will allow for smaller changes to be made to the weights in the network, possibly lowering the cost even more.

2.7.8 Learning duration

Depending on the model and data set size, the duration it took to learn a model could vary from a few minutes to hours and even days of learning. Most of the models were relatively basic, thus learning could be done under a day. Initially a Lenovo Y500 laptop was used to do training with. The specifications were as follows:

- Processor: Intel Core i7-3630QM CPU @ 2.4GHz.
- Ram: 8GB DDR3 1600 MHz.
- Graphics processor unit (GPU): NVIDIA GeForce GT 650M

Unfortunately, doing training on the laptop's CPU proved to be unfeasible for prototyping due to time constraints. Using a GPU, machine learning could be accelerated considerably. Training a model on an Asus NVidia 980ti STRIX GPU can be up to 100 times faster than training on a Dual Core CPU Intel i7 @ 2.5 GHz [34]. Unfortunately, both Keras and Tensorflow did not support the GPU in the laptop, since it was outdated.

Building a high specification computer, dedicated to do machine learning, seemed like the obvious next step. Fortunately, an alternative exists in this day and age - cloud computing. Several cloud service providers exist, such as: Google Cloud, Amazon Web Services and Microsoft Azure. These cloud services provide full powerful computer builds with high end GPUs. These virtual computers can be rented at a per hour basis. Microsoft Azure was used for experimentation since they offer free $100 student credits. The virtual machine that was used was: Standard NC6 (6 vcpus, 56 GiB memory, Nvidia Tesla K80 GPU) and cost $0.754/hour.

Before hardcore machine learning could be done on the Microsoft Azure virtual machine, an even better alternative was found - Google Colab. Google Colab is a Cloud based Python notebook. The advantages of using Google Colab are as follows:

- It is completely free but has some specification constraints.
- Google Colab has the latest version of Python installed with all the necessary libraries required in this project, such as Tensorflow, Keras, Numpy and Matplotlib.
- Google Drive integrates with Google Colab, making it extremely easy to access data sets that are located on a local drive of a personal laptop with Google Drive installed.

The specifications of the virtual machine which powers the Python Notebook of Google Colab can be found by requesting the system specifications in the Notebook itself using Python code. The specifications were as follows:

- CPU: 1 x single core hyper threaded Xeon Processor @2.2Ghz
- GPU: 1 x Tesla K80
- RAM: 12 GB Available
- Disk: 312 GB

2.8 Convolutional neural network training

2.8.1 Overview

All network typologies described in section 2.5 have been trained. The mini batch sized used during training was set to 128. The learning rate can be seen in tables 2.1 - 2.6, with each model having a different learning rate. The learning rates were obtained during prior test for convergence. The learning duration for each model hovered around 11 - 13 seconds for every 5 epochs. Each model was trained for a total of 10 000 epochs.

In tables 2.1 - 2.6, the accuracy for the different classes was provided at different instances during training. The average training and test accuracy were also provided at different instances during training. It is expected that the training accuracy would be better than the test accuracy. An indication of a network that is overfitting its data is when the training accuracy is significantly better than its test accuracy. Ideally the training and test accuracy should be the same or closely in range with each other, with both having high percentage accuracy.

The cost during training for each network is displayed in figures 2.27 - 2.32. As described in section 2.7.7, a general downward trend in the cost is expected until convergence occurs. The outcome of the various network results is discussed in the following subsections. The different typologies will be compared to one another.

2.8.2 Training results: Network 1

Evaluating table 2.1, it can be seen that there was a rapid increase in training accuracy up to 1500 epochs. Although the training accuracy was high at 10 000 epochs, the test accuracy did not provide satisfactory results. The high train accuracy with the low-test accuracy is an indication that the model is overfitting the data. The topology of network 1, as discussed in section 2.5.5, has many layers with many parameters.

Having many trainable parameters with a small dataset can easily lead to overfitting, as seen in this case. Another contribution to the bad performance of this network is the use of too large filters with excessive zero padding to keep the dimensions of the layers correct. Reducing the filter's x - y dimensions and increasing the number of channels in each filter will retain a larger dimension from the original input size, while still providing sufficient trainable parameters.

In figure 2.27, it can be seen that the network is steadily converging around a cost of 0.16 at 10 000 epochs with a train accuracy of 94%. Training for more epochs and a smaller learning rate will improve the train accuracy slightly, but no significant change to the test accuracy is expected. Overall, this network performed the worst of all the networks, and so was not used to conduct images classification with.

Table 2.1: Training performance of convolutional neural network 1.

		Class test accuracy (%)									Average (%)	
Epochs	Learning rate	0	1	2	3	4	5	6	7	8	Train	Test
5	0.0005	0	0	49	82	0	0	0	100	0	39	39
50	0.0005	80	82	45	73	14	13	68	60	69	62	60
150	0.0005	89	78	55	65	32	84	72	58	73	74	65
500	0.0005	89	72	44	67	41	68	63	72	73	85	65
1500	0.0005	88	61	50	58	53	63	59	71	74	91	63
3000	0.0005	82	58	58	53	43	59	60	70	71	92	62
5000	0.0005	86	61	43	68	39	56	61	70	72	93	62
7500	0.0005	84	63	51	54	48	52	59	67	75	94	61
10000	0.0005	82	60	56	54	44	55	57	66	77	94	61

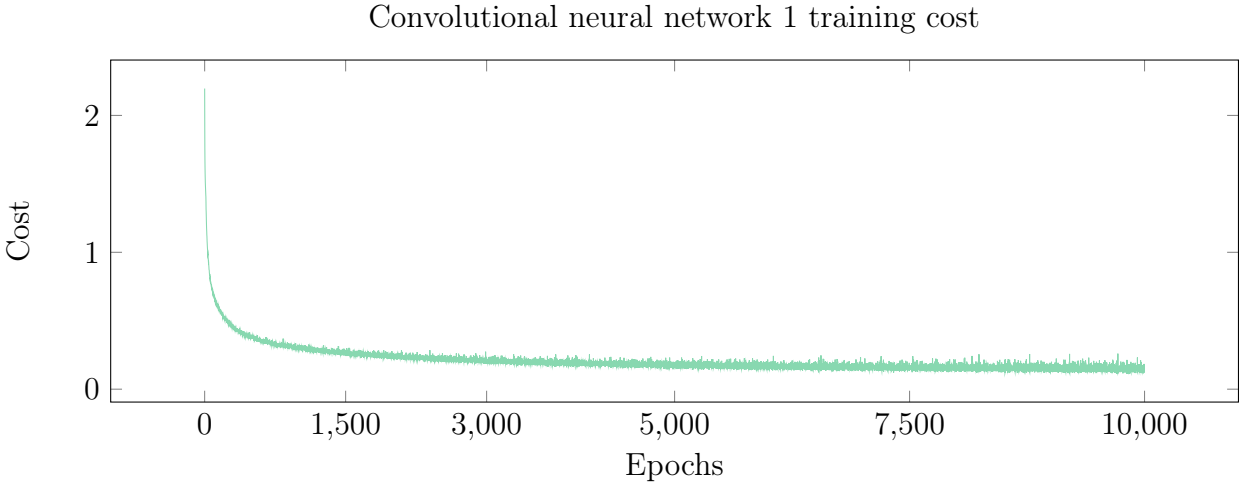

Figure 2.27: Cost after each epoch network 1.

2.8.3 Training results: Network 2

Table 2.2: Training performance of convolutional neural network 2.

		Class test accuracy (%)									Average (%)	
Epochs	Learning rate	0	1	2	3	4	5	6	7	8	Train	Test
5	0.0001	0	0	0	100	0	0	71	69	65	50	49
50	0.0001	0	0	0	100	1	70	80	84	72	59	58
150	0.0001	0	0	0	99	10	88	93	87	82	64	63
500	0.0001	93	0	0	87	53	94	94	97	90	71	69
1500	0.0001	93	0	71	74	60	97	93	91	89	84	76
3000	0.0001	94	0	67	75	61	94	94	94	88	88	76
5000	0.0001	94	0	64	75	59	93	93	94	88	88	75
7500	0.0001	93	0	65	72	61	93	93	94	88	88	75
10000	0.0001	95	0	63	72	59	90	92	94	87	88	74

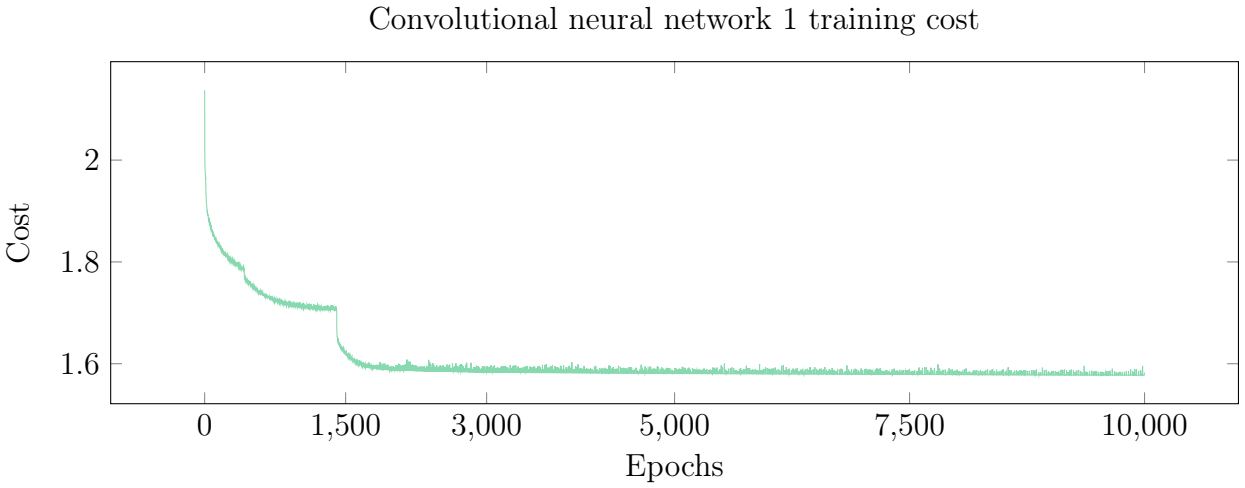

Figure 2.28: Cost after each epoch network 2.

2.8.4 Training results: Network 3

Table 2.3: Training performance of convolutional neural network 3.

		Class test accuracy (%)									Average (%)	
Epochs	Learning rate	0	1	2	3	4	5	6	7	8	Train	Test
5	0.0001	0	0	0	100	0	0	78	88	0	45	45
50	0.0001	0	88	45	81	0	90	89	85	80	74	72
150	0.0001	0	70	49	95	0	95	91	96	88	79	77
500	0.0001	87	81	67	89	0	97	97	97	89	90	83
1500	0.0001	92	83	74	82	0	98	96	96	92	92	83
3000	0.0001	92	84	71	79	69	96	97	96	91	97	86
5000	0.0001	91	85	69	82	70	97	97	96	90	98	87
7500	0.0001	91	87	69	79	70	96	97	96	90	98	86
10000	0.0001	91	86	70	80	67	97	97	96	90	98	86

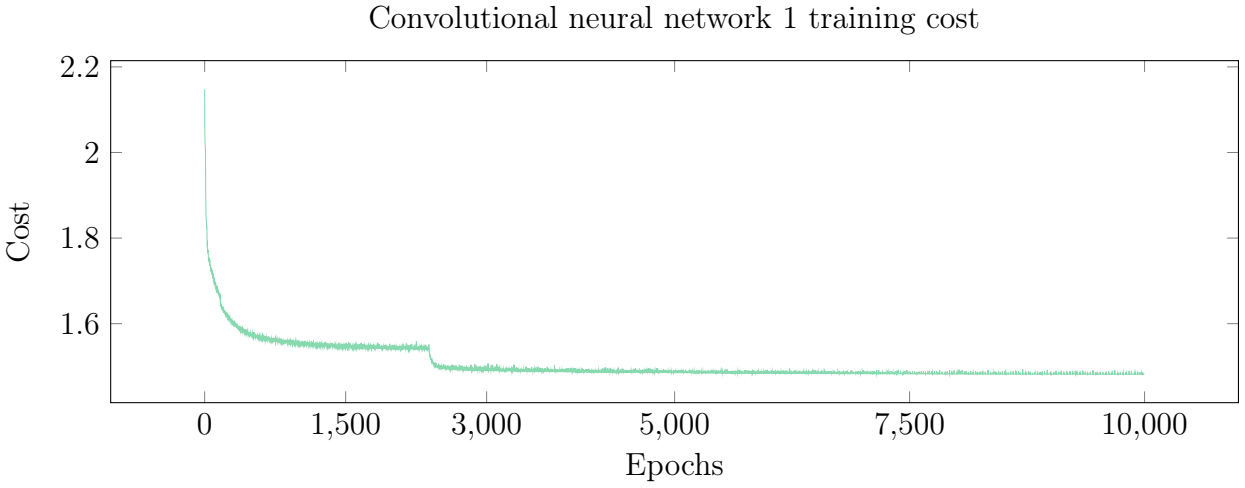

Figure 2.29: Cost after each epoch network 3.

2.8.5 Training results: Network 4

This network was inspired by the Alexnet design. The network was trained using a small learning rate of 0.00001. It can be seen that the test and training accuracy was in close range to one another of up to 1500 epochs. From thereon, the train accuracy surpassed the test accuracy by 10%. With a test accuracy of 83%, this network provided remarkable results, given that the dataset does contain some labeling errors. The labeling errors will be discussed in section 2.8.8.

It should be noted that class 4 obtained a 0% test accuracy for the entire training process up to 10 000 epochs. A possible reason for this is because class 4 and 5 have similar attributes. With class 4 having only 2870 images compared to other classes with 9000 images, it can also be that there was not enough data provided to distinguish between class 3 and 5.

As early results of this network proved promising, alternate versions were developed namely network 5 and 6 in sections 2.5.9 and 2.5.10.

Table 2.4: Training performance of convolutional neural network 4.

		Class test accuracy (%)									Average (%)	
Epochs	Learning rate	0	1	2	3	4	5	6	7	8	Train	Test
5	1e-05	0	0	0	100	0	0	82	71	0	42	42
50	1e-05	0	79	25	79	0	0	79	81	68	61	60
150	1e-05	0	86	40	75	0	78	86	78	70	68	67
500	1e-05	0	96	39	66	0	87	94	84	60	68	67
1500	1e-05	0	88	60	85	0	94	91	90	93	82	78
3000	1e-05	88	84	65	89	0	97	93	92	93	90	82
5000	1e-05	93	76	66	92	0	95	88	94	94	91	82
7500	1e-05	95	89	69	86	0	97	95	90	90	92	82
10000	1e-05	95	84	68	88	0	96	91	94	92	93	83

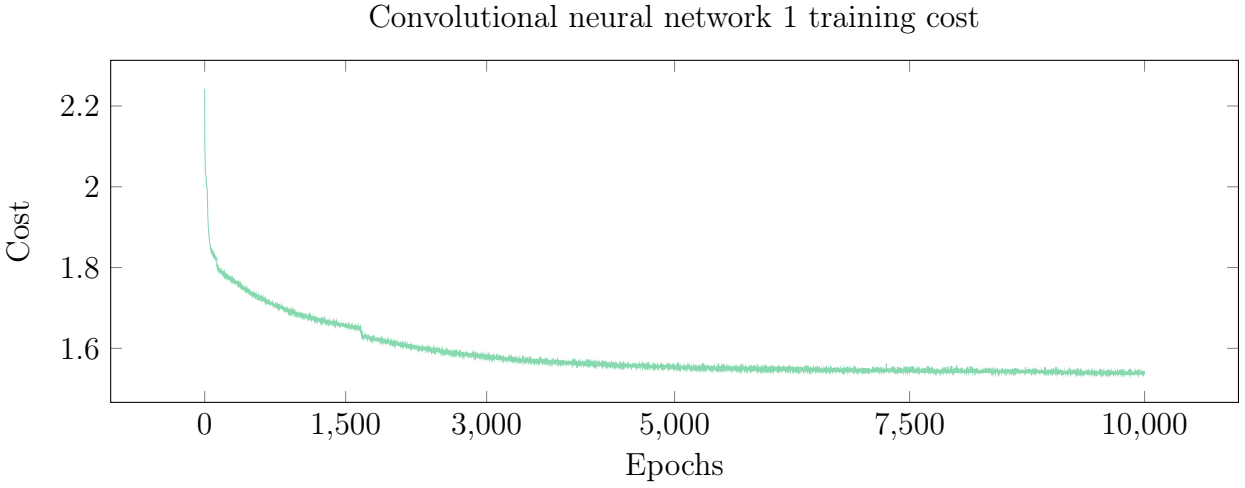

Figure 2.30: Cost after each epoch network 4.

2.8.6 Training results: Network 5

This network performed very similar that network 4. Once again, there was a close relationship with the train and test accuracy, with an end difference in accuracy of 12%. Unfortunately, there is still a 0% accuracy for class 4.

Table 2.5: Training performance of convolutional neural network 5.

		Class test accuracy (%)									Average (%)	
Epochs	Learning rate	0	1	2	3	4	5	6	7	8	Train	Test
5	0.0001	0	0	5	97	0	0	83	66	61	50	50
50	0.0001	0	92	40	66	0	0	80	84	75	64	63
150	0.0001	78	81	57	84	0	0	88	87	90	75	73
500	0.0001	83	91	60	87	0	0	95	91	95	84	78
1500	0.0001	86	81	63	89	0	0	95	91	96	88	78
3000	0.0001	84	85	70	80	0	92	93	95	93	93	82
5000	0.0001	85	83	67	86	0	92	91	94	94	94	82
7500	0.0001	88	84	67	87	0	93	94	92	94	94	82
10000	0.0001	88	84	65	86	0	92	92	94	94	94	82

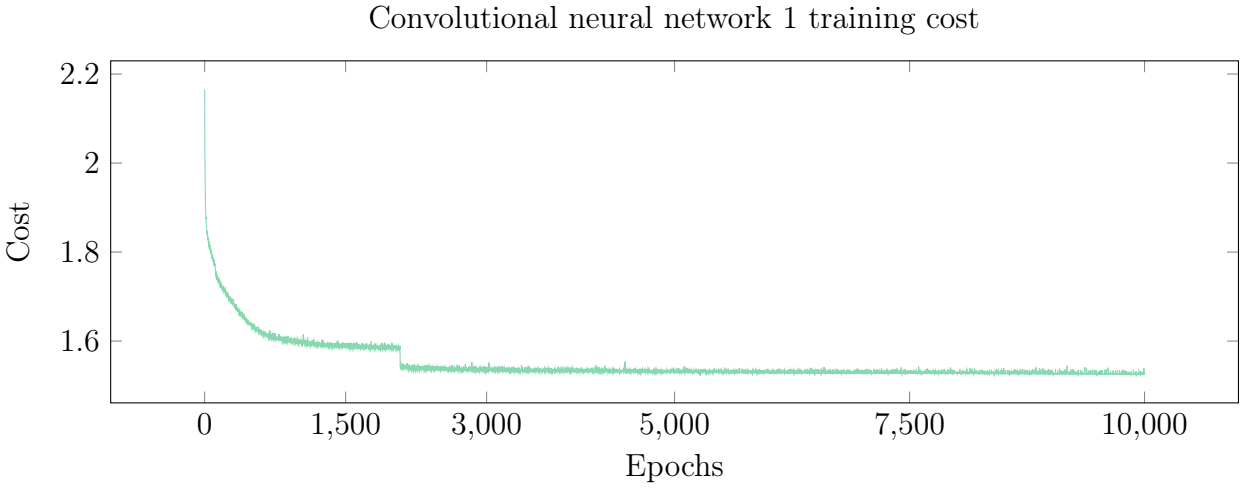

Figure 2.31: Cost after each epoch network 5.

2.8.7 Training results: Network 6

This network displayed the most promising results. With a final test accuracy of 85% at 10000 epochs, it is expected that this network will be able to accurately classify sub-images into their respective classes.

Evaluating table 2.6, it can be seen that this network can easily classify any sub-image within an accuracy range of 59 - 96%. Class 4 displayed a 0% accuracy for each epoch number up to 5000. Thereafter, the network started finding a pattern for class 4 sub-images, increasing the accuracy to 59%, but with a penalty to the accuracy of class 3. This is an indication that class 3 and 4 share similar patterns. Evaluating figure 2.32, it can be seen that convergence occurred. With a training accuracy of 98%, additional training will not significantly increase the test accuracy. Thus, 85% is most likely as good as the test accuracy will be. From previous testing, it was observed that training a network to 100% train accuracy will not

necessarily provide better test results. In fact, it might sometimes provide worse results, as the network overfits the train data.

Table 2.6: Training performance of convolutional neural network 6.

		Class test accuracy (%)									Average (%)	
Epochs	Learning rate	0	1	2	3	4	5	6	7	8	Train	Test
5	0.0001	0	0	0	100	0	0	75	86	0	45	44
50	0.0001	0	79	51	84	0	83	66	92	73	70	69
150	0.0001	0	68	49	94	0	76	83	82	92	74	73
500	0.0001	0	87	67	87	0	96	99	90	90	86	80
1500	0.0001	81	88	73	78	0	98	96	95	90	91	82
3000	0.0001	82	83	75	81	0	97	94	94	91	92	82
5000	0.0001	86	83	71	85	0	98	96	93	90	93	83
7500	0.0001	83	90	65	76	52	93	96	94	90	97	84
10000	0.0001	85	86	71	77	59	96	94	94	91	98	85

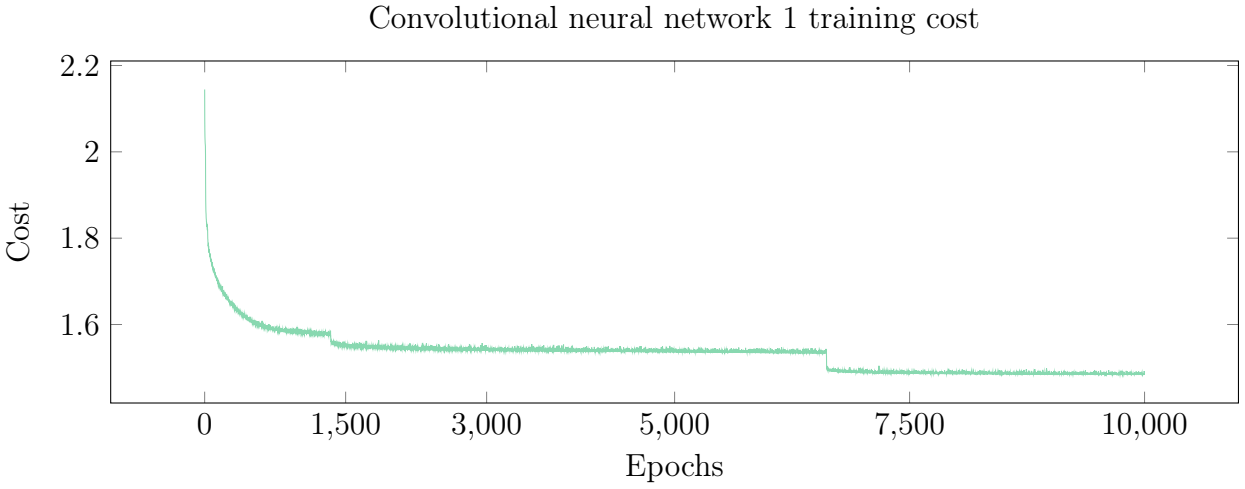

Figure 2.32: Cost after each epoch network 6.

2.8.8 Error compensation results

During the image classification process for data harvesting, misclassification can occur. This happens when an image of a droplet is classified to the incorrect class. Predominantly, misclassified images are allocated to the neighboring classes (i.e. one class up or down) from the correct class. This occurs because of water droplet formations falling within the boundary of two classes.

Both images in figure 2.33 were labeled as a class 3. Observing the images, a second time, one might re-classify figure 2.33a as a class 2 and figure 2.33b as a class 4.

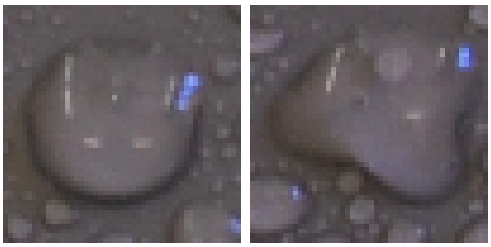

(a) Class 2. (b) Class 4.

Figure 2.33: Class 3 images that can also be subsequently classified in class 2 and class 4.

Consistent image classification by humans proves to be a difficult task, even after several iterations of re-classifying classified images. Obtaining a consistent image classification machine learning model is even more strenuous, since the performance of the machine learning model is dependent on the quality and accuracy of data that it is being trained with.

Initially, when different machine learning models were explored, results were disappointing. This gave rise to an error compensation metric (ECM). The ECM is applied to the test set results. It provides a prediction accuracy based on whether the class predicted by the machine learning model is the correct class that was labeled, and if it is within range of the boundary classes of the correct class.

Determining the significance of the prediction made by the machine learning model, one would like to compare it to the worst possible prediction that the trained model can make. Having nine classes, the worst expected average train accuracy would be to predict an image to be any random class between 0 - 8. This would result in an accuracy of $\frac{1}{9} \times 100 = 11\%$.

In order to compute the worst possible prediction a CNN can make with the ECM, the probability for the network to choose a given class should be determined. Two scenarios exist. The rule for probability addition can be applied, since the events are mutually exclusive. Equation 2.10 will be used to determine the probabilities for each class to be chosen at random.

$$P(A \cup B) = P(A) + P(B) \tag{2.9}$$

1. **Class 0 and 8:** With the outer classes (0, 8), there exists only one boundary class for each outer class, (1,7). If the correctly labeled class is 0, then a correct prediction made by the CNN can either be 0 or 1. The same applies for the boundary class 8.

   The chance that class 0 or 1 is chosen by random is $\frac{1}{9}$. Thus, the probability for a labeled class 0 to be predicted by random is:

$$\begin{aligned} P(A \cup B) &= P(A) + P(B) \\ &= \frac{1}{9} + \frac{1}{9} \\ &= \frac{2}{9} \\ &= 22.22\% \end{aligned} \tag{2.10}$$

   This probability also applies for outer class 8.

2. **Class 1 - 7:** Each one of these classes can have two boundary classes. There is therefore a total of 3 correct classes that can be predicted for a given labeled class. With any

class being chosen at random, the probability of that is $\frac{1}{9}$. Thus, the probability for a predicted class that was chosen at random to be correct is:

$$\begin{aligned} P(A \cup B \cup C) &= P(A) + P(B) + P(C) \\ &= \frac{1}{9} + \frac{1}{9} + \frac{1}{9} \\ &= \frac{1}{3} \\ &= 33.33\% \end{aligned} \tag{2.11}$$

Now that a boundary error is excepted for each class, it can be used to determine the accuracy of the networks. A classification accuracy of better than a random prediction is expected. The classification accuracy for all the classes is therefore compared by results from equation 2.10 and 2.11.

The ECM was applied to the test set results of all six CNN after 10 000 epochs and is seen in table 2.7. All the networks did significantly better than choosing a class at random, indicating that the networks are all able to do classifications when compensation is applied for the initial dataset labeling error.

Table 2.7: Error compensation results on network 1 - 6

Network no.	Average test set accuracy (%)	Average test set accuracy with ECM (%)
1	61	91
2	74	95
3	86	94
4	83	98
5	82	97
6	85	98

2.9 Insulator analysis

2.9.1 Overview

Now that a neural network exists to do image classification with, the next step is to interpret the results of the classified sub-images. With around 168 sub-images present in one photo of an insulator, it is not possible to get a conclusive result whether the insulator exhibits hydrophobic or hydrophilic properties on its surface. A discussion into acquiring images of an insulator for hydrophobicity analysis will follow with the method of interpreting all the classified sub-images present on its surface.

2.9.2 Image harvesting

Images for insulator analysis were obtained in the same manner than described in section 2.6.1 for the image harvesting process. Instead of taking photos every 5 seconds, a singular photo was taken as soon as the first water droplet slid of the insulator's surface. The water to isopropyl mixtures were kept the same as for the laser method and is discussed in section 3.4.4.

2.9.3 Features interpretation

In chapter 4, the machine learning technique that was developed will be used to do analysis on several insulators in order to determine their hydrophobicity. Features that will be examined to obtain a better understanding of the insulator's hydrophobicity states are:

- **Histogram distribution analysis of classified sub-images in section 4.3.2:** A histogram of all the classified sub-images within a picture of a wet insulator surface will be created. The histogram will then be analysed to find a pattern between the insulator's hydrophobicity and the distribution of classified sub-image classes.
- **Average sub-image classification analysis in section 4.3.3:** The average of all the classified sub-images will be determined. It is expected that this average will have a strong correlation to the overall surface hydrophobicity of the insulator.
- **Sub-image standard deviation and variance in section 4.3.4:** The variance and standard deviation will be used to determine the quality of the of the classified data. The insulator will be sprayed uniformly with an isopropyl mixture; thus it is expected that the entirety of the insulator should reflect the same order of classified sub-images for each isopropyl mixture.

2.9.4 Conclusive overview

The neural networks discussed in this chapter provided promising results, especially neural network 6. The train and test results for network 3 - 6 were close to each other, indicating that the network is able to classify sub-images in the correct category without overfitting the training images.

A more complex network with more training parameters could be developed to reduce overfitting even more, though a better option would be to improve the training data. Since the training data also exhibits some labeling errors as described in 2.8.8, improving the labeled data set will probably provide a better improvement in test and training results.

Accounting for classification uncertainty to which a classified image can be in either of the neighboring classes around the correct class, it was shown that the neural networks could achieve an accuracy in the high 90%. After evaluating all the different networks and their results, it was decided that CNN 6 will be used to do image analysis within chapter 4. The interpretation of the features collected from the classified sub-images will also follow in chapter 4.

Chapter 3

Laser technique

3.1 Introduction

3.1.1 Overview

As described in chapter 1, the ideal method to measure hydrophobicity is to measure the contact angle of the water droplet on the insulator's surface. This method works great for a singular droplet on a small patch of the insulator's surface, but when the overall hydrophobicity of the surface needs to be taken into consideration, it becomes unfeasible to measure the contact angle of hundreds of water droplets. Not only does the contact angle of the water droplet play an important role in characterizing the performance of the insulator, the percentage wetted area of the surface is also a very important factor to take into consideration. The greater the wetted area, the more paths there are for leakage current to flow.

The ideal solution to measuring contact angle and percentage wetted area would be to model a 3D representation of the water droplets on the surface of the insulator. To determine the contact angle of water droplets from a simple 2D image of the insulator is close to impossible, as there is no accurate way of determining depth over the entire image.

In this section, different techniques will be looked at for creating a 3D model of a surface. Accuracy will be an important requirement as this will enable us to find the exact contact angles of the water droplets on the surface. Another important aspect to keep in mind is the ease of applying these techniques on insulators, not only in the lab but possibly in the field.

3.1.2 Different 3D surface profiling techniques

Three different 3D profiling technologies were investigated:

- **Laser spot:** This method determines the angles of the reflected light relative to a baseline. Using triangulation, a 3D surface can be constructed with multiple sample points [35].
- **Laser line:** Similar to the laser spot method, this method uses triangulation to collect the angles of the reflected line laser relative to a baseline to reconstruct a 3D surface [35].
- **Structured light:** A light pattern is projected onto a surface and the deformation of the light pattern is calculated with triangulation, such that a 3D surface can be reconstructed [35].

The laser spot is not ideal for creating a high resolution 3D surface, since thousands of samples would be required to achieve it. The Structured light requires a projector to project patterns of light which increase the cost.

It was decided that laser line scanning would be used, since it could reconstruct an accurate 3D surface profile without the use of expensive equipment. A high-quality line laser with a perfectly straight projection of the laser line and a DSLR camera capable of taking 30 fps 1080p video is all that was required.

3.1.3 Requirements and limitations of 3D surface profiling techniques

Current 3D surface profiling techniques require that the object being scanned is highly reflective. The more reflective a surface is, the easier it is to detect deformation of the projected light sequence onto the surface.

External lighting can also affect the level of accuracy. Having a greater contrast between the projected light and external light makes it easier to detect the projected light sequence.

3.1.4 Similar applications of 3D laser scanners

3D laser scanning can be found in many quality control environments where it is essential to rapidly obtain an accurate 3D surface. An experiment was done using a 3D laser scanning device to accurately scan a steel pipe. The 3D laser technique provided more accurate results than the ultrasonic method used for quality control [1]. The laser scanning method used a line laser scanning device to scan the pipe's surface. Three additional cameras were used to track the position of the 3D laser scanning device, thus providing more maneuverability to move the device around an object freely [1].

The use of 3D laser scanning techniques for hydrophobicity analysis has not been attempted. Measuring a surface hydrophobicity state requires the analysis of water formations on an insulator's surface. Lasers require reflective surfaces to be effective. Therefore, this technique would be ideal for obtaining a 3D surface profile of water formations on an insulator's surface.

3.2 3D Surface profiler development

3.2.1 Development goal

The process of developing the methodology to measure hydrophobicity of polymer insulators with a 3D surface profiler requires determining how this method can assist in better measurements that are more consistent, less subjective to human perception and less dependent on extensive training.

The ideal hydrophobicity measurement device must have the following characteristics:

- A device that can conduct lab measurements as well as field measurements. The lab and field measurement fidelity should coincide with each other. Also, the mythology to measure the polymers hydrophobicity under lab conditions vs field conditions should stay the same.
- Individual person operation could proof beneficial for field measurements. The less people required to take a measurement, the more cost effective the method becomes

and is thus more attractive for commercial product development. Having a singular person operation also makes it easier to take measurements in the field, especially considering that measurements can then be taken while the insulator is still mounted on the supporting structure.

- Measurements obtained by this device should not be affected by external lighting, and so different light sources from various angles should not affect the measurement results. A downfall of existing image processing techniques is that different light exposures on an image greatly affect the ability to detect water droplet formations on the insulator's surface, giving inconsistent results.

- Having a high-resolution 3D profile is of paramount importance to extract valuable data. It is required that this method can measure all the different angles present on each individual water droplet formation, since the contact angle of a water droplet represents a direct correlation to the surface hydrophobicity.

3.2.2 Proposed 3D profiling method

After evaluating all the different techniques, a decision was made to use a line laser to project a line perpendicular to the surface being scanned. This method works by using a camera at an angle to observe the deformation of the straight line as it moves along a surface. By evaluating the deformation of the line at several set intervals on the surface, a 3D image can be reconstructed.

3.2.3 Constraints and possible solutions

One of the first issues coming to light when attempting to use a line laser 3D profiler to scan a surface sprayed with water, is that water droplets do not reflect light off its surface. Water is transparent, thus allowing visible light to penetrate its surface and scatter within the water droplet. The following possible solutions are being considered:

- To use non-visible medium infrared light. Medium infrared light spectrum at a wavelength of 3 um water absorbance depth is at 1 um. This means that medium infrared light does not penetrate water deeper than 1um. The result is that a 3D surface profile can be obtained of a surface with water droplets on it. This in theory might work, but unfortunately, medium infrared lasers and cameras are very expensive. This type of equipment is bulky as well, making it infeasible to use in a one-man operational device.

- To add colourant to the water being sprayed on the surface. This would enable visible light to more easily reflect off the water droplet's surface. A concerning factor with this solution is that it will influence the hydrophobicity characteristics of the water on the insulator surface.

When attempting to recreate a 3D profile from a series of images of the deformed line laser, it is important to keep the scanning rate in mind so that scaling is being done appropriately afterwards. It is also important that scanning rate should be kept constant over the entire surface, otherwise the 3D profile would not be an accurate representation of the surface. An easy solution would be to implement motion tracking and apply adaptive scaling according to the rate of movement.

It is desired to have a great contrast between the projected line laser and external light sources on the recorded video. It is expected that the projected line will be substantially brighter

than the external lighting, in turn lowering the camera's sensor sensitivity. Therefore, an adequate contrast can be achieved to assist in line laser contour detection. It should be emphasized that if the line laser is barely visible to the human eye, it will not be sufficient to do contour detection in post-analysis. A possible solution is to increase the laser power or eliminate external light sources.

3.2.4 Line laser isolation in post processing image analysis

Color filtering

In order to detect deformation of the line laser projected on a surface, one would need to isolate the front-end, which is the laser light, from the back-end, which is any background visuals. Several methods will be discussed that were attempted to achieve line laser isolation.

One of the first properties that can be exploited using a visible red line laser is that it is the only red color present in the video being taken when a surface is scanned with it. This is because most high voltage polymer insulators are grey. By first applying color filtering a mask of the original image can be created that only contains the red laser line. In this case, a mask is a secondary image containing pixel values, zero or one; zero is for background and one for where red colours are present.

The first method that was attempted was colour filtering using the default colour space of the image, BGR color filtering. An image in BGR color space is a matrix of pixels, each pixel containing three colors: red, green, and blue, each with an intensity ranging between 0–255. By creating a color filter that only accepts red pixels, one might think that an adequate mask of the red line can be obtained. Unfortunately, the red line laser reflected off the polymer's surface is not perfectly red. Thus, each BGR pixel of the red line laser will contain high values of red, but also contain green and blue in it. With some fine tuning, a filter with the following ranges was obtained:

$$\begin{bmatrix} Blue \\ Green \\ Red \end{bmatrix} = \begin{bmatrix} 130 - 227 \\ 74 - 150 \\ 159 - 255 \end{bmatrix} \tag{3.1}$$

This colour filter was able to obtain the mask in figure 3.1b from the image in figure 3.1a under uniform lighting conditions. Applying the mask to the original image results in the isolated line seen in figure 3.1c. It can also be seen that the line is not perfectly uniform.

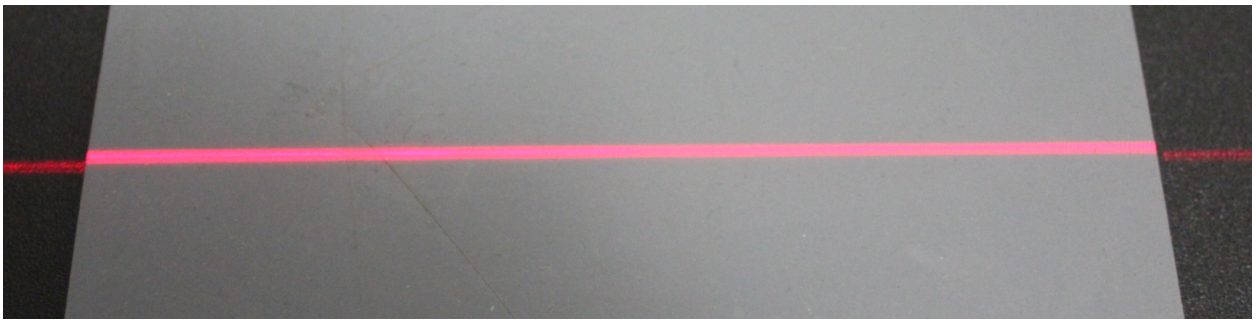

(a) Original image.

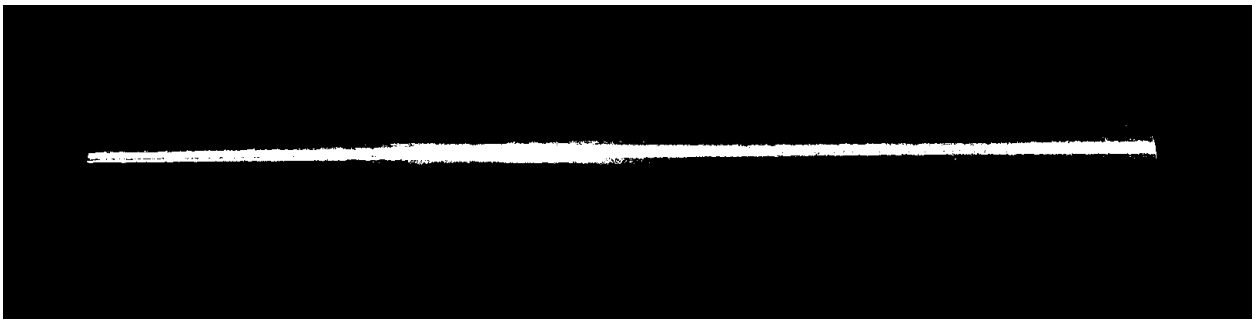

(b) Mask after color filtering.

(c) Mask applied to original image.

Figure 3.1: Laser line isolation with BGR color filtering with uniform external lighting.

Unfortunately, when non-uniform external lighting is applied, the filter fails to create an adequate mask, as seen in 3.2 This is because the filter is sensitive to changes in light intensity.

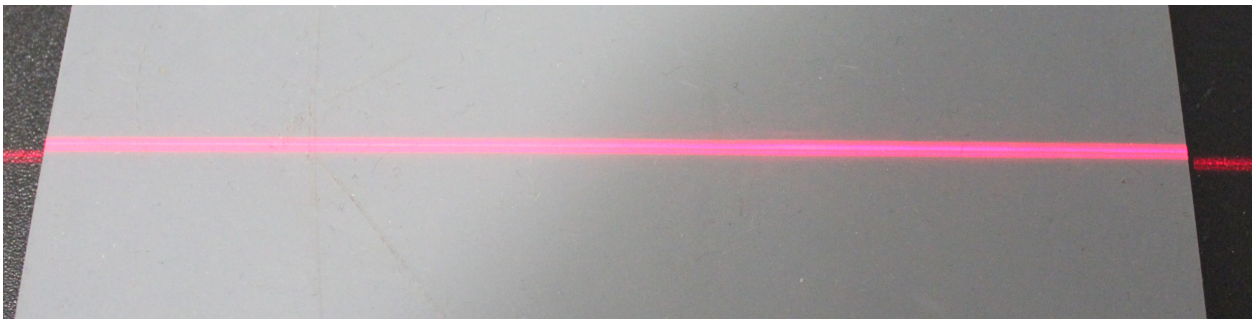

(a) Original image.

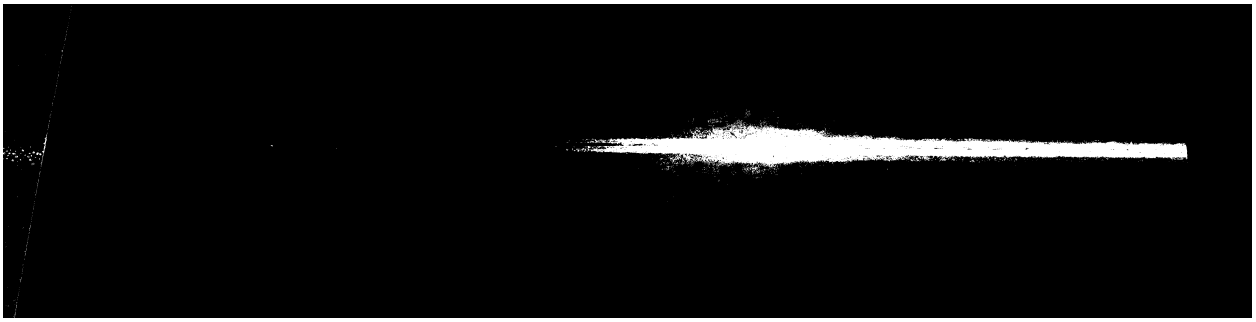

(b) Mask after color filtering.

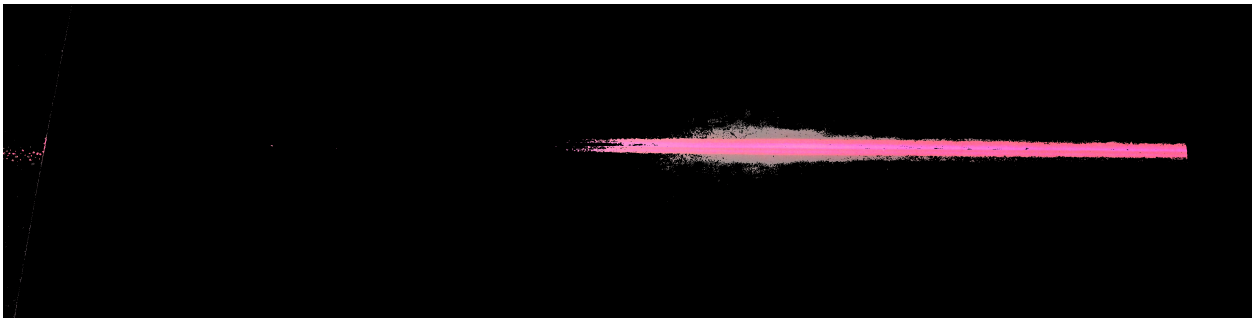

(c) Mask applied to original image.

Figure 3.2: Laser line isolation with BGR color filtering with non-uniform external lighting.

The second method attempted was color filtering in the HSV color space. HSV stands for hue, saturation and value. Using the HSV color space, a range of red-like colors can be selected (for example a red-pinkish color). Another advantage of using the HSV color space is that a mask can be created with this filter that consists of only red colors brighter that a certain value, making it easy to ignore background red colors that are not part of the laser line. Figure 3.3 is a representation of a HSV cylinder. Hue is represented by the degrees of rotation of the cylinder, saturation is represented by the radius of the cylinder and value is represented by the height of the cylinder.

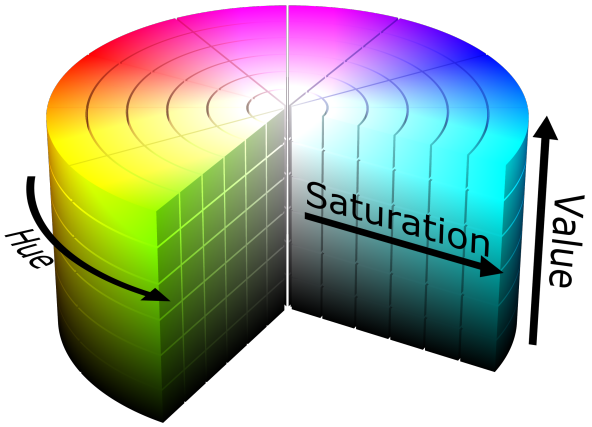

Figure 3.3: HSV color cylinder.

A Python library called Open Computer Vision (CV2) was used to do image manipulation and analysis. The HSV model in CV2 has the default following ranges:

$$\begin{bmatrix} Hue \\ Saturation \\ Value \end{bmatrix} = \begin{bmatrix} 0° - 180° \\ 0 - 255 \\ 0 - 255 \end{bmatrix} \tag{3.2}$$

It was found that, by creating a HSV color filter using the ranges in (3.3), a mask could be created that was sufficient to isolate the line laser from the background as seen in figure 3.4.

$$\begin{bmatrix} Hue \\ Saturation \\ Value \end{bmatrix} = \begin{bmatrix} 0° - 15° \\ 0 - 255 \\ 220 - 255 \end{bmatrix} + \begin{bmatrix} 155° - 179° \\ 0 - 255 \\ 220 - 255 \end{bmatrix} \tag{3.3}$$

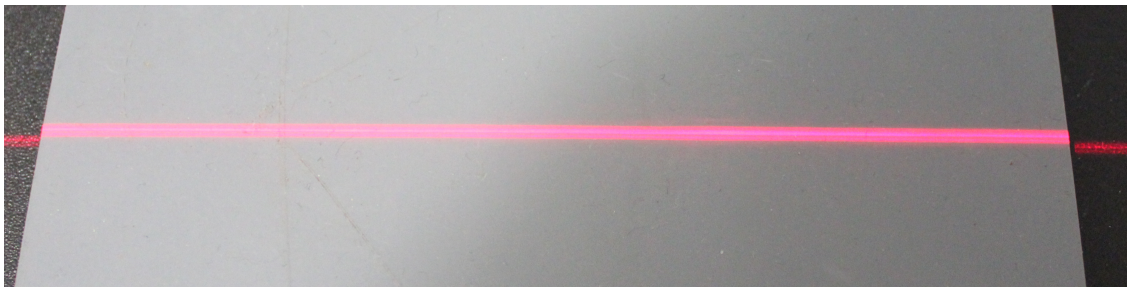

(a) Original image.

(b) Mask after color filtering.

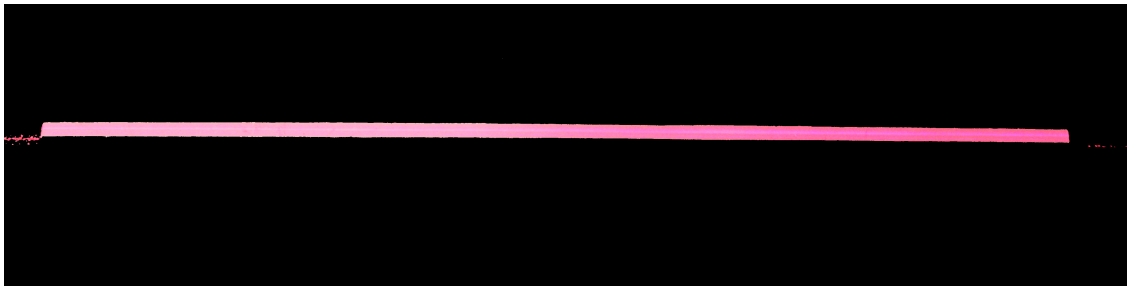

(c) Mask applied to original image.

Figure 3.4: Laser line isolation with HSV color filtering with non-uniform external lighting.

Contour detection

Now that the line laser is isolated from the background, the next step is to find the coordinates of the line's edge. This can be done by using contour detection built into the Open Computer Vision library. The contour detection algorithm outputs a matrix with all the contours present on the image. Contour detection was done on the output mask after color filtering as seen in figure 3.4b. By eliminating every contour except the one encompassing the line laser, one can then use the coordinates to do further analysis. This was achieved by isolating the largest contour from all the contours that were detected. Figure 3.5 displays the output of contour detection over the original image.

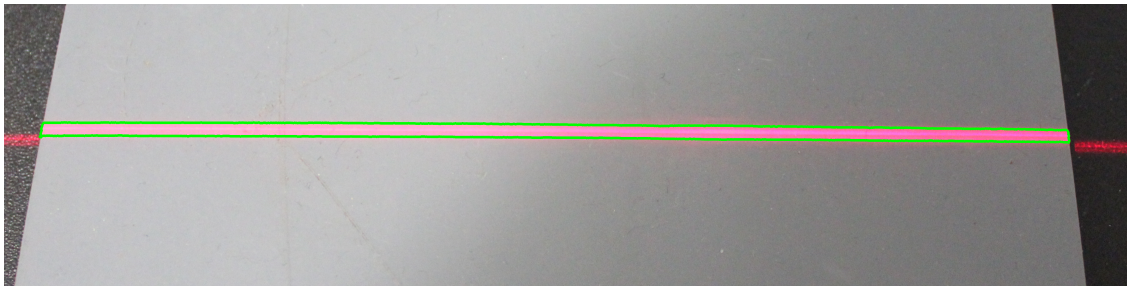

Figure 3.5: Contour detection output on original image.

3.2.5 Elementary surface constructor

The process of creating a 3D surface model requires the coordinates of the line laser over all the 2D images to be stitched together, creating a 3D mesh of the surface that was scanned as seen in figure 3.6. The resolution of the 3D model depends on the resolution of the 2D image and the number of samples that were taken over the entire surface being scanned.

(a) Top view of insulator being scanned.

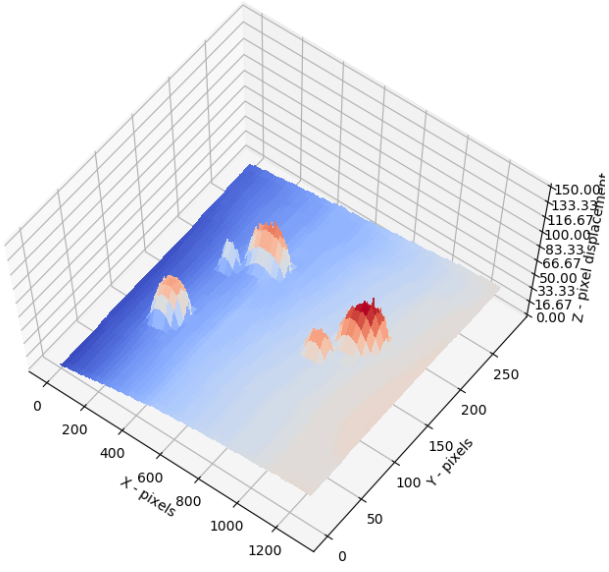

(b) 3D Mesh of insulator scanned at a constant rate.

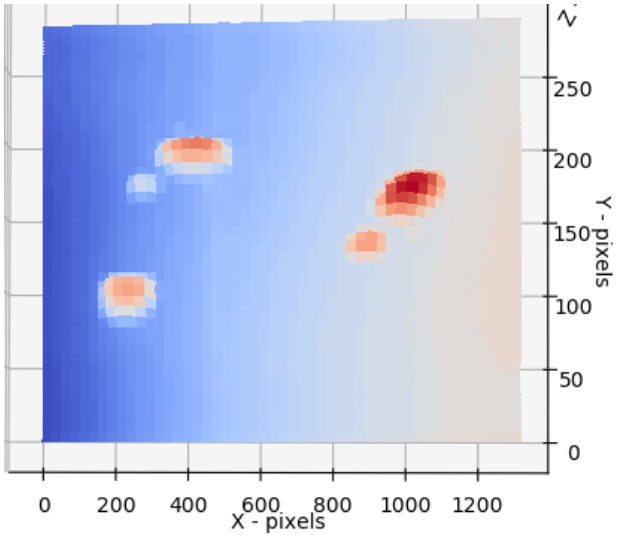

(c) Top view of insulator being scanned.

Figure 3.6: Elementary surface constructor.

3.2.6 Surface tracking

The first problem encountered is inconsistent sample spacing over the surface being scanned. In other words, the 2D image samples are not being taken at exactly x-number of millimeters. It is difficult for a human to move the line laser over a surface being scanned at a constant rate. This results in a skewed 3D image being generated, as seen in figure 3.7.

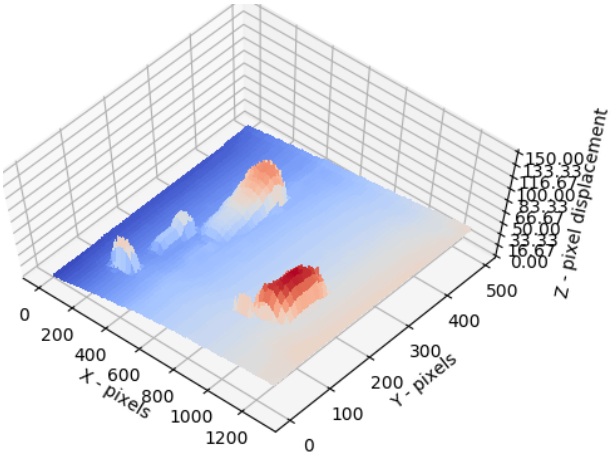

(a) Top view of insulator being scanned.

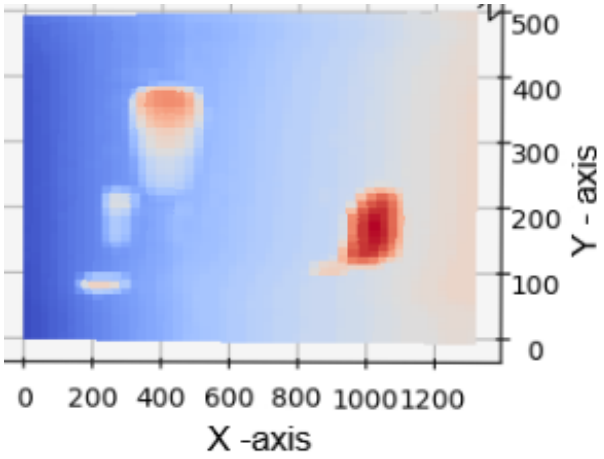

(b) 3D Mesh of insulator scanned at a constant rate.

Figure 3.7: Inconsistent scanning rate.

To resolve this issue, surface tracking can be implemented, which can then be used to scale the spacing between the samples accordingly. Two surface tracking methods were investigated:

Optical surface tracking

Optical surface tracking works on the same principle which an optical laser mouse works. An optical laser mouse has a low-resolution optical sensor which samples images at high rates. Movement in the X-Y direction is detected by comparing two subsequent images to one another by using the mouse image processing chip. The image processing chip calculates the distance that reference pixels on the first image traveled to a subsequent image, which is then translated into X-Y coordinates.

A similar attempt was made to do optical image tracking of the video being taken of the surface being scanned. The algorithm that was developed is as follows: A block of 50x50 pixels in the center of the first frame is convoluted over the entire subsequent frame of the video. Unfortunately, this method does not work well, since the camera's sensor sensitivity is set to a low level, causing the video to be dark. Dark images make it difficult to find reference frames, resulting in inaccurate tracking.

Tracking strip

An easy solution to low light image tracking is to use a tracking strip. By adding a strip of black and white boxes along the surface being scanned, one can count the number of boxes as the laser travels over the surface. The algorithm that was developed is described below.

The tracking strip is attached to the side of the surface being scanned, as seen in figure 3.8a. An assumption was made that the outermost point of the line laser is the edge where the tracking strip is located. A small box on the edge of the laser being detected is used for evaluation. All the pixels in the box are added and if the value of those pixels is above a certain level, the box is recognized as a white box. If the sum of all the pixels in the box

is below a certain level, the box is recognized as a black box. That is because white pixels carry high color values in the HSV space and dark pixels carry low values.

Now that it is possible to determine the speed at which the laser travels on the surface, dynamic frame scaling can be applied. Each black and white box represents a resolution of 25 pixels on the video time axis. All the frames in between two subsequent boxes are being placed in a frame buffer. The frame buffer is then being up-scaled by a factor of 40, which means that for every frame in the original frame buffer, there is 40 exactly the same frames in the new buffer. Every n-th evenly spaced frame is then chosen and placed into the final frame buffer to achieve a total frame count of 25 frames, representing the 25 pixels on the video time axis. This method works well to achieve a smooth final frame buffer, especially where the original frame buffer had less than 25 frames or a frame count that is not an exact factor of 25 frames. It can be seen that the scaled 3D mesh in figure 3.8c provide a more accurate representation of the water droplet formations seen in figure 3.8a than the non-scaled 3D mesh in figure 3.8b.

It should be noted that this method does not account for uneven vertical movement (i.e. if the one end of the line laser travels faster than the other end of the line laser), and therefore only square surfaces can be scanned. To create a 3D profile of a round insulator's surface, scaling has to be done so that a round 3D image can be reconstructed. This will be discussed in the next subsection.

Scanning a round HV polymer insulator

Since the inner and outer part of the line laser is being sampled at a set frame rate, a round surface being scanned will be reconstructed as a skewed square surface, as seen in figure 3.9b. By knowing the inner radius and outer radius of the line laser being projected on a round surface, trigonometry can be applied to scale the coordinates so that a round 3D image can be created.

The square 3D mesh is altered by scaling it with trigonometry in equation 3.4. The 3D mesh consists of multiple points with x, y coordinates indicating its location in the x, y plane. Each point also has a z-axis indicating its height. Only the x, y coordinates were altered as follow:

- **Degrees spin:** The total rotational scan of the insulator's surface. A complete scan will have a 360° insulator rotational scan.
- $C_{inner\ radius}$**:** The inner radius of the round insulator surface. Thus, the radius of support structure of the insulator.

$$X_{new} = (X_{old} + C_{inner\ radius}) \times cos\left[2\pi \times \frac{degrees\ spin}{360} \times \left(\frac{Y_{old}}{Y_{max}}\right)\right]$$
$$Y_{new} = (X_{old} + C_{inner\ radius}) \times sin\left[2\pi \times \frac{degrees\ spin}{360} \times \left(\frac{Y_{old}}{Y_{max}}\right)\right] \quad (3.4)$$

(a) Tracking strip attached to square insulator.

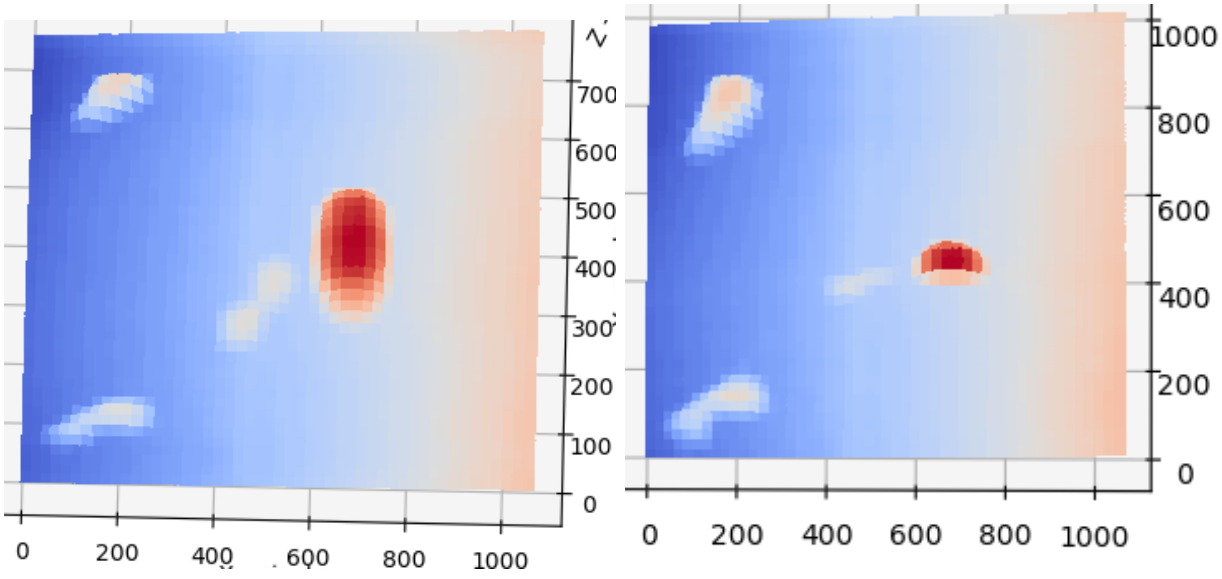

(b) 3D Mesh before scaling.

(c) 3D Mesh after scaling.

Figure 3.8: 2D line laser coordinates stitched together to form 3D mesh.

As seen in figure 3.9c, the skew square image was transformed to a round image representing the round surface of the image. A round tracking strip was also added so that consistent scaling could be applied.

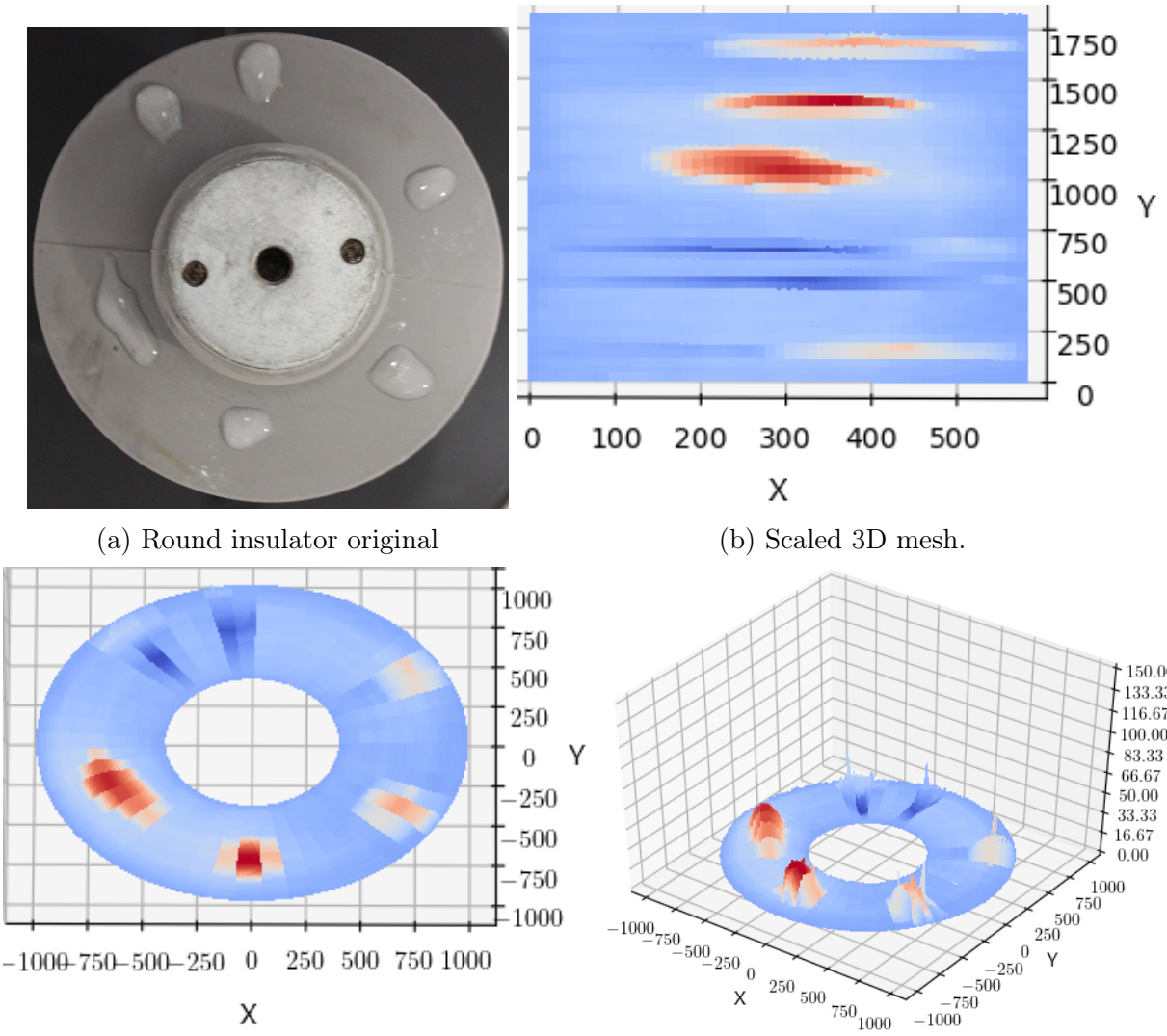

(a) Round insulator original

(b) Scaled 3D mesh.

(c) Scaled 3D mesh top view.

(d) Scaled 3D mesh angle view.

Figure 3.9: Transforming skewed 3D mesh from square to round.

3.3 Feature extraction from 3D surface

3.3.1 Water droplet isolation

Now that a 3D surface had been obtained, the next step would be to isolate the water droplets from the insulator's surface so that analysis can be done. It is desired to have a perfectly flat 3D image of the surface being scanned, with only the water droplets permeating the surface. This way, it is straightforward to do analysis on the water droplets and the surface because they can easily be separated.

From a 2D image of the line laser, one can observe that the line is not perfectly flat. This is because of the camera's lens is concave. A solution to this would be to create a reference concave line by taking a single frame of the line laser projected over a perfectly flat surface and then subtracting it from all the frames in the video. Another solution is to find the mathematical model of the lens and then scale each frame according to that model.

All these solutions will work if a perfectly flat surface is being scanned, but the method should also work on HV polymer insulators that has cone-shaped disks.

The 3D matrix used to create the figure can be transformed to a 2D gray-scale image, with

the 3D X,Y-axes representing the X,Y axes in the 2D image and the 3D Z-axis representing the gray-scale brightness value. Such a transformation can be seen in figure 3.10c.

Several morphologies exist in the 2D image domain. By using these morphologies, an attempt can be made to isolate the water droplets from the scanned surface.

Looking at the problem from the 2D image domain, a method should be found to eliminate contrast irregularities. It can be seen in figure 3.10 that non-uniform flatness in the 3D domain creates non-uniform contrasts on a 2D image seen in figure 3.10c

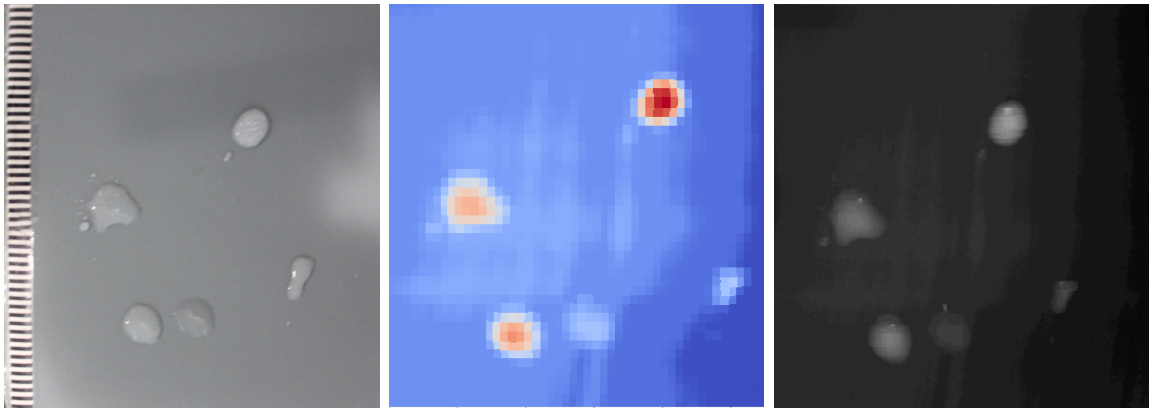

(a) (b) (c)

Figure 3.10: 3D Surface transformed to grayscale image domain.

By applying thresholding to the 2D image, an attempt was made to isolate the water droplets from the background. Three different thresholding techniques were tested.

Binary threshold:

This method creates a binary image. All values above a predefined fixed brightness level is represented by the binary value 1, and all values below are represented by 0. In figure 3.11 binary thresholding does an adequate job of isolating the water droplets from the scanned surface. Different levels of thresholding were applied.

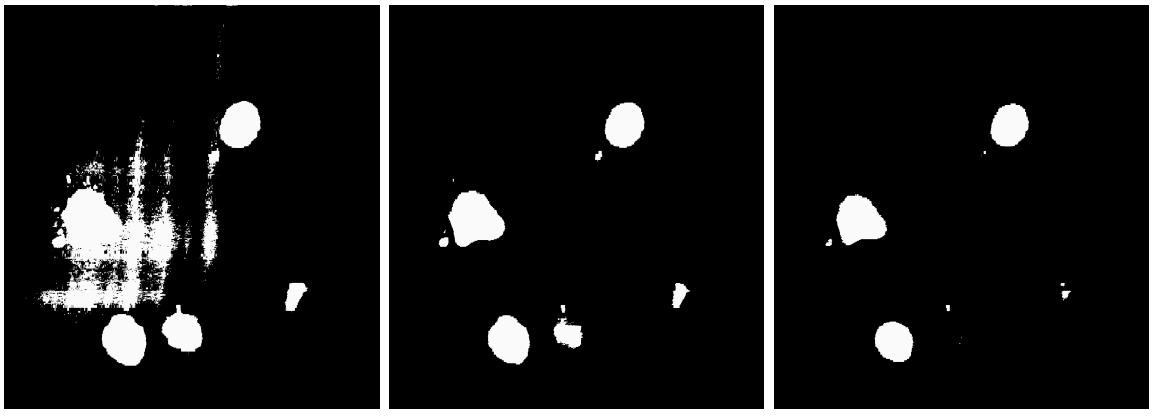

(a) Level 1. (b) Level 2. (c) Level 3.

Figure 3.11: Binary thresholding on grayscale image.

Adaptive threshold:

In order to account for variation in illumination of an image, adaptive thresholding can be applied. Adaptive threshold uses a different threshold value for each pixel in an image. Two methods were tested:

- **Mean adaptive thresholding:** For each pixel in an image, the threshold is calculated by evaluating the mean value of pixels for a certain block size. In figure 3.12 it can be seen that adaptive thresholding is able to isolate most of the water droplets from the background on flat and concave surfaces. An increasing in block sizes were evaluated.

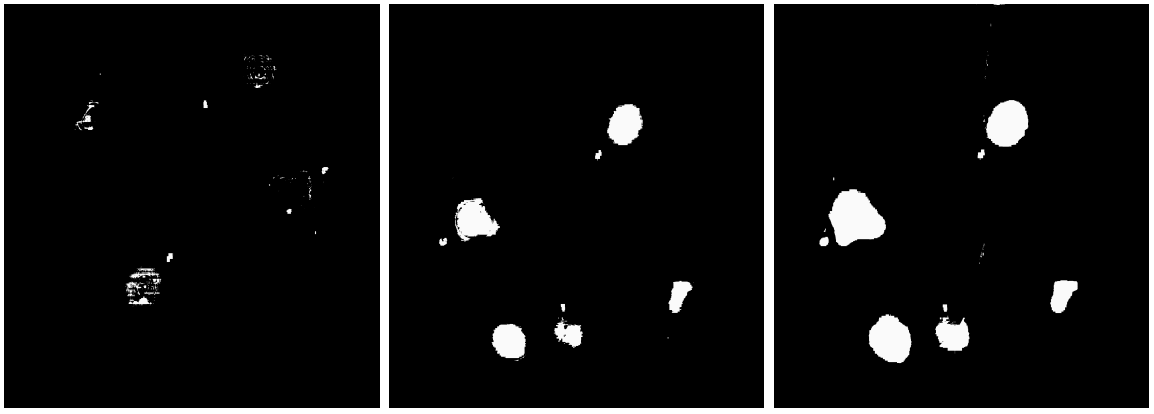

(a) Block size 1 (b) Block size 2 (c) Block size 3

Figure 3.12: Mean adaptive thresholding with different block sizes.

- **Gaussian adaptive thresholding:** For each pixel in an image the threshold is calculated by evaluating the weighted sum of a certain pixel block size where the weighted block is comprised of gaussian values. As seen in figure 3.13, gaussian adaptive thresholding provides even better water droplet isolation than adaptive mean thresholding.

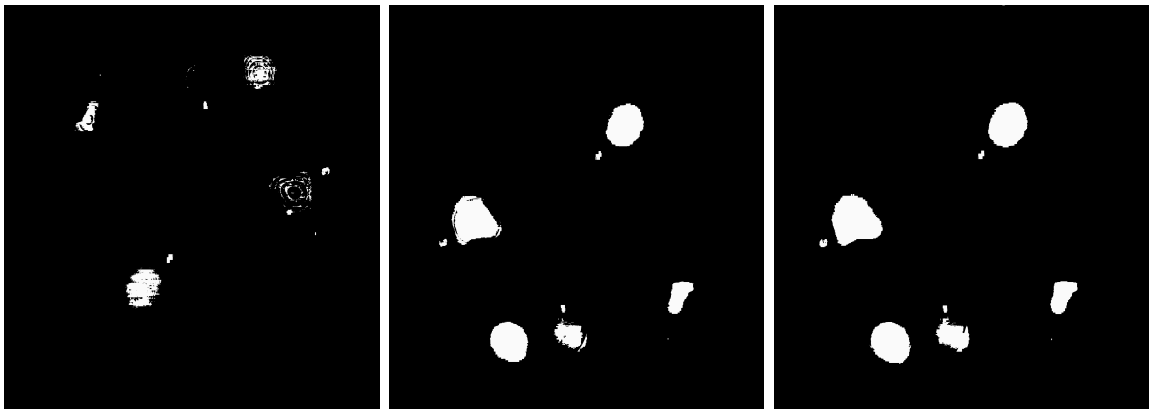

(a) Block size 1 (b) Block size 2 (c) Block size 3

Figure 3.13: Gaussian adaptive thresholding with different block sizes.

An important factor influencing the efficiency of this method is the block size over which the threshold calculations is being done. The greater the block size, the more prone to errors in water droplet isolation. The smaller the block size, the more difficult it is to detect large water droplet formations.

Gaussian adaptive thresholding with a block size of 2 generally provided the best results. Hence all further analysis will be done on the output mask of the Gaussian adaptive threshold.

3.3.2 Water droplet detection

Now that a mask is established that contains only the water droplets, it is possible to use contour detection to find the outline of all the water droplets. A discussion on contour detection can be found in section 3.2.4. The contours are used to separate the water droplets from the insulator. Only the contours with a length of more than 60 pixels were used. This eliminated all the small contours from small artifacts that were left after Gaussian adaptive thresholding was applied. The contours of the water droplets will be used in the subsequent sections do analysis on the water droplets. The result of contour detection can be seen by the green line drawn on the outer edge of the water droplets in figure 3.14.

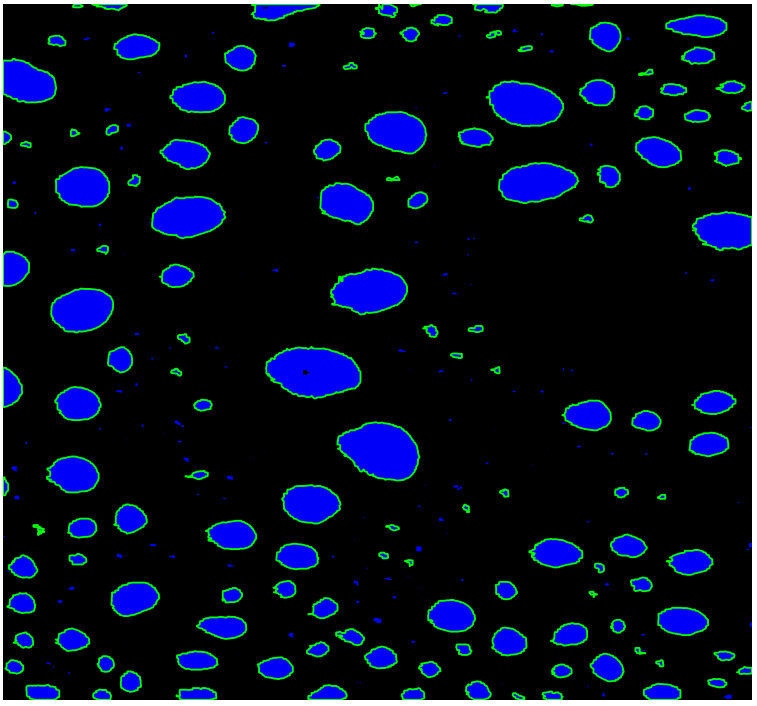

Figure 3.14: Contour detection after gaussian thresholding.

3.3.3 Surface wetness ratio

The primary drive towards creating a hydrophobicity measurement device for polymer insulators is to determine the performance of these insulators along with their ability to insulate a conductor from the supporting structure. Water mixed with pollutants on the insulator's surface create a path for current to flow, resulting in flashover currents. The more water accumulation there is on the insulator's surface, the greater the risk for leakage currents. From this a surface wetness ratio expression is formed.

The surface wetness ratio is the ratio between the area covered with water and the area without any water on it. The greater the ratio, the greater area is covered with water, causing a higher the risk for leakage current to flow over the insulator's surface.

In section 3.3.1, a mask was created to display the areas covered with water droplets. The surface wetness ratio can easily be determined by summing all the areas covered with water

and dividing it by the total number of pixels. Three insulator surfaces were examined, ranging from hydrophobic to hydrophilic. One can observe in figure 3.17 that the surface wetness ratio (WR) has a direct correlation to the hydrophobicity state of the insulator. It is therefore expected that, as the hydrophobicity performance of an insulator decreases, an increase in surface wetness ratio would appear.

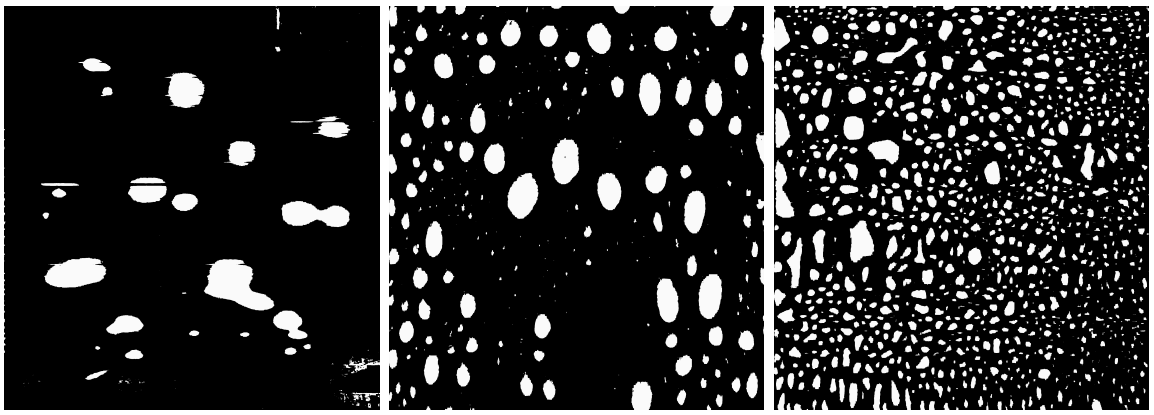

(a) Hydrophobic WR 1:16. (b) Neutral WR 1:7. (c) Hydrophilic: WR 1:5.

Figure 3.15: Surface wetness ratio for insulators with different hydrophobicity states.

3.3.4 Puddle size

An investigation into water puddle formation on the insulator's surface was conducted to see if a correlation could be found to its hydrophobicity state. By analysing the distribution, the different surface areas that the water droplets accommodate, a hypothesis was constructed as follows:

- **Small puddles:** This can indicate that the surface is mostly hydrophobic. As soon as a water droplet becomes too large, it will easily slide off a hydrophobic surface.
- **Large puddles:** With the majority of the water droplet formations on the insulator's surface being large, this can indicate that the surface is mostly hydrophilic. Hydrophilic surfaces tend to attract water, rather than repel it. Thus, as water is being sprayed on the surface, the accumulation of water droplets into puddles will grow until the insulator's surface attraction to water is unable to support the weight of the puddle that gravity imposes on it.
- **Various puddle sizes:** This can be an indication of different hydrophobicity states on the insulator 's surface. It might also be that water that was sprayed on the surface was done unevenly.

Three different insulator surfaces were investigated, ranging from hydrophobic to hydrophilic as seen in figure 3.16 - 3.18 histograms were constructed within each bin, representing the total puddles that fall within a certain range of surface areas. It can be seen from this that for figure 3.16, representing a hydrophobic surface that there is a large distribution of water puddles in the small surface area ranges. Figure 3.18 represents a hydrophilic surface that has a distribution over small and large puddles. It should be interpreted that, since large puddles take up a large surface area, the total number of large puddles will not dominate the total number of small puddles.

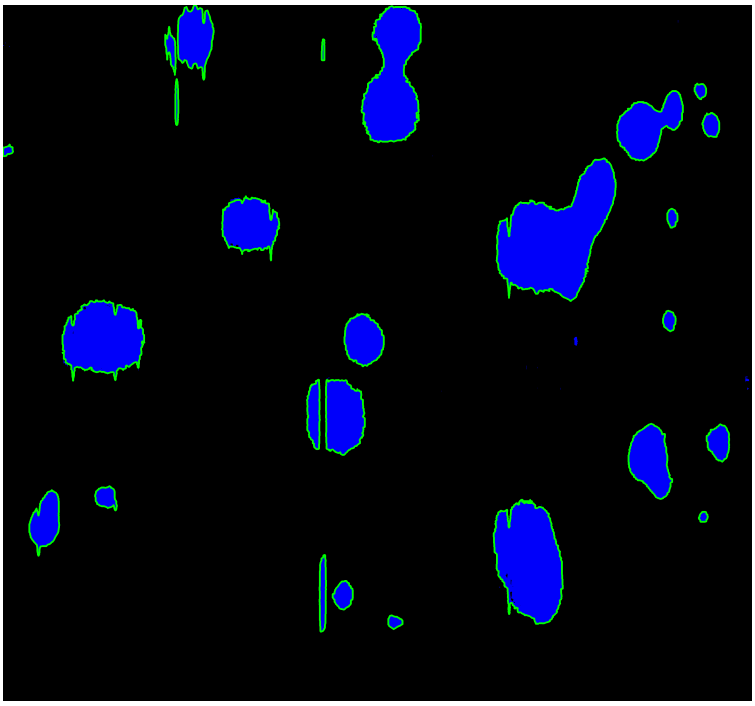

(a) Water droplet detection output

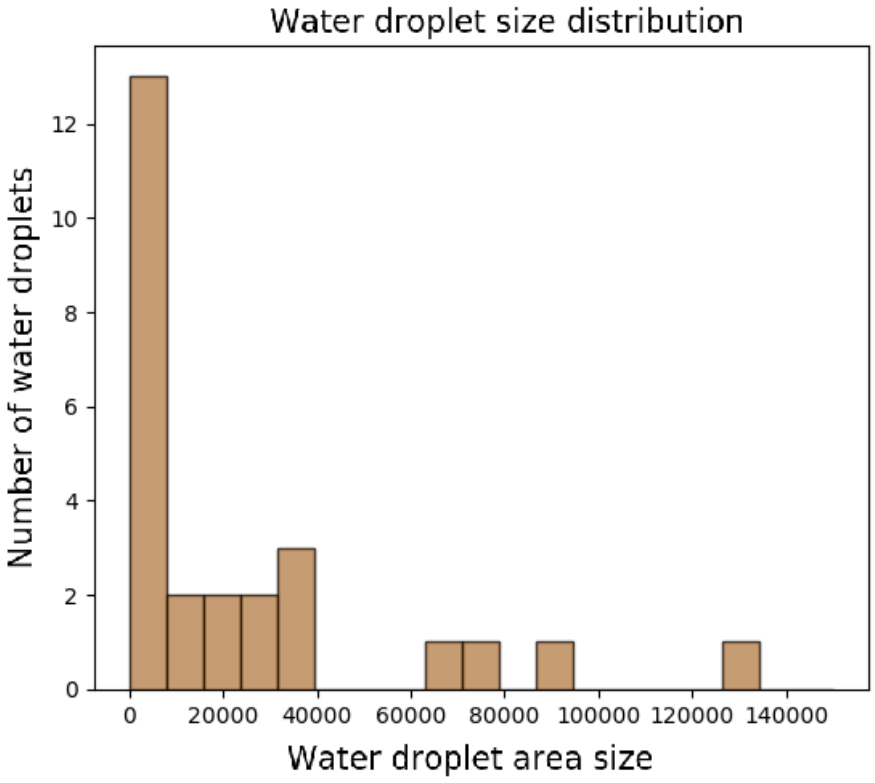

(b) Histogram distribution of puddle sizes

Figure 3.16: fig:Puddle size analysis of hydrophobic surface.

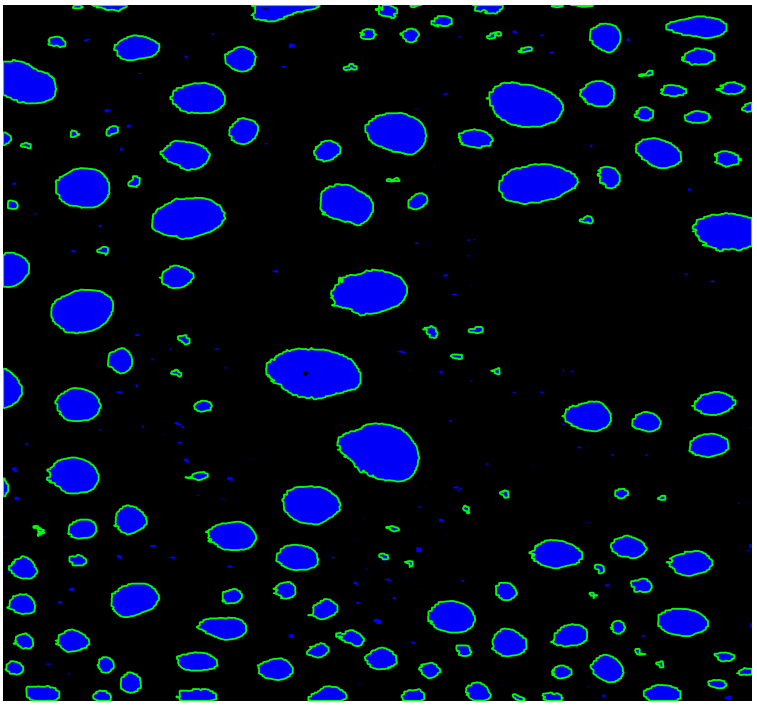

(a) Water droplet detection output

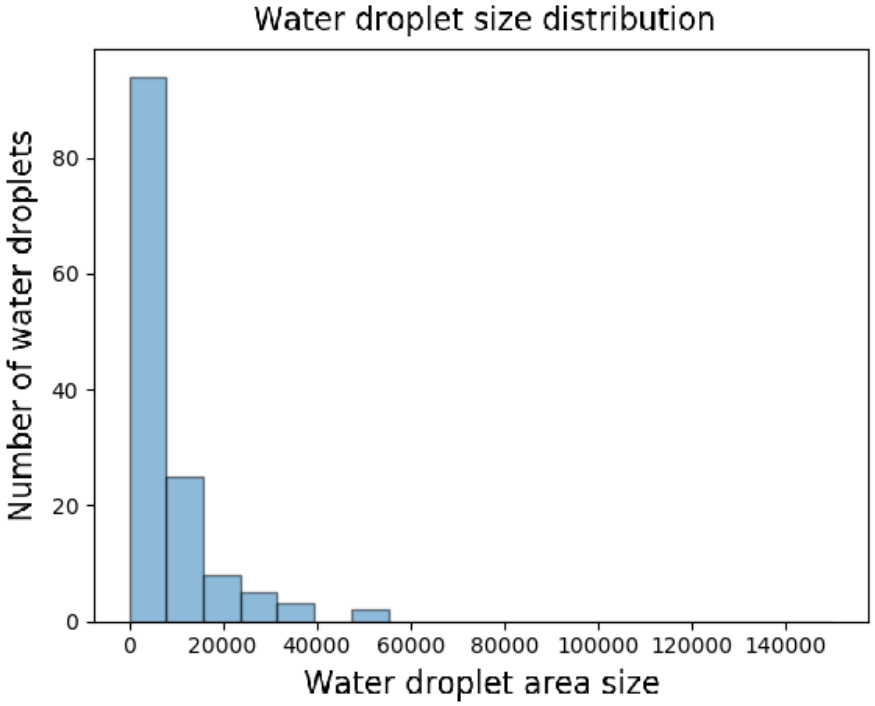

(b) Histogram distribution of puddle sizes

Figure 3.17: Puddle size analysis of medium hydrophobicity surface.

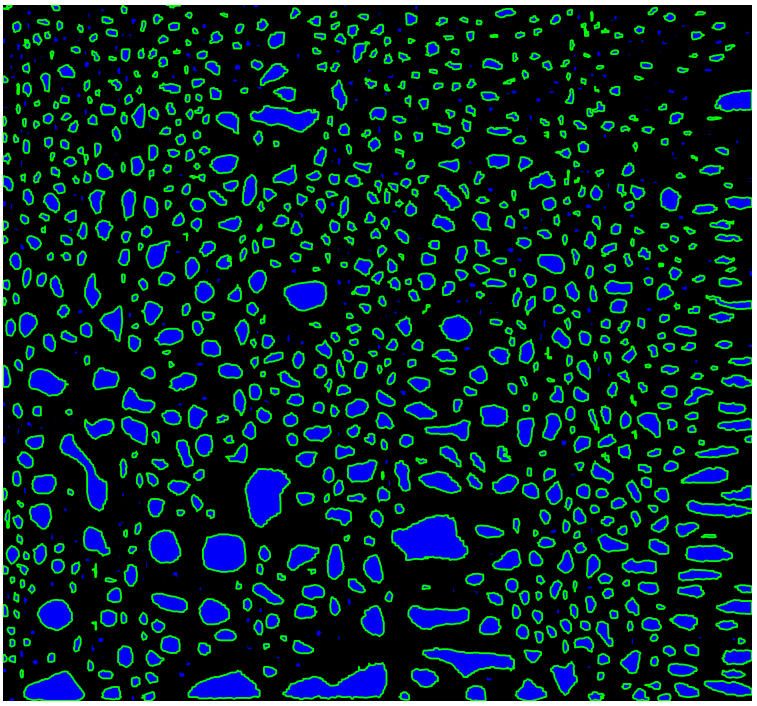

(a) Water droplet detection output

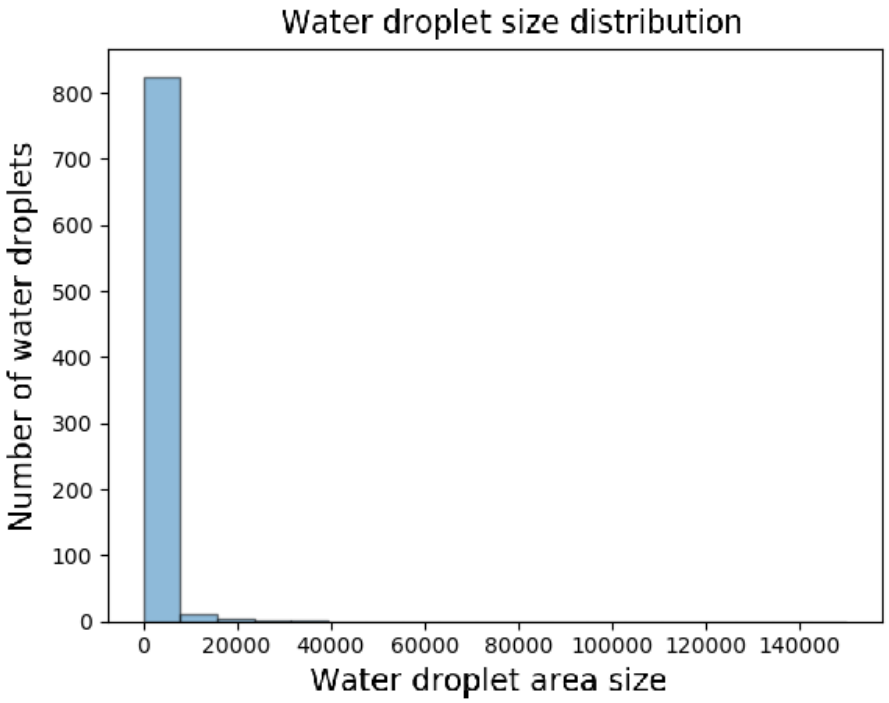

(b) Histogram distribution of puddle sizes

Figure 3.18: Puddle size analysis of hydrophilic surface.

3.4 Data harvesting

3.4.1 Camera setup

During the entire 3D laser profiling technique, a Canon EOS Rebel T6 was used to conduct experiments with. The camera was primarily used to capture videos. The camera had the following specifications:

Camera:

- Canon EOS Rebel T6
- Sensor: 18.0 Megapixel CMOS (APS-C)
- ISO: 100-6400
- Video Capture: 1920 x 1080 p - 30 fps, 1280 x 720 p - 60 fps

Lens:

- SeriesIS II Canon EF-S
- Aperture: f/3.5-5.6
- Focal depth: EF-S 18-55mm IS II lens

During experimentation, it was found that setting the camera sensor to a low ISO sensitivity resulted in less noise being generated on the line laser by the camera's sensor. It also aided in isolating the line laser from the background by only capturing the brightest parts of the image. By using an aperture of F3.5, the camera 's sensor was exposed to the maximum available light from the lens. This significantly helped to get a sharp image of the line laser and eliminated color washing around the line laser edge.

The resolution of the 3D profile is dependent on the resolution at which the video is being taken, as well as the frame rate. To achieve the same resolution in the X–Y direction of the 3D profile, the frame rate multiplied by the scanning time should be equal to the horizontal resolution of a frame in the video. Therefore, having a higher frame rate reduces the scanning time needed to get a corresponding resolution in the X–Y plane.

The higher the vertical resolution is of the video being taken, the better the resolution will be in the Z–coordinate of the 3D surface profile. It is important to take into consideration that the vertical displacement of the line laser, as it travels over water droplets on the surface being scanned, is not an exact representation of the vertical height of the individual water droplets. This is because the camera is set at an angle and not parallel to the horizontal line. This effect is negligible as long as the camera angle to the horizontal plane of the surface is kept the same.

3.4.2 Insulator selection and placement

For initial tests and proof of concepts, square polymer composite insulators will be used, sized at 120 mm x 140 mm. A selection of five squares was used. The square insulators were placed at 30° angle.

3.4.3 Water spray methods

It is important that the method being used to spray the insulator's surface can give repeatable results. Two methods were investigated, with a third modified method also used thereafter.

STRI method

According to the Swedish Transmission Research Institute (STRI) guide, a common spray bottle should be used to produce a fine mist of water. The surface should be sprayed with

about 20 pumps of the bottle over a span of 20 seconds. After 5 seconds, an image / scan should be taken for analysis.

Water misting system

The water misting system discussed in section 2.6.1 was used to spray the insulator's surface with isopropyl alcohol water mixtures.

This method unfortunately did not work that well. For various isopropyl alcohol water mixtures, the same formation of water droplets was observed. It almost appeared as if the isopropyl alcohol had no effect on the surface tension of the water droplets. It could have been due to the isopropyl alcohol evaporating before making contact with the insulator's surface, because it was sprayed as a fine mist. This method was subsequently abandoned.

Modified STRI method

This method builds on the principles of the STRI method. A water spray bottle is used to apply a fine mist of water to the insulator's surface. Mist is applied to the surface until the first waster droplet runs off the insulator's surface. Directly afterwards, the surface will be scanned to obtain a 3D profile.

3.4.4 Isopropyl alcohol mixtures

The goal of using isopropyl and water mixtures was to emulate different hydrophobicity states on the insulator's surface. New insulators are hydrophobic and as they degrade over the years, they become hydrophilic. Isopropyl alcohol mimics this behaviour by lowering the surface tension of water on the insulator's surface.

In order to analyse different degrees of surface tension, various ratios of isopropyl alcohol to deionized water were mixed in 500 ml glass bottles. The higher the ratios of isopropyl alcohol in the water solution, the more hydrophilic the insulators surface becomes. The concentration of isopropyl alcohol within the deionized water solution was as follows:

- 0% (Hydrophobic)
- 10%
- 20%
- 30%
- 40%
- 50%
- 60% (Hydrophilic)

After spraying the insulator's surface with 0% isopropyl alcohol, it is expected that uniform, well rounded droplets would be present. For medium concentrations, it is expected that water puddles will be present, with puddles becoming more prominent as the concentration increases. For high concentrations, it is expected that a film of the water mixture would cover the majority of the insulator's surface.

Chapter 4

Methods and results

4.1 Introduction

The machine learning and laser techniques discussed in chapters 2 and 3 were used to conduct tests on several different insulators with different hydrophobicity states. The various hydrophobicity states were emulated by adding different mixtures of water and isopropyl together, resulting in a change of water surface tension on the surface.

4.2 Laser technique

4.2.1 Overview

The laser technique developed in chapter 3 were used to measure the following attributes.

- Surface wetness ratio
- Amount of water droplets on surface
- Water droplet size distribution

It was expected that each of these attributes will have some correlation to the insulator's surface hydrophobicity. The shortcomings of these analysis were investigated to why certain measurements failed.

Five insulators were used to conduct the exact same tests in order to find a general trend in the measurement results. Seven different mixtures of water and isopropyl were used starting from 0% isopropyl up to 60%. Higher concentrations of isopropyl were not necessary because a mixture of 60% and above resulted in the same complete hydrophobicity loss.

4.2.2 Surface wetness ratio

By analysing the surface wetness ratio, it is desired that a pattern between different hydrophobicity states and the area covered by water would be present. The greater the area covered by water; the more preferential leakage current flow paths would be present.

In section 3.3.3, the method for determining a surface wetness ratio was discussed. Five insulators were evaluated with seven water:isopropyl mixtures. Insulators were scanned and water droplets were isolated from the insulators. The results for this analysis can be seen in figure 4.1.

By looking at the dashed line representing the average of the surface area covered by water droplets, a general trend appears, indicating an increase in surface area covered by water droplets as the percentage of isopropyl increases.

Insulators 2, 4 and 5 provide a general upward trend as the percentage isopropyl mixture increases. Insulator 1 displays a decrease in percentage water cover at 50% isopropyl mixture. With a 30% water cover at 50% isopropyl mixture, it can be seen that there is a 7% water cover drop from the general trend. With a high concentration of isopropyl water mixture, the surface tension of the water sprayed onto the insulator's surface is very low. This results in water droplets which are low in height. The laser scanning method is very sensitive to changes in height, but when a shallow film of water is formed on the insulator's surface, it becomes extremely difficult to detect deformation of the line laser as it moves across the surface. In fact, given the low height of a film water formation, it is spectacular to observe the ability of this technique to still detect these water formations. Unfortunately, with a shallow film of water, the results are not that consistent, given that it cannot always detect the shallow water film formations.

By observing the surface area covered with water on insulator 2 over the entire range of water:isopropyl mixtures, it can be seen that initially, the surface area covered is 36% for pure water, decreasing for 10% and 20% isopropyl mixtures. With a decrease of only 2.4%, one can point this behaviour to random spray patterns and random water formations. As for each of the water:isopropyl mixtures, the insulator's surface was cleaned and left to dry before another water:isopropyl mixture was sprayed and scanned.

Overall, this method provides an indication to the surface hydrophobicity; however, because of random water formations, multiple scans should be done to get a more accurate idea of the insulator's hydrophobicity state. This analysis works well on low to medium hydrophobic surfaces. For surfaces with hydrophilic behaviour, this method is still capable of detecting water formations, although results would not be consistent.

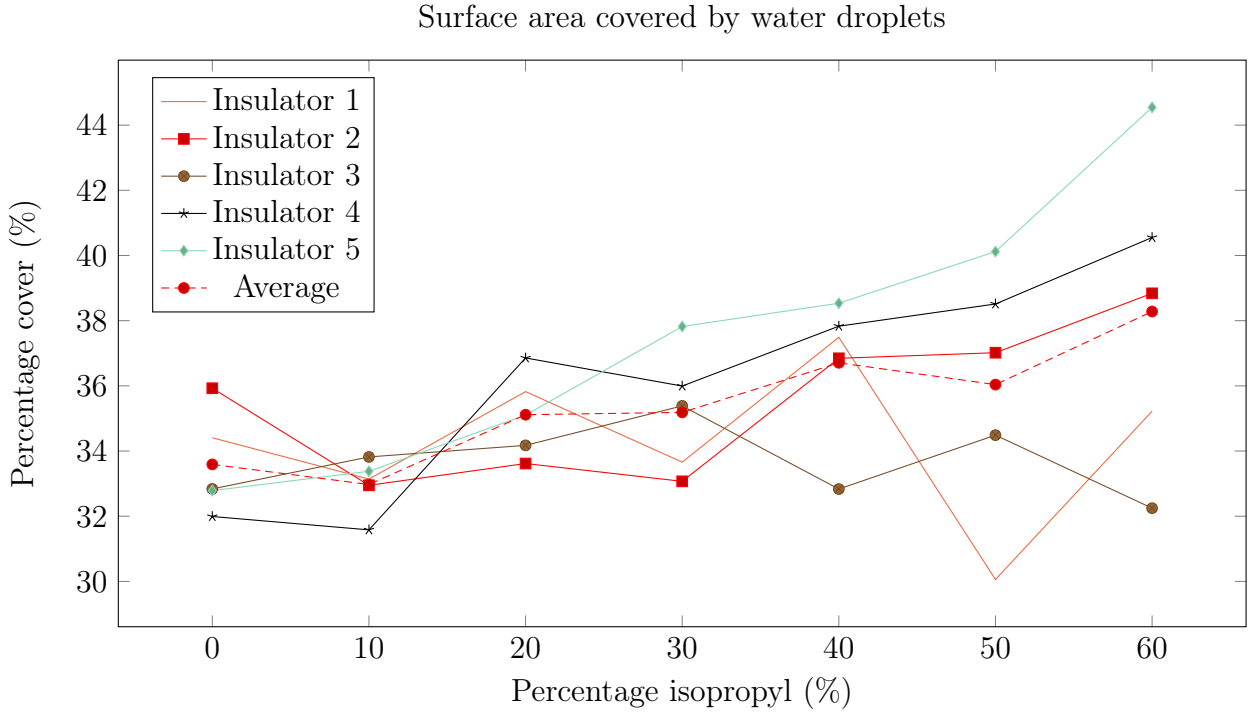

Figure 4.1: Cost after each epoch.

4.2.3 Amount of water droplets on surface

In section 3.3.4, a description of the behaviour of the puddle size on different hydrophobicity surfaces was discussed. With a decrease in hydrophobicity, it is expected that larger water formations would start to form. Therefore, a decrease in the amount of water droplets on the insulator's surface are expected for a decrease in hydrophobicity. However, this did not hold up.

In section 3.3.2, the method of counting the total number of water droplets on an insulator's surface was discussed. After analysing five different insulators for various ratios of water:isopropyl mixtures, results were obtained as displayed in figure 4.3

By looking at the average amount of water droplets for all five insulators, one can observe that there is an upward trend in the amount of water droplets for a decrease in hydrophobicity. This contradicts the idea that as a surface becomes hydrophilic, water puddles become larger, occupying a larger part of the insulator and resulting in a smaller amount of water droplets.

An investigation into this behaviour was made by looking at all results from the water droplet detection for each of the water:isopropyl mixtures. One of the deficiencies of the laser scanning method found was in fact aiding in providing a meaningful trend with the amount of water droplets on the insulator's surface.

In figure 4.2, it can be seen that for a higher concentration isopropyl water mixture, the water droplets become less uniform and irregular puddles start to form. At the highest water:isopropyl mixture (60%), it can be seen that the laser method fails to accurately reconstruct the film of water on the surface of the insulator, as expected from the discussion above in section 4.2.2.

What is interesting is that, although an accurate reconstruction of the water film formations is not possible, the algorithm believes that there are more water droplets than there actually is. This in turn supports the general trend seen in figure 4.3

In summary, the less hydrophobic a surface becomes, the more artifacts on the reconstructed surface will appear and the higher the water droplet count would be. A strong correlation exists between the increase of isopropyl in the water mixture and the number of water droplets.

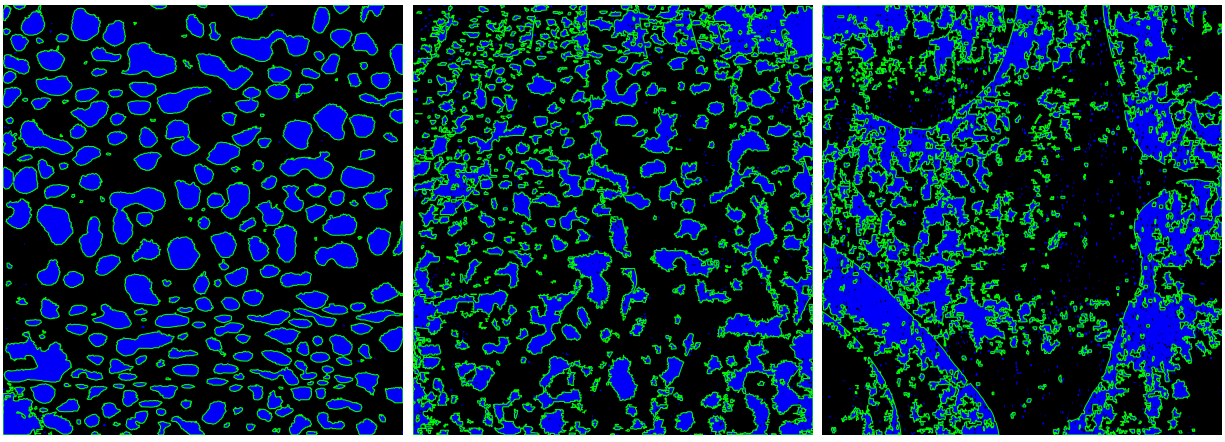

(a) 0% (b) 40% (c) 60%

Figure 4.2: Water droplet detection for different water:isopropyl mixtures.

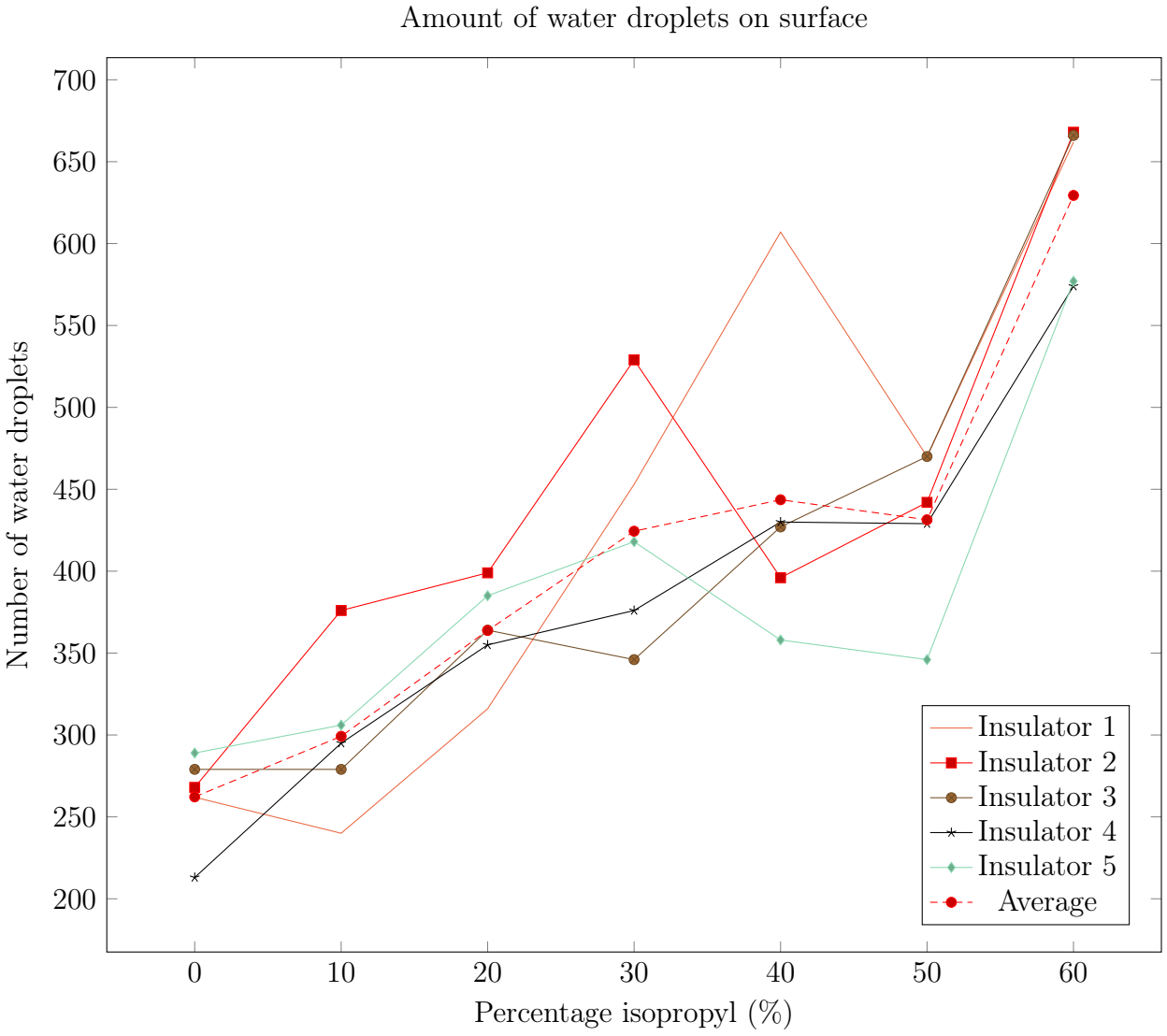

Figure 4.3: Amount of water droplets for different water:isopropyl mixtures.

4.2.4 Water droplet size distribution

It is expected that the size of the water droplets will provide insight into the hydrophobicity state of the insulator. In figure 4.4, the histogram distribution is displayed for insulator 1 for various water:isopropyl mixtures. The data displayed in the histograms will be discussed for each mixture. Note that the Y-axis on the histogram representing the number of water droplets is different for each histogram. The area of the water droplet is determined by counting all the pixels in an image covered by a water droplet.

Figure 4.4a

With 0% water:isopropyl mixture, it can be seen that there is a wide distribution of water droplet sizes with only about 30 very small water droplets. Since large water droplets encompass a large surface area on the insulator, it can be seen that there are not many water droplets. Although there are not many large water droplets, the existence of them provides insightful meaning to an insulator with hydrophobic behaviour.

Figure 4.4b

It can be seen that, for the 10% water:isopropyl mixture, there is a significant change in the water droplet area size distribution. With a lower water droplet surface tension, it can be seen that large water droplets cease to exist. There is an increase in smaller water droplets by a factor of 3 from the 0% water:isopropyl mixture.

Figure 4.4c

As the water:isopropyl mixture increases, an increase in smaller water droplets can be observed.

Figure 4.4d

A decrease in smaller water droplets and increase in medium sized water droplets can be observed. This is due to the random formation of water droplets. It is expected that with only a 10% isopropyl mixture increase, the insulator might provide the same or slightly worse results than its neighboring water:isopropyl mixture.

Figure 4.4e

With a 40% water:isopropyl mixture, the surface tension of the water on the insulator's surface is very low. As discussed in section 4.2.3, the laser technique fails to accurately reconstruct a film of water. The result is that the algorithm detects large quantities of small water droplets, which coincidentally fits the general trend of the water droplet size distribution.

Figure 4.4f and 4.4g

A small number of large water droplet formations exist with a large amount of small water droplets. This is an indication that the surface is completely hydrophilic and that many artifacts exist because of inaccurate scanning.

Summary

The water droplet size distribution provides meaningful data of which a conclusion can be drawn for surface hydrophobicity state.

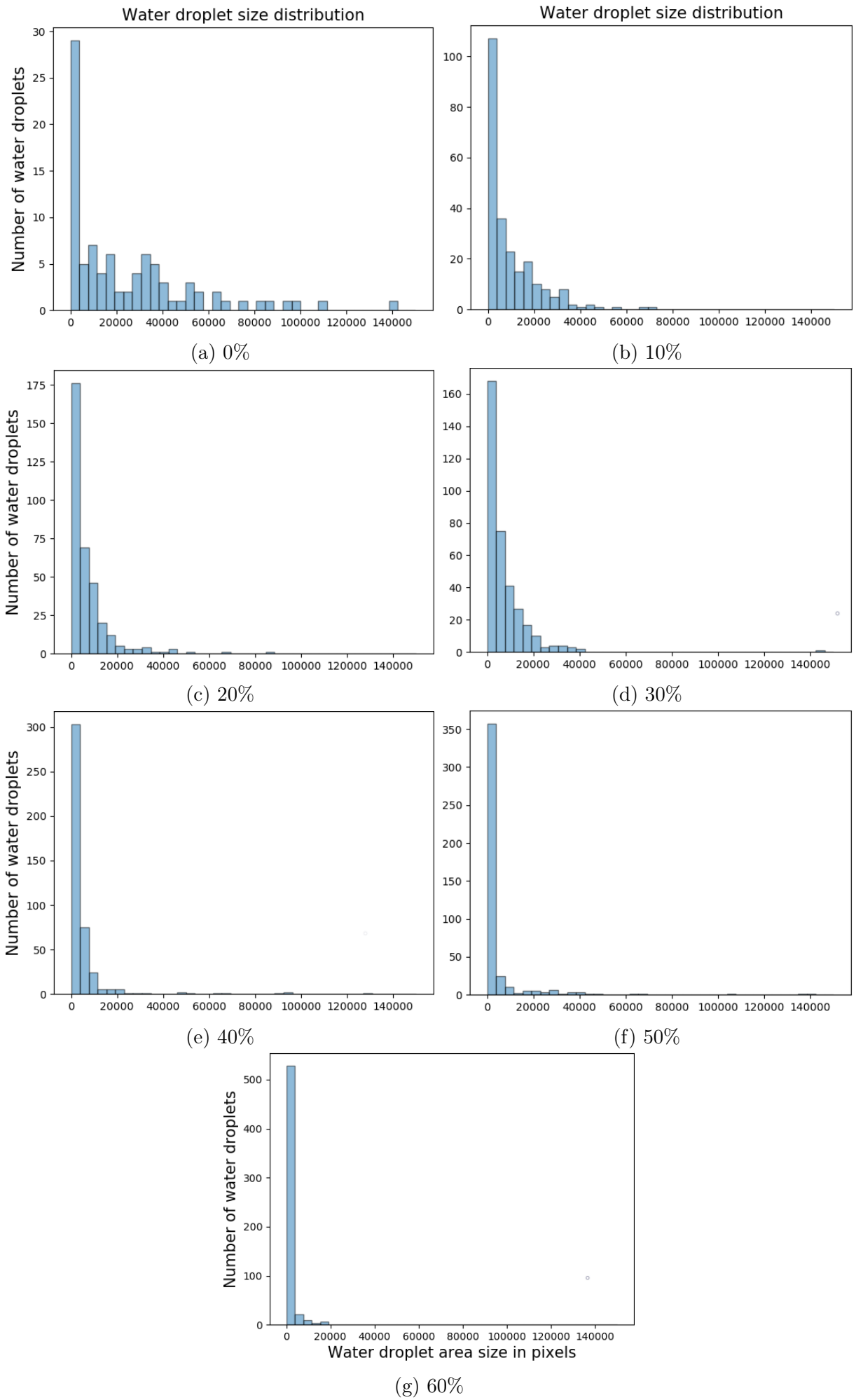

(a) 0%

(b) 10%

(c) 20%

(d) 30%

(e) 40%

(f) 50%

(g) 60%

Figure 4.4: Water droplet size distribution.

4.3 Machine learning method

4.3.1 Water droplet hydrophobicity classification

In chapter 2, a machine learning method was used to train a convolutional neural network. The implementation of this method was as follows:

- A high-resolution image of the insulator was acquired.
- The image was then divided up into blocks with the same size as which the neural network was trained on (10 mm),
- Fed the images into the neural network for classification

After classifying all the individual images, analysis could begin to get an overall understanding of the hydrophobicity state of the insulator.

In the following figures, insulators with different water formations, representing different degrees of hydrophobicity states, will be discussed. In each figure, sub-figure (a) is the original image and sub-figure (b) is the original image with a heat map overlay. The heat map contains the different numbers that are the classes in which the neural network classified each sub-image. Lighter colors of the heat map display a hydrophobic instance of the water droplets within the sub-image, while darker colors represent a hydrophilic behaviour.

It should be noted that, during the beginning stages of developing machine learning method to do image analysis, the algorithms were unable to classify images into their correct class. Even though the training set provided acceptable training test results, testing it on unseen images provided poor results. This was due to a lack of training data and neural networks that were trained to be biased. A biased network generally starts to learn to recognize the data that it was provided with, rather than learning the patterns that exist within each class of the data. The result is that, when new data is introduced to the neural network, it is unable to provide accurate results.

All the images that were classified below were images that the neural network has not seen before. Thus, the neural network does a classification based on the patterns it recognized from the training data for each class.

Figure 4.5 breakdown

Evaluating figure 4.5a, one can see that there are many hydrophobic water droplets on the surface of the insulator. There is also a patch where a water droplet ran down taking all other water droplets with it in its path. At the bottom of the insulator there are medium sized puddles that formed.

After sub-image analysis, the labeled sub-images can be seen in figure 4.5b. It can be seen that there is a general class 1 classification for the majority of the sub-images. This corresponds to the predefined classes used to classify the training set in section 2.6.2. Class 0 sub-images can be seen where the water droplet ran down the insulator. This is correct, as the training set contained sub-images with empty patches with some having very small water droplets on it. There are also several class 2 and 3 sub-images that were classified correctly. However, there are some errors existing in the classified image, especially along the bottom of the image and almost all of the class 4 images.

The majority of the sub-images that were classified incorrectly can be attributed to the sub-image division process. Inspecting the sub-image (x,y) = (4,10) classified as class 4

on its own, it is not possible to tell in which class it belongs to from class 2 - 4. However, evaluating the general trend of all the classified sub-images, it can be concluded that adequate classifications were made.

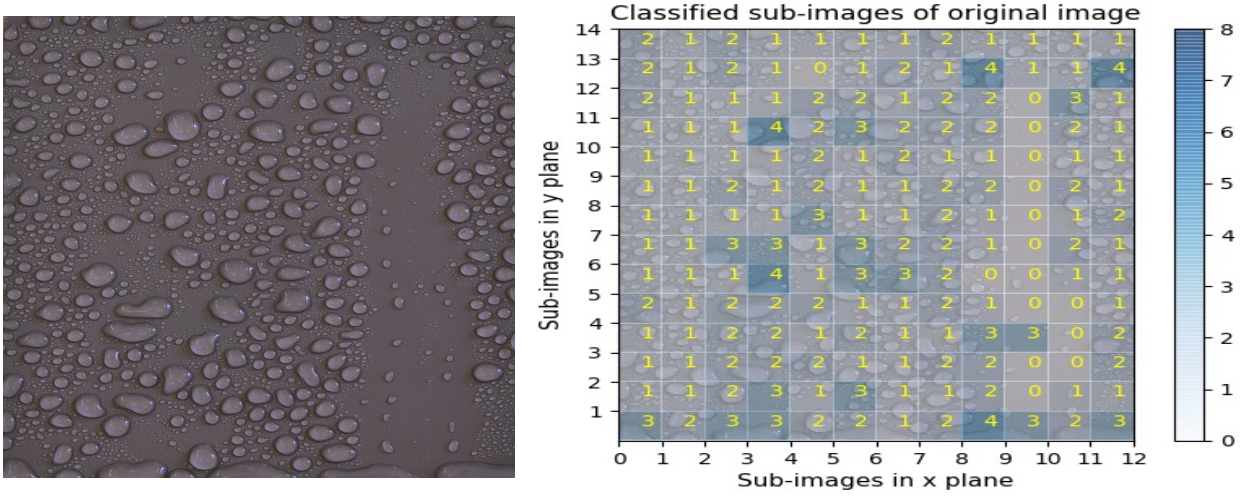

(a) (b)

Figure 4.5: Original image with heat map and classified sub-images insulator 1.

Figure 4.6 breakdown

It can be seen in figure 4.6a that the majority of the water droplets can be categorized as class 1. Several empty patches relating to class 0 exist. The larger water droplets can be classified as a class (2 - 3). There should be nothing in class 4 and higher.

Observing the classified sub-images in Figure 4.6b, it can be seen that the majority of the sub-images where classified into their correct classes. However, looking closely at the class 4 sub-images, one can see that they should be moved to either class 1 or 2. The same could be said for the class 3 sub-images, with an exception for (x,y) = (9,12). Some of the class 2 sub-images could also be moved into class 1. Nonetheless, class 1 and class 2 have many similarities, making this classification acceptable.

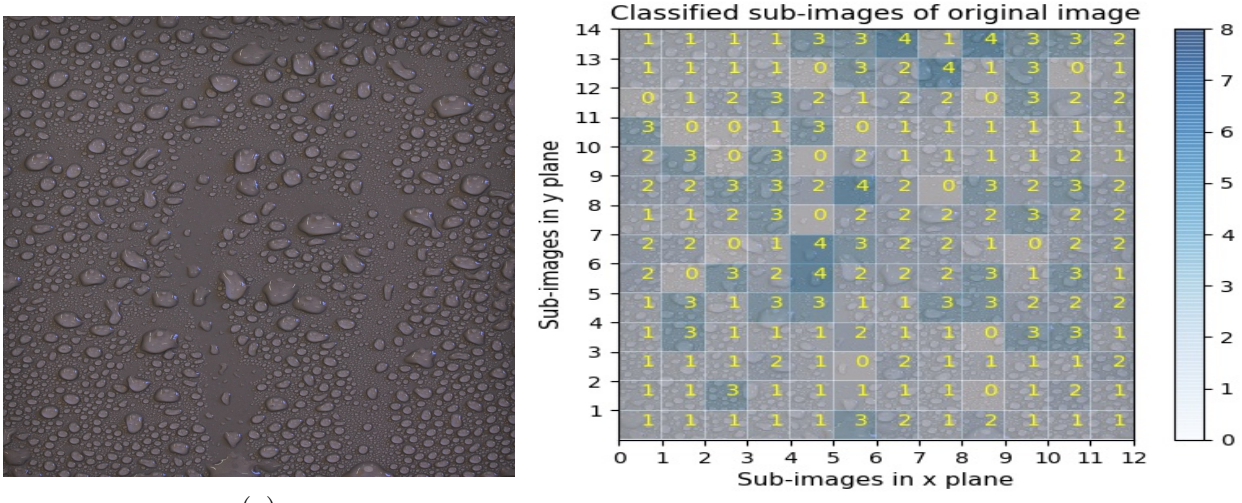

(a) (b)

Figure 4.6: Original image with heat map and classified sub-images insulator 2.

Figure 4.7 breakdown

Evaluating figure 4.7a, it can be seen that the majority of the sub-images from (x) = (0 - 2) should be classified as a class 0 or 1. For (x) = (3 - 8), some sub-images should be classified into class 0 and others into class 2 - 3.

It can be seen in figure 4.7b that for (x) = (0 - 2) there exists several errors. This is because the training set did not contain such images on which the neural network could be trained on. For (x) = (2 - 8) some sub-images should have been classified into a class 0 rather than class 3.

Although some errors are present in this image, the general classification of all the sub-images is class 4 and smaller. This gives an indication that the insulator behaves in a somewhat hydrophobic manner. These types of errors are expected, given the relatively small dataset used for training.

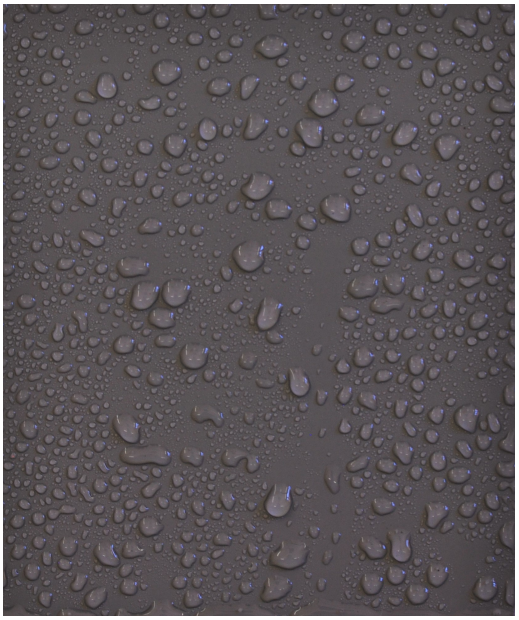

(a)

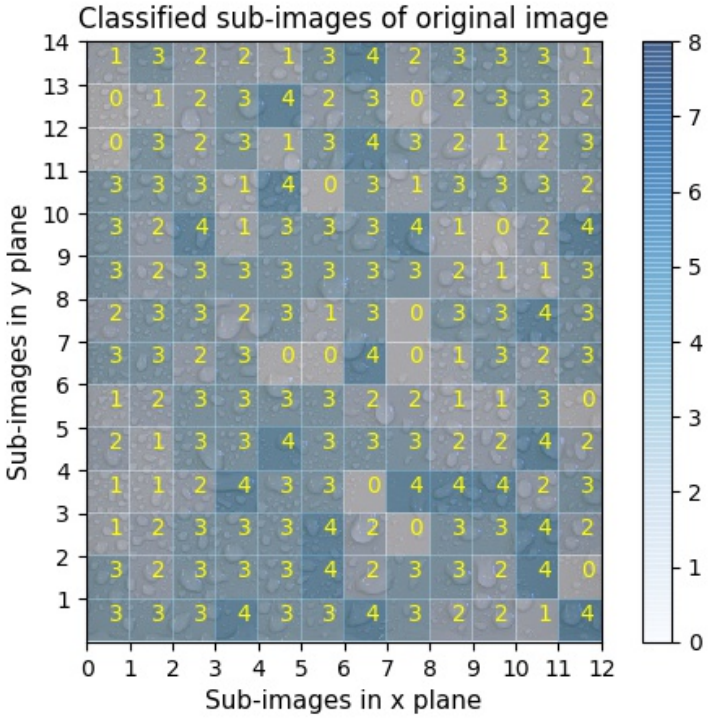

(b)

Figure 4.7: Original image with heat map and classified sub-images insulator 3.

Figure 4.8 breakdown

Assessing the general hydrophobicity state of the water formations on figure 4.8a, it can be seen that the surface tension of the water droplets is medium to low.

With the majority of the sub-images in figure 4.8b being class 3, the neural network was able to successfully do a correct classification. It should be noted that there are several sub-images that should have been classified as class 1, such as in the bottom right hand corner.

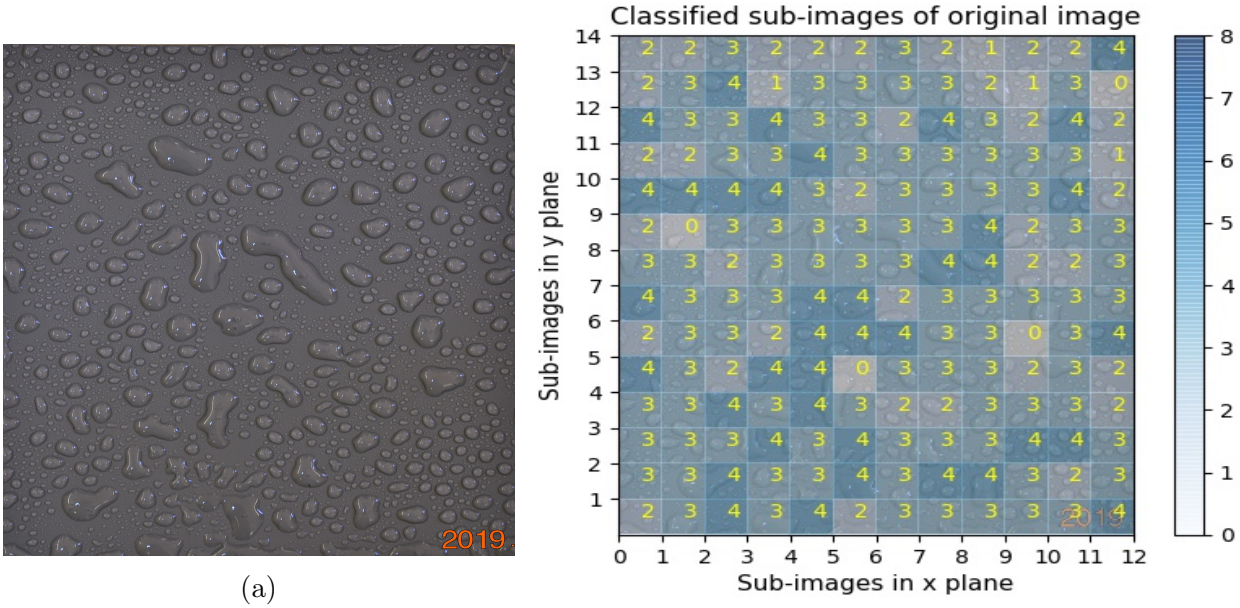

(a) (b)

Figure 4.8: Original image with heat map and classified sub-images insulator 4.

Figure 4.9 breakdown

In figure 4.9a, it can be seen that the surface tension on the water droplets is very low. Water tears can be seen with no sign of hydrophobic behaviour on the surface. The overall prediction of this image should be hydrophilic.

The classified sub-images in figure 4.9b describe a surface which behaves in between a hydrophobic and hydrophilic surface. However, the correct classification would be that this surface is hydrophilic. The majority of the classifications should be in the range of class 5 - 6.

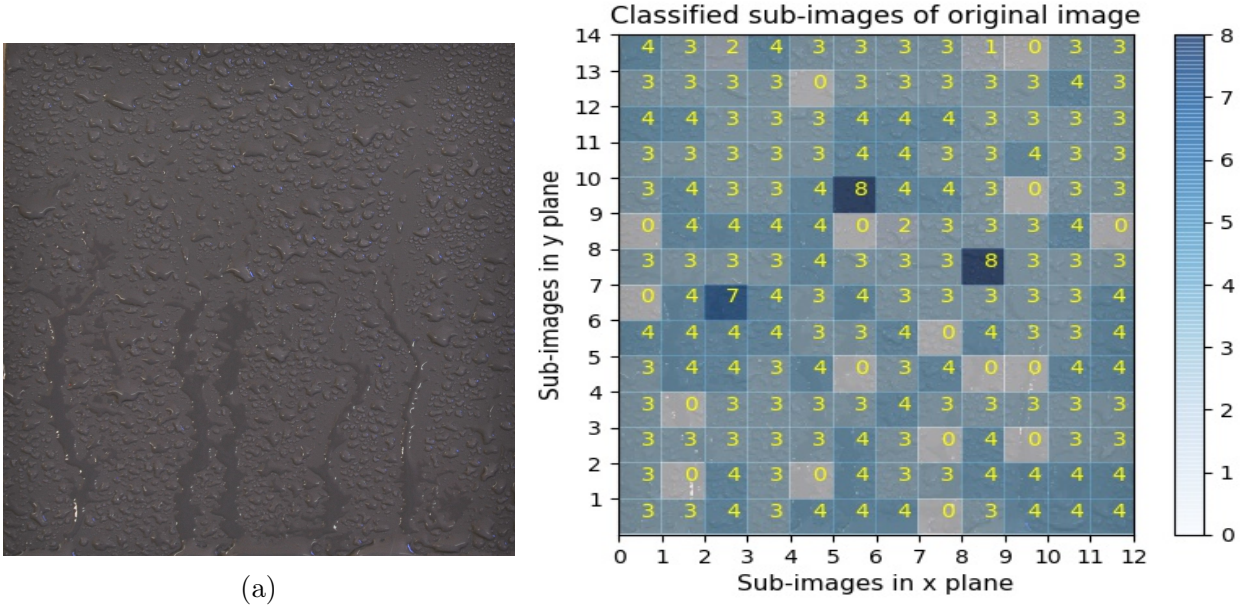

(a) (b)

Figure 4.9: Original image with heat map and classified sub-images insulator 5.

Figure 4.10 breakdown

As with the previous figure, in figure 4.10a, the water droplets show hydrophilic behaviour. There is not a film of water that has formed, indicating that the sub-images cannot be classified as a class 8. Non uniform water droplets that look as if they are flat to the surface can be seen. This indicates to classes 5 - 7.

In figure 4.10b, the neural network was able to successfully classify the sub-images into class 5 - 7 where the majority of sub-images are class 5. This confirms the poor hydrophobicity state of the insulator.

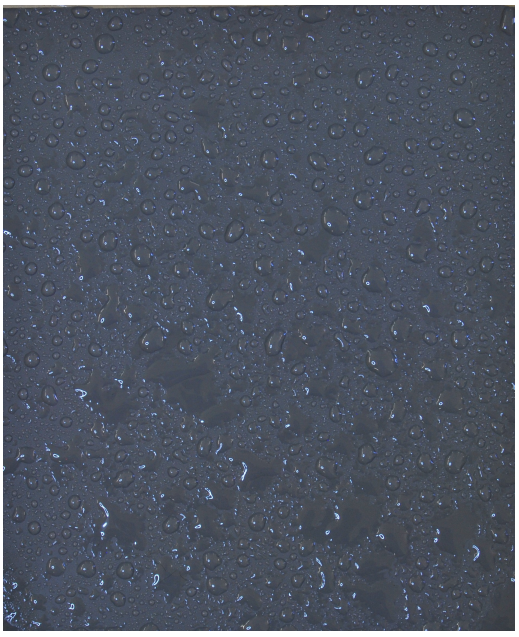

(a)

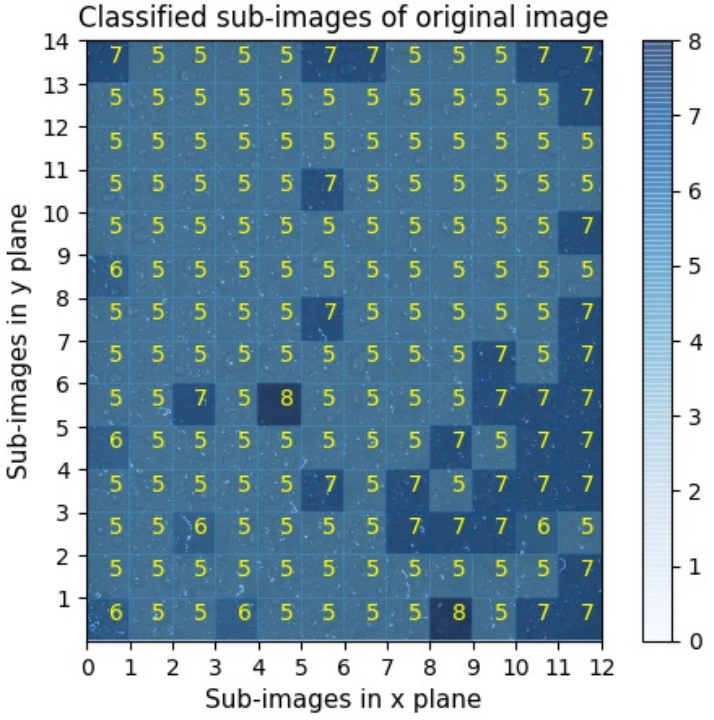

(b)

Figure 4.10: Original image with heat map and classified sub-images insulator 6.

Figure 4.11 breakdown

The surface seen in figure 4.11a can be categorized as completely hydrophobic. With the entire surface covered with water, there is no sign of hydrophobic patches on the insulator.

The neural network was able to make a correct classification. It should be noted that class 7 and 8 are very similar. Even when sub-images were labeled for dataset harvesting, it was hard to distinguish between them. Thus, it is no surprise that uncertainty exists within the neural network by seemingly randomly classifying the sub-images into classes 7 and 8.

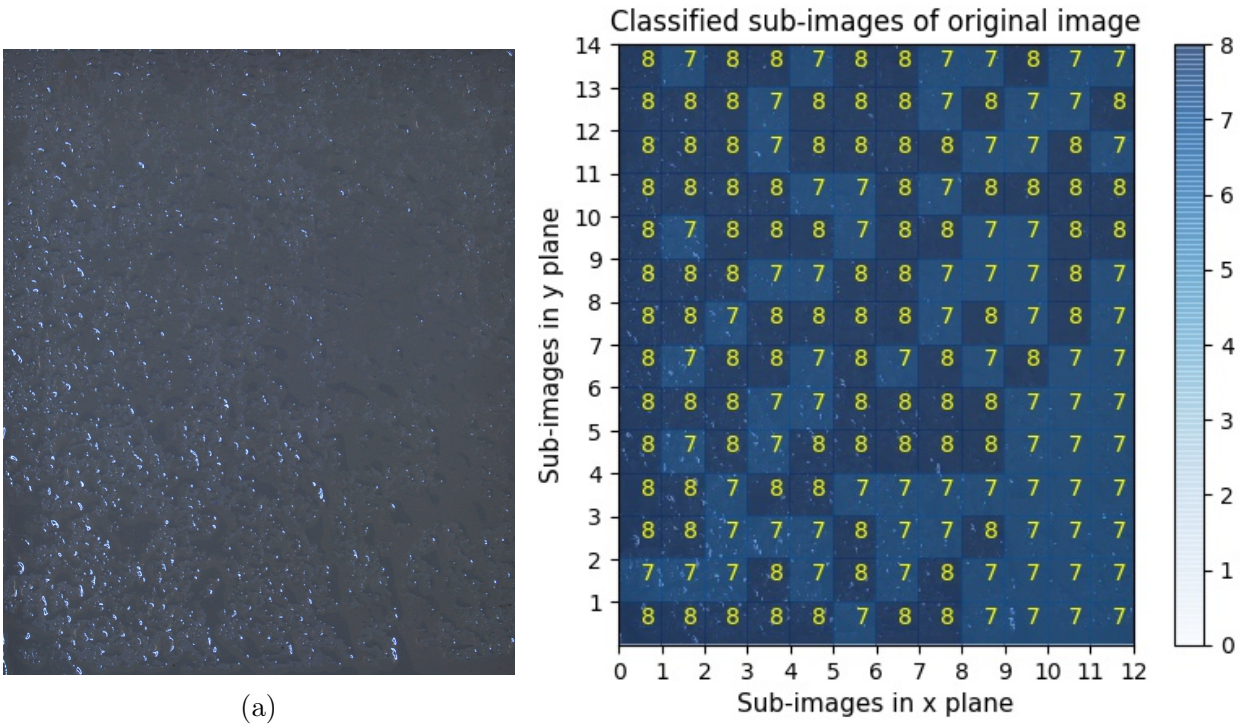

(a)

(b)

Figure 4.11: Original image with heat map and classified sub-images insulator 7.

4.3.2 Histogram distribution analysis of classified sub-images

A histogram of the sub-images for each of the individual figures 4.5b - 4.11b were constructed. Each bin of the histogram represents a classification class. Note that the y-axis differs for each histogram. The goal of histogram analysis was to get a better understanding to what extent each classification class contributes to the insulator's hydrophobicity state. Instead of only classifying an insulator into 9 classes, histogram analysis can provide a more in-depth description on how the insulator's surface behaves. The insulators in figures 4.5b - 4.11b represents the histograms in figures 4.12a - 4.12g.

The histogram in figure 4.12a displays a strong presence for class 1 and 2 with the adjacent classes 0 and 3 also present. By only evaluating the histogram, a conclusion can be drawn that the majority of the insulator's surface is hydrophobic, translating into an insulator with good water repellent properties. Although the existence of class 4 sub-images is present, it is nothing of concern given the overall trend is around class 1. The class 4 sub-images could point to the fact that there are small patches on the insulator that might have more pollution on it, resulting in less hydrophobic water formations on those patches.

With histogram in figure 4.12b revealing similar properties than in figure 4.12a, it can also be concluded that this insulator is hydrophobic. It is important to note, however, that in figure 4.12b, there is an increase of class 3 sub-images. This indicates that there are patches on the insulator that display a small degradation in its water repellent properties. Since that majority of the sub-images are below class 3, the general conclusion is that the surface is still hydrophobic.

In figure 4.12c, the histogram displays a strong presence for class 3, with an increase in class 4 sub-images. This indicates to a loss of strong hydrophobic properties. The patches where classes 3 and greater sub-images are present point to a future failing point where leakage current might start to flow under wet conditions. As discussed with the figure 4.7 breakdown,

many classified errors exist in figure 4.7. Thus, the histogram analysis is not true for the specific figure 4.7, but stays true for the histogram in figure 4.12c.

The histogram distribution in figure 4.12d is situated around class 3. There is a minority presence of class 0 and 1. With the majority of the sub-images classified as class 3 and its neighboring classes, there is a strong indication that this surface is starting to behave hydrophilic. Class 3 - 4 point to possible points of failure in the nearby future. With no indication of classes 6 - 8, it should be noted that the neural network was unable to recognize a film of water on the surface.

The histograms in figures 4.12d and 4.12e have very similar features. Figure 4.12e displays an even more hydrophilic surface with the majority of the sub-images located at class 3 and 4. This displays an insulator at the brink of complete hydrophobicity loss.

In figure 4.12f, the histogram distribution points to a definite hydrophilic surface, since there is no indication of classes 0 - 4. Class 5 indicates that there are non-uniform water droplets that are flat to the surface, while the traces of class 7 and 8 indicates that a film of water is present. This insulator lost its ability to repel water and has high change of providing a preferential flow path for leakage current to flow.

As with figure 4.12f, the histogram in figure 4.12g displays a complete loss of hydrophobic properties, only in an even more extreme manner. The fact that there are no classes other than 7 and 8 indicates that the insulator should be completely covered by a film of water. This insulator is on the extreme hydrophilic state side. It should be noted that since class 7 and 8 share many similarities, the neural network finds it hard to distinguish between them and so one can recognize the two classes as one as the same.

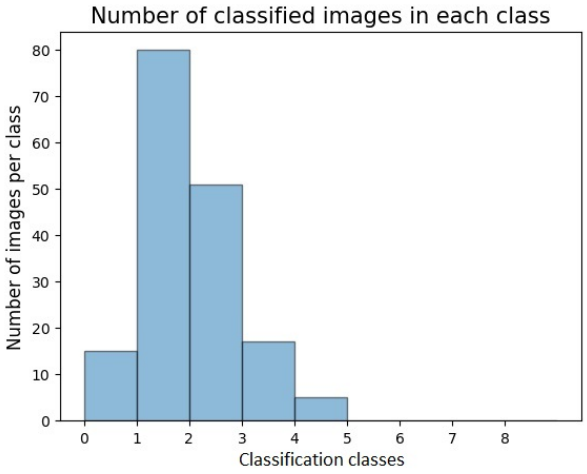

(a)

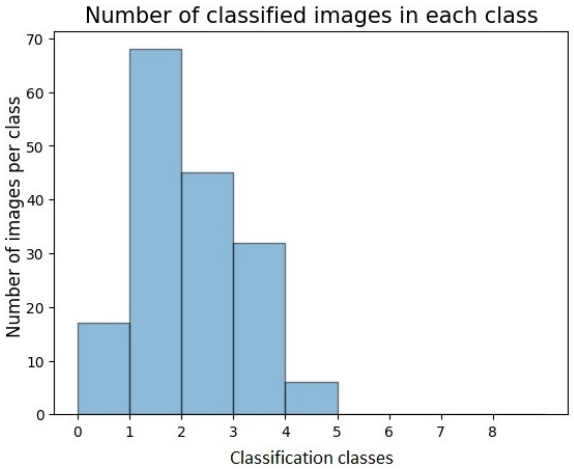

(b)

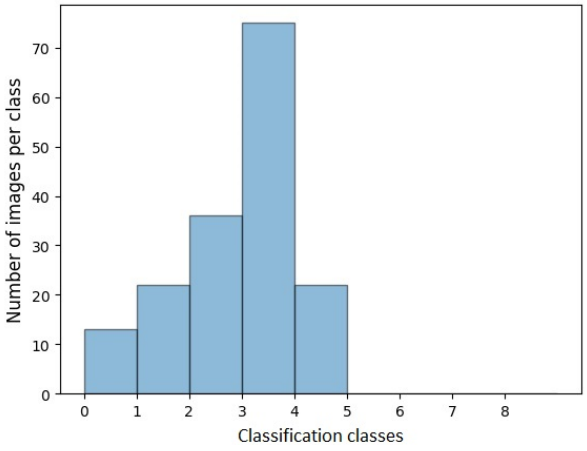

(c)

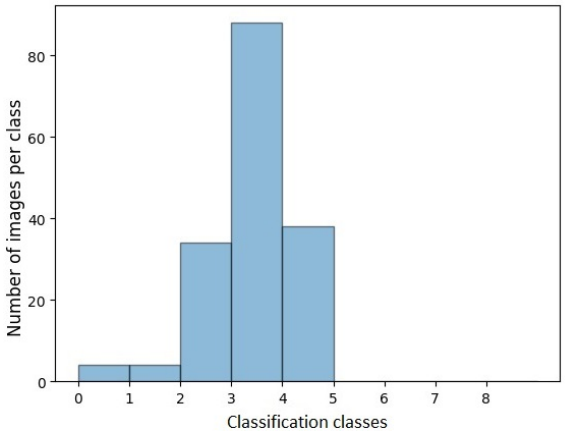

(d)

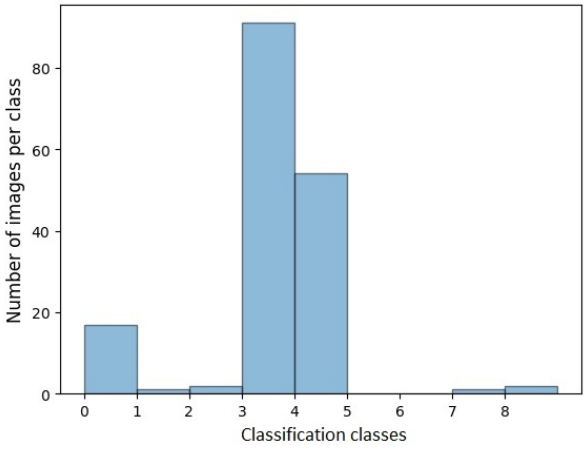

(e)

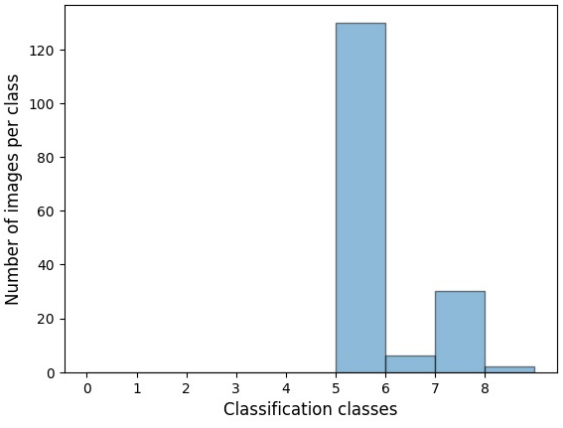

(f)

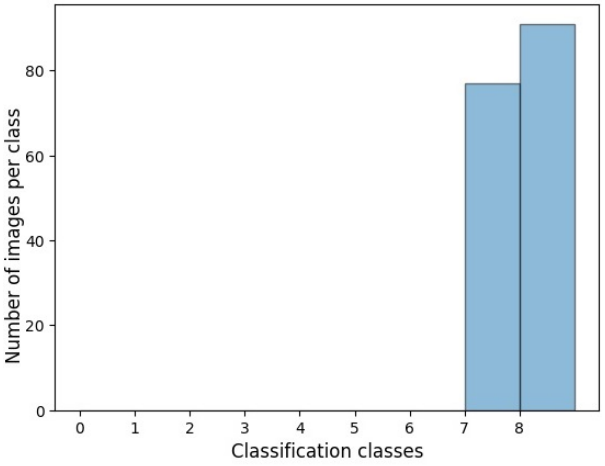

(g)

4.3.3 Average sub-image classification analysis

The histogram analysis provided an in depth understanding of the current state of the insulator. Having a simple hydrophobicity rating is also desired, such as the STRI guide described in section 1.2.2. Taking the average class of all the classified sub-images on the insulator can provide a simple indication of the insulator's hydrophobicity state. However, this does not provide a proper explanation of what is going on. For instance, half of the surface might be perfectly hydrophobic, and the other half might be completely hydrophilic. The average classification class might be around class 3 - 4. Classifying an insulator as such is not advised, as the most hydrophilic part of the insulator can provide a large enough surface area for leakage current to flow.

The average sub-image of each individual figure 4.5b - 4.11b represents insulator 1 - 7 in figure 4.13.

- **Insulator 1** has an average classification class of 1.5. Glancing at the original image of the insulator in figure 4.5a, one can confirm that this is in fact a good average for the hydrophobicity of the insulator on a scale from 0 - 8.
- **Insulator 2** has a very similar average classification class at 1.7. Figure 4.5a behaves the same as figure 4.6a and so it is no surprise that their average classification classes are almost the same.
- **Insulator 3** with an average classification class of 2.5 should be less hydrophobic than insulator 1 and 2. Due to classification error in figure 4.7b, the average classification class has an offset of 1 class. Considering that there were some errors in the classification, having an offset of 1 class is not bad at all.
- **Insulator 4** is where some loss of hydrophobicity is prevalent, as seen in figure 4.8a. This partial loss of hydrophobicity is also reflected in the average classification class, which amounts to a classification of 2.9
- **Insulator 5** displays an average classification class of 3.1. However, glancing back at figure 4.9a, an average classification of around 5 is expected. This is also due to classification errors in figure 4.9b.
- **Insulator 6** has an average classification class of 5.4. This indicates that there is a significant loss of the water surface tension to the insulator's surface. The original image in figure 4.10a displays exactly such behaviour.
- **Insulator 7** has an average classification class of 7.5, giving a good indication that a film of water is covering almost the entire insulator's surface. With a theoretical maximum of 8 for the average classification class, this surface is behaving completely hydrophilic according to figure 4.13. This assumption is supported by looking at figure 4.11a.

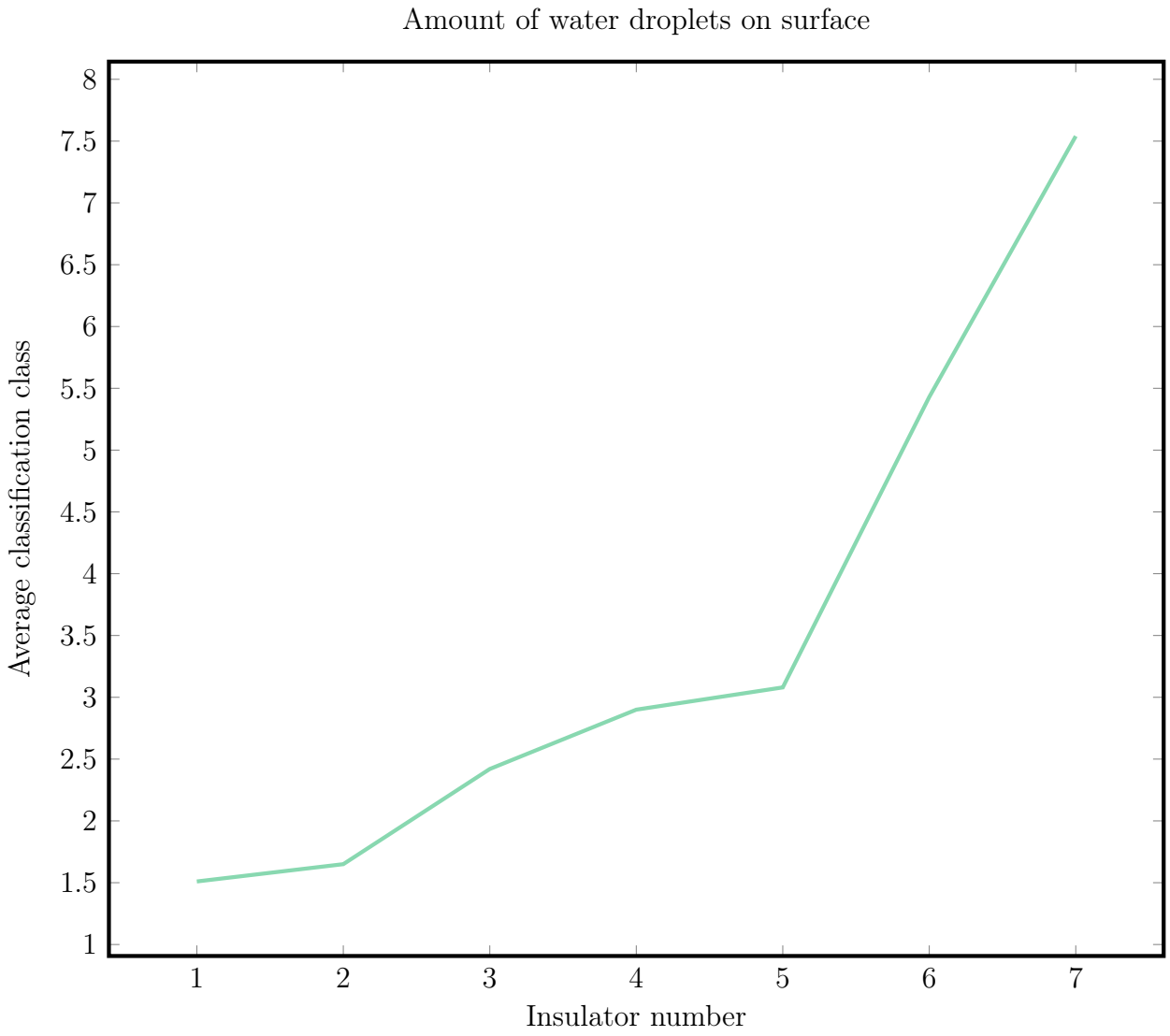

Figure 4.13: Average class for all classified sub-images

4.3.4 Sub-image standard deviation and variance discussion

Evaluating the standard deviation of all the sub-images in each of the figures 4.5b - 4.11b, the authenticity of the results in the average classification class can be determined.

- **Standard deviation:** An insulator that has a uniform hydrophobicity state should provide a small standard deviation for its classified sub-images, as almost all the sub-images should be classified into the same class. Table 4.1 displays standard deviation of the sub-images in figure 4.5b - 4.11b.

  The general standard deviation for all the figures is around 1. This is an indication that the general classification of the sub-images deviates by about 1. This is in agreement with the origins of the error compensation discussed in section 2.8.8. Therefore, it is expected that a standard deviation of around 0.5 - 1 will exist because of classification errors during dataset harvesting.

- **Variance**: An insulator with a high variance indicates to sub-image classifications that are spread out over several classes, especially the boundary classes. If half of

a hydrophobic insulator's surface is covered by pollution, resulting in completely hydrophilic behaviour for that part, it will result in a high variance as half of the sub-image will be classified into class 0 - 1 and the other half into class 7 - 8.

Given that the insulators had uniform hydrophobicity properties displayed over the entirety of their surfaces, the variance for each one of the insulators was quite low, as seen in table 4.1.

Table 4.1: Standard deviation and variance for sub-images in figure 4.5b - 4.11b

Figure	Standard deviation	Variance
4.12a	0.9	0.81
4.12b	1.01	1.02
4.12c	1.11	1.23
4.12d	0.85	0.73
4.12e	1.29	1.65
4.12f	0.82	0.67
4.12g	0.5	0.25

4.4 Machine learning method vs laser method

Both the machine learning method and laser method provided promising results. The machine learning method was able to display a correlation between the insulator's surface hydrophobicity and the features extracted from the classified sub-images.

The laser method was able to create an accurate 3D representation of the water droplets on the insulator's surface. The features extracted from the 3D surface provided a good indication to the insulator's surface hydrophobicity.

Both the machine learning and laser methods were able to display similar trends for different classes of hydrophobicity.

Chapter 5

Conclusions and recommendations

5.1 Conclusion

The drive behind developing new hydrophobicity measurement techniques was to establish a new method to measure an insulator's surface hydrophobicity in the field and lab. The machine learning technique provided promising test results during the training of different models. Six different models were evaluated. It was determined that errors during the dataset labeling process had a degraded effect on the test results of the convolutional neural networks. Taking into account that boundary errors may exists, the results were significantly better. Model 6 was chosen to be used in evaluating insulators with different emulated hydrophobicity states. Good classification results of network 6 were obtained, although errors did exist for sub-images in classes 5 - 7. Errors were contributed to not having enough training data and variation in lighting conditions of training data. Histogram distribution analysis of the classified images provided good insight into the water formations present on the insulator surfaces with their respective hydrophobicity classifications. The average of all the sub-images that were classified on an insulator's surface provided a good estimation of the insulator's hydrophobicity state, which is similar to the STRI classification. The sub-image classification variance and standard deviation provided confidence for the average sub-image classification metric. The machine learning method was considered a success. However, a higher quality dataset with more labeled images is required to improve on this method. Given that only a picture of a wet insulator is required to do analysis with, this method is ready to be used outside in the field.

The laser method was able to reconstruct an accurate 3D representation of the water droplet formations present on the insulator's surface. Effective laser line isolation was established in conjunction with contour detection needed to track the deformation of the laser line as it moved across the insulator's surface. Surface tracking was employed to compensate for an irregular scanning rate. The result was an accurate 3D mesh of the insulator's surface. The 3D mesh was converted to a gray scale image with the z -axis representing the light intensity in the gray-scale image. Having a gray-scale image allowed the use of well-established image morphology transformations to isolate the water droplets from the insulator's surface, even when it was not perfectly flat. Knowing the size and location of the water droplets enabled analysis to be done. The laser method was able to find that as the hydrophobicity of the insulator decreased, an increase in covered surface area was detected. However, this was not accurate for extremely hydrophilic surfaces, as it was difficult for the laser method to detect a very small change in the laser line height on the insulator's surface. Counting all the water droplets on the insulator provided a good correlation between amount of water droplets and surface hydrophobicity. Individual water droplet size analysis provided good insight into the

hydrophobicity state of the insulator. Although errors occurred for the extreme hydrophilic case, the fact that a significant amount of small water droplets was detected contributed into identifying the hydrophilic cases. The laser method provided accurate results for the hydrophobic surfaces. Water droplets on hydrophilic surfaces were shallow, making it difficult to detect deformation of the laser line as it is scanned over a surface. The result is that many errors occurred during water droplet isolation of hydrophilic surfaces. However, taking note of how these errors presented themselves indicated that a hydrophilic surface was present. Therefore, this technique proved to be effective. A drawback to this technique is that the laser light source disappears under outdoor lighting, making it ineffective to use in the field during the day.

5.2 Recommendations

The machine learning method does have some classification errors, especially when an insulator is illuminated with a different light source than what the labeled images were trained on. To improve on the machine learning classification, additional labeled images should be acquired. An additional data augmentation step can be implemented to artificially change the light intensity on labeled sub-images. This will increase the dataset size and also combat classification errors.

The big caveat to the laser method is when external light sources are greater than the laser light intensity. Acquiring a more powerful laser can mitigate this issue. A perfectly uniform line laser would also be beneficial. Further research can be done into finding a water colouring additive to provide better laser light reflection of the water droplet's surface. With the 3D surface constructor that was developed in the laser method, creating an algorithm to find the path of least resistance for leakage current to flow can also be beneficial to do in depth analysis.

List of References

[1] K.-Y. Law, "Definitions for hydrophilicity, hydrophobicity, and superhydrophobicity: Getting the basics right," *The Journal of Physical Chemistry Letters*, vol. 5, no. 4, pp. 686–688, 2014, pMID: 26270837. [Online]. Available: https://doi.org/10.1021/jz402762h

[2] R. Cardoso Buontempo, J. Pissolato, J. L. De Franco, S. Abreu, D. Da Silva, M. Romano, E. Costa, and L. Innocentini-Mei, "Hydrophobicity classification of distribuition silicone arresters before and after solid layer contamination," 08 2013.

[3] H. Chen, J. L. Muros-Cobos, and A. Amirfazli, "Contact angle measurement with a smartphone," *Review of Scientific Instruments*, vol. 89, no. 3, 2018.

[4] A. Bojovschi, T. V. Quoc, H. N. Trung, D. T. Quang, and T. C. Le, "Environmental effects on hv dielectric materials and related sensing technologies," *Applied Sciences*, vol. 9, no. 5, 2019. [Online]. Available: https://www.mdpi.com/2076-3417/9/5/856

[5] M. GenÃ§oÄlu and M. Cebeci, "The pollution flashover on high voltage insulators," *Electric Power Systems Research*, vol. 78, pp. 1914–1921, 11 2008.

[6] M. T. GenÃ§oglu and M. Cebeci, "Computation of ac flashover voltage of polluted hv insulators using a dynamic arc model," 2009.

[7] A. E. Vlastos and E. Sherif, "Natural ageing of epdm composite insulators," *IEEE Transactions on Power Delivery*, vol. 5, no. 1, pp. 406–414, 1990.

[8] S. Horikoshi, H. Hidaka, and N. Serpone, "Environmental remediation by an integrated microwave/uv illumination technique. 3. a microwave-powered plasma light source and photoreactor to degrade pollutants in aqueous dispersions of tio2 illuminated by the emitted uv/visible radiation," *Environmental science & technology*, vol. 36, no. 23, pp. 5229–5237, 2002.

[9] R. T. Waters, A. Haddad, H. Griffiths, N. Harid, P. Charalampidis, and P. Sarkar, "Dry-band discharges on polluted silicone rubber insulation: control and characterization," *IEEE Transactions on Dielectrics and Electrical Insulation*, vol. 18, no. 6, pp. 1995–2003, 2011.

[10] D. Ghosh and D. Khastgir, "Degradation and stability of polymeric high-voltage insulators and prediction of their service life through environmental and accelerated aging processes." *ACS omega*, vol. 3, no. 9, pp. 11 317–11 330, 2018. [Online]. Available: http://search.proquest.com/docview/2281844618/

[11] Y. Hirano, T. Inohara, M. Toyoda, H. Murase, and M. Kosakada, "Accelerated weatherability of shed materials for composite insulators," *IEEE Transactions on Dielectrics and Electrical Insulation*, vol. 8, no. 1, pp. 97–103, 2001.

[12] Arshad, A. Nekahi, S. G. McMeekin, and M. Farzaneh, "Effect of pollution severity on electric field distribution along a polymeric insulator," in *2015 IEEE 11th International Conference on the Properties and Applications of Dielectric Materials (ICPADM)*, July 2015, pp. 612–615.

[13] M. Farzaneh and W. A. Chisholm, *Insulators for icing and polluted environments*. John Wiley & Sons, 2009, vol. 47.

[14] R. Sundararajan, A. Mohammed, N. Chaipanit, T. Karcher, and Z. Liu, "In-service aging and degradation of 345 kv epdm transmission line insulators in a coastal environment," *IEEE Transactions on Dielectrics and Electrical Insulation*, vol. 11, no. 2, pp. 348–361, 2004.

[15] M. N. Horenstein and J. R. Melcher, "Particle contamination of high voltage dc insulators below corona threshold," *IEEE Transactions on Electrical Insulation*, vol. EI-14, no. 6, pp. 297–305, Dec 1979.

[16] W. Lampe, T. K. E. Hoglund, C. L. Nellis, P. E. Renner, and R. D. Stearns, "Long-term tests of hvdc insulators under natural pollution conditions at the big eddy test center," *IEEE Transactions on Power Delivery*, vol. 4, no. 1, pp. 248–259, Jan 1989.

[17] M. Amin, M. Akbar, and S. Amin, "Hydrophobicity of silicone rubber used for outdoor insulation (An overview)," *Reviews on Advanced Materials Science*, vol. 16, no. 1-2, pp. 10–26, 2007.

[18] *CRC materials science and engineering handbook*, 2nd ed. Boca Raton: CRC Press, 1994.

[19] A.-B. Mostafa and M. Ebrahim, "3d laser scanners' techniques overview," *International Journal of Science and Research (IJSR)*, vol. 4, pp. 5–611, 10 2015.

[20] N. J. Nilsson, "Introduction to machine learning: An early draft of a proposed textbook. http://robotics.stanford.edu/people/nilsson/mlbook.ht ml," 1996.

[21] G. Wang, "An Introduction to Artificial Neural Network Modelling," *The Journal of Business Forecasting*, vol. 28, no. 3, pp. 17–20, 2009.

[22] S. Cross, R. Harrison, and R. Kennedy, "Introduction to neural networks," *The Lancet*, vol. 346, no. 8982, pp. 1075 – 1079, 1995. [Online]. Available: http://www.sciencedirect.com/science/article/pii/S0140673695917462

[23] C. Nwankpa, W. Ijomah, A. Gachagan, and S. Marshall, "Activation functions: Comparison of trends in practice and research for deep learning," 11 2018.

[24] D. M. Hawkins, "The problem of overfitting." *Journal of chemical information and computer sciences*, vol. 44, no. 1, pp. 1–12, 2004. [Online]. Available: http://search.proquest.com/docview/80118607/

[25] D. Brain and G. Webb, "On the effect of data set size on bias and variance in classification learning," *Proceedings of the Fourth Australian Knowledge Acquisition Workshop*, 06 2000.

[26] S. Indolia, A. K. Goswami, S. Mishra, and P. Asopa, "Conceptual understanding of convolutional neural network-a deep learning approach," *Procedia computer science*, vol. 132, pp. 679–688, 2018.

[27] Q. Sun, F. Lin, W. Yan, F. Wang, S. Chen, and L. Zhong, "Estimation of the hydrophobicity of a composite insulator based on an improved probabilistic neural network," *Energies*, vol. 11, no. 9, p. 2459, 2018. [Online]. Available: http://search.proquest.com/docview/2108556172/

[28] X. Huang, T. Nie, Y. Zhang, and X. Zhang, "Study on hydrophobicity detection of composite insulators of transmission lines by image analysis," *IEEE Access*, vol. 7, pp. 84 516–84 523, 2019.

[29] P. A. Kowalski, "Determining significance of input neurons for probabilistic neural network by sensitivity analysis procedure." *Computational Intelligence*, vol. 34, no. 3, pp. 895–917, 2018.

[30] J. G. Carney and P. Cunningham, "The Epoch Interpretation of Learning," p. 5, 1998. [Online]. Available: http://citeseerx.ist.psu.edu/viewdoc/download?doi=10.1.1.48.5940{\&}rep=rep1{\&}type=pdf

[31] M. Li, T. Zhang, Y. Chen, and A. Smola, "Efficient mini-batch training for stochastic optimization," in *Proceedings of the 20th ACM SIGKDD international conference on knowledge discovery and data mining*, ser. KDD '14. ACM, 2014, pp. 661–670.

[32] D. Masters and C. Luschi, "Revisiting small batch training for deep neural networks," *arXiv.org*, 2018. [Online]. Available: http://search.proquest.com/docview/2072054947/

[33] N. Cui, "Applying gradient descent in convolutional neural networks," in *Journal of Physics: Conference Series*, vol. 1004, no. 1. IOP Publishing, 2018, p. 012027.

[34] J. Lawrence, J. Malmsten, A. Rybka, D. A. Sabol, and K. Triplin, "Comparing tensorflow deep learning performance using cpus, gpus, local pcs and cloud," 2017.

[35] N. Farahani, A. Braun, D. Jutt, T. Huffman, N. Reder, Z. Liu, Y. Yagi, and L. Pantanowitz, "Three-dimensional imaging and scanning: current and future applications for pathology," *Journal of pathology informatics*, vol. 8, 2017.